Bioactive exometabolites drive maintenance competition in simple bacterial communities

John L. Chodkowski[1] and Ashley Shade[2*]

[1]Department of Microbiology and Molecular Genetics, Michigan State University, East Lansing, MI 48824, USA

[2]Universite Claude Bernard Lyon 1, Laboratoire d'Ecologie Microbienne, UMR CNRS 5557, UMR INRAE 1418, VetAgro Sup, 69622 Villeurbanne, France

* Corresponding author and material requests. Email: ashley.shade@cnrs.fr; ORCiD: 0000-0002-7189-3067

Competing Interests

The authors declare no competing financial interests.

Abstract

During prolonged resource limitation, bacterial cells can persist in metabolically active states of non-growth. These maintenance periods, such as those experienced in stationary phase, can include upregulation of secondary metabolism and release of exometabolites into the local environment. As resource limitation is common of many environmental microbial habitats, we hypothesized that neighboring bacterial populations employ exometabolites to compete or cooperate during maintenance, and

that these exometabolite-facilitated interactions can drive community outcomes. Here, we evaluated the consequences of exometabolite interactions over stationary phase among three environmental strains: *Burkholderia thailandensis* E264, *Chromobacterium subtsugae* ATCC 31532, and *Pseudomonas syringae* pv.*tomato* DC3000. We assembled them into synthetic communities that only permitted chemical interactions. We compared the responses (transcripts) and outputs (exometabolites) of each member with and without neighbors. We found that transcriptional dynamics were changed with different neighbors, and that some of these changes were coordinated between members. The dominant competitor *B. thailandensis* consistently upregulated biosynthetic gene clusters to produce bioactive exometabolites for both exploitative and interference competition. These results demonstrate that competition strategies during maintenance can contribute to community-level outcomes. It also suggests that the traditional concept of defining competitiveness by growth outcomes may be narrow, and that maintenance competition could be an additional or alternative measure.

Importance

Free-living microbial populations often persist and engage in environments that offer few or inconsistently available resources. Thus, it is important to investigate microbial interactions in this common and ecologically relevant condition of non-growth. This work investigates the consequences of resource limitation for community metabolic output and for population interactions in simple synthetic bacterial communities. Despite non-growth, we observed active, exometabolite-mediated competition among the bacterial

populations. Many of these interactions and produced exometabolites were dependent on the community composition, but we also observed that one dominant competitor consistently produced interfering exometabolites regardless. These results are important for predicting and understanding microbial interactions in resource-limited environments.

Introduction

Bacteria interact with other bacteria and their environment within complex, multi-species communities. Bacterial interactions rely on the ability to sense and respond to both biotic and abiotic stimuli [1, 2]. These stimuli include physical, chemical or molecular cues, and can alter bacterial behaviors [3, 4], and ultimately, can also alter community functioning [5, 6]. It is expected that interspecies interactions play an important role in shaping microbial community dynamics [7]. However, multiple stimuli in the environment make it difficult to disentangle the separate influences of abiotic versus biotic stimuli on microbial community dynamics [8]. Therefore, efforts to characterize and distinguish community responses to biotic stimuli, such as those that facilitate interspecies interactions, will provide insights into the specific roles that microbial interactions play in shaping their communities [9].

Interspecies interactions can be facilitated through small molecules [10]. Extracellular small molecules are collectively referred to as exometabolites [11, 12, 13]. Depending on the exometabolite produced, these molecules can mediate interspecies interactions that range from competitive to cooperative [14]. Of these interaction types,

65 competition has been shown to have a major influence in structuring microbial
66 communities [15, 16, 17]. Thus, competitive interactions that are mediated by
67 exometabolites are also expected to influence microbial community dynamics. In
68 addition, different types of exometabolites can be employed by bacteria to gain
69 advantage in both exploitative (e.g. nutrient scavenging) and interference (direct cell
70 damage) categories of competition.

71 Traditionally, competition has been viewed through the lens of resource
72 acquisition [18]. In previous studies, competitiveness is modeled with respect to yield
73 given resource consumption and growth [19, 20]. However, competition for *survival* or
74 *maintenance* may be just as important as competition for yield, especially during periods
75 of resource limitation [21, 22]. Competition during maintenance is likely common in
76 environments that experience relatively long periods of nutrient famine punctuated by
77 short periods of nutrient influx, for example such as in soils, sequencing batch reactors,
78 and the gut [23, 24, 25, 26]. The stationary phase of a bacterial growth curve falls within
79 this context of growth cessation, and pulses of nutrients may be transiently available as
80 cells die and lyse (necromass), while the total population size remains stagnant.
81 Stationary phase is often coordinated with a metabolic shift to secondary metabolism
82 [27, 28]. Therefore, an effective “maintenance” competitor may produce bioactive
83 exometabolites, like antibiotics, which are often produced because of secondary
84 metabolism. Bacteria can activate biosynthetic gene clusters (BSGCs) to produce
85 bioactive exometabolites [29]. The activation of BSGCs is closely tied to stress
86 responses, suggesting that bacteria can sense the stress of competition [30, 31]. While
87 it is known that certain exometabolites can trigger BSGC upregulation and, more

generally alter transcription [32], there is much to understand about the outcomes of interspecies interactions for BSGCs in multi-member microbial communities.

Here, we build on our previous research to understand how exometabolite-mediated interactions among bacterial neighbors contribute to community outcomes in a simple, three-member community (Table 1). These three members are commonly associated with terrestrial environments (soils or plants) and were chosen because of reported [33] and observed interspecies exometabolite interactions in the laboratory. We used a synthetic community (SynCom) approach [34] by applying our previously described transwell system [35], which allowed for evaluation of "community goods" within a media reservoir that was shared among members. The members' populations were physically isolated by membrane filters at the bottom of each transwell, but could interact chemically via the reservoir. In our prior work, we investigated each member's exometabolites and transcription over stationary phase, and the objective was to understand monoculture responses (in minimal glucose media) before assembling the more complex 2- and 3- member communities. We previously found that each member in monoculture produced a variety of exometabolites in stationary phase, including bioactive molecules involved in competition [36]. In this work, we build to 2- and 3-member communities to ask: How do members interact via exometabolites in simple communities during maintenance (stationary phase), and what are the competitive strategies and outcomes of those interactions? What genetic pathways, molecules, and members drive the responses?

We found that *B. thailandensis* had a major influence on the transcriptional responses of both *C. subtsugae* and *P. syringae*, and that this influence could be

attributed to an increase in both interference and exploitative competition strategies. These findings show that diverse competitive strategies can be deployed even when bacterial neighbors are surviving rather than exponentially growing. Therefore, we suggest that contact-independent, exometabolite-mediated interference and exploitation are important competitive strategies in resource-limited environments and support the non-yield outcome of maintenance.

Materials and Methods

Bacterial strains and culture conditions

We selected three environmental bacterial strains for the SynCom experiments that were originally isolated from various plant/soil habitats and that had prior evidence of exometabolite interactions among them in the laboratory [Table 1; 33, 37-40]. Freezer stocks of *B. thailandensis*, *C. subtsugae*, and *P. syringae* were plated on half-concentration Trypticase soy agar (TSA50) at 27°C for at least 24 h. Members were inoculated in 7 ml of M9–0.2% glucose medium and grown for 16 h at 27°C, 200 rpm. Cultures were then diluted into 50 ml M9-0.2% glucose medium such that exponential growth phase was achieved after 10 h of incubation at 27°C, 200 rpm. Members were diluted in 50 ml M9 glucose medium to target ODs (*B. thailandensis* 0.3 OD, *C. subtsugae*: 0.035 OD, *P. syringae* 0.035 OD). The high initial OD for *B. thailandensis* was necessary such that stationary phase would be achieved by all members within a 2 h window after 24 h incubation in the transwell plate. The glucose concentration in the final dilution varied upon community membership- 0.067% for monocultures, 0.13% for

pairwise cocultures, and 0.2% for the 3-member community. For each member, 48 ml of diluted culture was transferred as 4 mL aliquots in 12, 5 mL Falcon tubes to more efficiently prepare replicate transwell plates.

Synthetic community experiments

Transwell plate preparation was performed as previously described [35]. Briefly, we used sterile filter plates with 0.22-µm-pore polyvinylidene difluoride (PVDF) filter bottoms (Millipore MAGVS2210). Prior to use, filter plates were washed three times with sterile water using a vacuum apparatus (NucleoVac 96 vacuum manifold; Clontech Laboratories). The filter of well H12 was removed with a sterile pipette tip and tweezer, and 31 ml of M9 glucose medium was added to the reservoir through well H12. The glucose concentration in the reservoir varied upon community membership- 0.067% for monocultures, 0.13% for pairwise cocultures, and 0.2% for the 3-member community. Glucose concentration was adjusted to plate occupancy (e.g., 3-member communities had higher number of wells occupied than 2- or 1-member). Our aim was for each member to achieve stationary phase at similar times across all conditions to compare transcripts and exometabolites under similar growth trajectories. In other words, available resources were standardized while keeping the well occupancy for each member constant. With this design, transcripts and exometabolites in cocultures that deviated from those in monocultures could be attributed to interspecies interactions and not complicated by offset in member growth trajectories across the experimental conditions.

Each well was filled with 130 µL of culture or medium (prepared as described, above; see methods section: Bacterial strains and culture conditions). For each plate, a custom R script (RandomArray.R [see script at https://github.com/ShadeLab/PAPER_Chodkowski_mSystems_2017/blob/master/R_analysis/RandomArray.R]) was used to randomize community member placement in the wells so that each member occupied a total of 31 wells per plate. In total, there were 7 community conditions- 3 monocultures, 3 pairwise cocultures, and the 3-member community. Each member occupied 31 wells per plate regardless of experimental condition. Thus, “baseline” exometabolites could be determined in the monocultures, and then deviations in exometabolite abundance or detection in the cocultures could be attributed to interspecies interactions. A time course was performed for each replicate. The time course included an exponential phase time point (12.5 h) and 5 time points assessed every 5 h over stationary phase (25 h – 45 h). Four biological replicates were performed for each community condition for a total of 28 experiments. For each experiment, 6 replicate filter plates were prepared for destructive sampling for a total of 168 transwell plates.

Filter plates were incubated at 27°C with gentle shaking (~0.32 rcf). For each plate, a custom R script (RandomArray.R [see script at https://github.com/ShadeLab/PAPER_Chodkowski_mSystems_2017/blob/master/R_analysis/RandomArray.R]) was used to randomize wells for each organism assigned to RNA extraction (16 wells) and flow cytometry (5 wells). The following procedure was performed for each organism when a transwell plate was destructively sampled: i) wells containing spent culture assigned to RNA extraction were pooled (~100 µL/well) into a

178 1.7 mL microcentrifuge tube and flash frozen in liquid nitrogen and stored at -80 until
179 further processing. ii) 20 µL from wells assigned for flow cytometry were diluted into 180
180 µL Tris-buffered saline (TBS; 20 mM Tris, 0.8% NaCl [pH 7.4]). In community
181 memberships where *P. syringae* was arrayed with *B. thailandensis*, *P. syringae* had a
182 final dilution of 70-fold in TBS. In community memberships where *P. syringae* was
183 arrayed in monoculture or in coculture with *C. subtsugae*, *P. syringae* had a final dilution
184 of 900-fold in TBS. Final dilutions for *B. thailandensis* and *C. subtsugae* were 1 300-fold
185 and 1 540-fold, respectively. Each member was diluted differently to achieve a suitable
186 events/second range on the flow cytometer for accurate cell counting. Populations were
187 then stained and analyzed on the flow cytometer for live/dead counting (see
188 Supplementary Methods). iii) Spent medium (~31 ml) from the shared reservoir was
189 transferred to 50 mL conical tubes, flash-frozen in liquid nitrogen and stored at −80 °C
190 prior to metabolite extraction.
191
192 **RNA-seq**
193 RNA extraction, sequencing, quality control, and count matrix generation was performed
194 as previously published [36, see Supplementary Methods].
195
196 **Transcriptomics**
197 *Quality filtering and differential gene expression analysis*
198 Count matrices for each member were quality filtered in two steps: genes
199 containing 0 counts in all samples were removed, and genes with a transcript count of
200 ≤10 in more than 90% of samples were removed. DESeq2 [41] was used to extract size

factor and dispersion estimates. These estimates were used as external input into ImpulseDE2 for the analysis of differentially regulated genes [42]. ImpulseDE2 determines differential expression by comparing longitudinal count datasets. Case-control (Cocultures-monoculture control) analyses were analyzed to identify genes with differences in temporal regulation at an FDR-corrected threshold of 0.01. Genes that passed the FDR threshold were further filtered for genes that had at least one time point with a log2 fold-change (LFC) >= 1 or <= -1. Thus, we defined differentially expressed genes (DEGs) as genes that met both the FDR-corrected and LFC thresholds. For each member, differences in gene regulation between the three coculture conditions was visualized with Venn diagrams using the VennDiagram package [43].

Differentially expressed genes were first determined by comparing each coculture condition to the monoculture control and applying a LFC threshold (see above). We then determined a second set of DEGs by comparing pairwise cocultures to each other. ImpulseDE2 case-control analyses were performed as follows: *B. thailandensis* coculture with *C. subtsugae* (case) compared to *B. thailandensis* coculture with *P. syringae* (control), *C. subtsugae* coculture with *B. thailandensis* (case) compared to *C. subtsugae* coculture with *P. syringae* (control), and *P. syringae* coculture with *B. thailandensis* (case) compared to *P. syringae* coculture with *C, subtsugae* (control). Genes that passed the FDR-corrected threshold of 0.01 based on ImpulseDE2 analysis and had at least one time point with a LFC of >= 1 or <= -1 represented coculture specific DEGs. The DEGs determined from monoculture comparisons and coculture comparisons were then categorically grouped using Clusters of Orthologous Groups (COG).

224

225 *COG analysis*

226 Protein fasta files were downloaded from NCBI and uploaded to eggNOG-
227 mapper v2 (http://eggnog-mapper.embl.de/) to obtain COGs. The DEGs determined
228 from ImpulseDE2 and LFC thresholds were categorized as upregulated or
229 downregulated based on temporal expression patterns. DEGs with consistent positive
230 LFC throughout all stationary phase time points were categorized as upregulated. DEGs
231 with consistent negative LFC throughout all stationary phase time points were
232 categorized as downregulated. These DEGs were then assigned to COGs, grouped
233 based on temporal up/downregulation patterns, and plotted using ggplot2 [44].

234

235 *Principal coordinates analysis and statistics*

236 Normalized gene matrices were extracted from DESeq2 and filtered to only
237 contain DEGs (coculture to monoculture comparisons) based on our previously
238 described definition. A variance-stabilizing transformation was performed on normalized
239 gene matrices using the rlog function in DESeq2. A distance matrix based on the Bray-
240 Curtis dissimilarity metric was then calculated on the variance-stabilized gene matrices
241 and principal coordinates analysis was performed using the R package vegan [45].
242 Principal coordinates were plotted using ggplot2. Coordinates of the first two PCoA axes
243 were used to perform PROTEST analysis using the PROTEST function in vegan.
244 Dissimilarity matrices were used to perform PERMANOVA and variation partitioning
245 using the adonis and varpart functions in vegan, respectively. The RVAideMemoire
246 package [46] was used to perform a post-hoc pairwise PERMANOVAs. Lastly,

247 distances were extracted from the Bray-Curtis dissimilarity matrix that compared each
248 coculture condition to the monoculture condition at each time point within each member.
249 These distances were used to produce time series distance plots.
250
251 *Biosynthetic gene cluster (BSGC) analysis*
252 NCBI accession numbers were uploaded to antiSMASH 6 beta bacterial version
253 [47] to identify genes involved in BSGCs using default parameters. Where possible,
254 literature-based evidence and BSGCs uploaded to MIBiG [48] were used to better
255 inform antiSMASH predictions. Log2 fold-changes (LFCs) were calculated for all
256 predicted biosynthetic genes within each predicted cluster by comparing coculture
257 expression to monoculture expression at each time point. Average LFCs were
258 calculated from all predicted biosynthetic genes within a predicted BSGC at each time
259 point. Temporal LFC trends were plotted using ggplot2. An upregulated BSGC was
260 defined as a BSGC that had at least two consecutive time points in stationary phase
261 with a LFC > 1.
262
263 *Network analysis*
264 Unweighted co-expression networks were created from quality filtered and
265 normalized expression data. Networks were generated for pairwise cocultures
266 containing *B. thailandensis*. First, data were quality filtered as previously described
267 (see methods section: *Quality filtering and differential gene expression analysis*). Then,
268 normalized expression data was extracted from DESeq2. Twenty-three and twenty-
269 four RNA-seq samples from each member were used for network analysis in the *B.*

thailandensis-C. subtsugae and B. thailandensis-P.syringae cocultures, respectively (23/24 samples/member; 6 time points, 4 biological replicates). Only 23 samples were used in the *B. thailandensis-C. subtsugae* network analysis because RNA-seq failed for *C. subtsugae* at 45 h, biological replicate 2. Interspecies networks were then inferred from the expression data using the context likelihood of relatedness [49] algorithm within the R package Minet [50]. Gene matrices for each coculture pair were concatenated to perform the following analysis. Briefly, the mutual information coefficient was determined for each gene-pair. To ensure robust detection of co-expressed genes, a resampling approach was used as previously described [51]. Then, a Z-score was computed on the mutual information matrix. A Z-score threshold of 4.5 was used to determine an edge in the interspecies network. Interspecies networks were uploaded into Cytoscape version 3.7.1. for visualization, topological analysis, and enrichment analysis [52].

Gene annotation and gene ontology (GO) files were obtained for *B. thailandensis*, *P. syringae,* and *C. subtsugae* for enrichment analyses. For *B. thailandensis,* annotation and ontology files were downloaded from the Burkholderia Genome Database (https://www.burkholderia.com). For *P. syringae*, annotation and ontology files were downloaded from the Pseudomonas Genome Database (http://www.pseudomonas.com/strain/download). Annotation and ontology files for *C. subtsugae* were generated using Blast2GO version 5.2.5 [53]. InterProScan [54] with default parameters were used to complement gene annotations from *C. subtsugae*. GO terms were assigned using Blast2GO with default parameters. In addition, genes involved in secondary metabolism were manually curated and added to these files as

293 individual GO terms. These genes were also used to update the GO term GO:0017000
294 (antibiotic biosynthetic process), composed of a collection of all the biosynthetic genes.
295 (see methods section: *Biosynthetic gene cluster (BSGC) analysi*s).
296 Topological analysis was performed as follows: Nodes were filtered from each
297 coculture network to only select genes from one member at a time. The GLay
298 community cluster function in Cytoscape was used to determine intra-member modules.
299 Functional enrichment analysis was then performed on the modules using the BiNGO
300 package [55] in Cytoscape.
301 To determine interspecies co-regulation patterns, we filtered network nodes that
302 contained an interspecies edge. Functional enrichment analysis was performed on the
303 collection of genes containing interspecies edges for each member using the BiNGO
304 package in Cytoscape. Then, we selected all genes contained within modules of interest
305 (e.g. *B. thailandensis* modules containing either thailandamide or malleilactone genes in
306 the *B. thailandensis*-*C. subtsugae* coculture network or *B. thailandensis*-*P. syringae*
307 coculture network, respectively) in Cytoscape. Node selection was extended by
308 selecting the first neighbors of the selected nodes. This resulted in interspecies edges.
309 The resultant nodes were transformed into a circular layout and exported for manual
310 edits in InkScape.. The biosynthetic gene cluster organization of thailandamide and
311 malleilactone were obtained from MIBig and drawn in InkScape.
312 Protein sequences from an interspecies gene of interest (CLV_2968) within a
313 network module that also contained thailandamide genes from the *B. thailandensis*-*C.*
314 *subtsugae* network and an interspecies gene of interest (PSPTO_1206) within a
315 network module that also contained malleilactone genes from the *B. thailandensis*-*P.*

316 *syringae* network were obtained. A protein blast for each protein was run against *B.*
317 *thailandensis* protein sequences. *B. thailandensis* locus tags were extracted from the
318 top blast hit from each run. Normalized transcript counts for these 4 genes of interest
319 were plotted in R. Time course gene trajectories were determined using a loess
320 smoothing function.
321
322
323 **Metabolomics**
324 *LCMS, feature detection, and quality control*
325 Standard operating protocols were performed at the Department of Energy Joint
326 Genome Institute as previously described [36]. MZmine 2 [56] was used for feature
327 detection and peak area integration as previously described [36]. Select exometabolites
328 were identified in MZmine 2 by manual observation of both MS and MS/MS data. We
329 extracted quantities of these identified exometabolites for ANOVA and Tukey HSD post-
330 hoc analysis in R. We filtered features in three steps to identify coculture-accumulated
331 exometabolites. The feature-filtering steps were performed as follows on a per-member
332 basis: (i) retain features where the maximum peak area abundance occurred in any of
333 the coculture communities ; (ii) a noise filter, the minimum peak area of a feature from a
334 replicate at any time point needed to be 3 times the maximum peak area of the same
335 feature in one of the external control replicates, was applied; (iii) coefficient of variation
336 (CV) values for each feature calculated between replicates at each time point needed to
337 be less than 20% across the time series.

Four final feature data sets from polar and nonpolar analyses in both ionization modes were analyzed in MetaboAnalyst 5.0 [57], as reported in our prior work [36, see Supplementary Methods]. In addition, exometabolites categorized as primary metabolites were identified according to Metabolomics Standards Initiative (MSI) level 1 criteria [58], as reported in our prior work [36, see Methods].

Principal coordinates analysis and statistics

A distance matrix based on the Bray-Curtis dissimilarity metric was used to calculate dissimilarities between exometabolite profiles. Principal coordinates analysis was performed using the R package vegan. Principal coordinates were plotted using ggplot2. Coordinates of the first two PCoA axes were used to perform Protest analysis using the protest function in vegan. Dissimilarity matrices were used to perform PERMANOVA and variation partitioning using the adonis and varpart functions in vegan, respectively. The RVAideMemoire package was used to perform a post-hoc pairwise PERMANOVAs. Monoculture controls were removed to focus on coculture trends.

Results

Overview

Our major data types included both transcriptomics and metabolomics, and we integrate these to interpret SynCom dynamics and interactions. Our longitudinal design resulted in 288 RNAseq samples across the three members, and 168 community metabolomics samples analyzed in each of four mass spectral modes (polar/nonpolar, positive/negative modes = 672 total mass spectral profiles). After quality control, we were left with 281 RNAseq and 605 total mass spectral profiles for the integrated analyses [https://github.com/ShadeLab/Paper_Chodkowski_3member_SynCom_2021/tree/master/SummaryOfSamples]. First, we present a summary of experiments and cell viability (section 1). Then, we present results of general responses of transcription (section 2) and exometabolomics (section 3), separately. Then, we integrate transcriptomic and metabolomic efforts to determine the upregulation of biosynthetic gene clusters (BSGCs) and identify exometabolites of interest from mass spectrometry (section 4). Lastly, we then present a transcriptomics co-expression network to ask how the upregulation of BSGCs influenced interspecies interactions through coordinated longitudinal gene expression (section 5).

1. *SynCom design/sampling scheme and membership cell viability*

We had four replicate, independent timeseries for each of seven community memberships (three of each monoculture, three of each pair in coculture, and the 3-member community). We define membership as the specific strains present in a given condition. Here, we focus on the multi-member analyses (2 and 3-member combinations) to gain insights into community outcomes (Fig. 1A). The SynCom transwell system isolated member populations among separate transwells but permitted

383 exchange of their collective exometabolites via the plate's shared media reservoir (Fig.
384 1B). We collected data (transcripts, metabolites, etc) over a timeseries that included one
385 exponential phase time point (12.5 h) followed by 5 stationary phase time points (25-45
386 h sampled at 5-hour intervals; Fig. 1C).

387 We observed relatively unchanged viability in *B. thailandensis* across all conditions
388 (Fig. S1; panels A-D). On the contrary, we observed a slight reduction (~2.1 log2 fold
389 change) in *C. subtsugae* live cell counts, and a drastic reduction (~4.7 log2 fold change)
390 in *P. syringae* live cell counts, when either member was cocultured with *B. thailandensis*
391 (Fig. 2; panels A vs C and panels D vs F, respectively). Reductions in cell viability of *C.*
392 *subtsugae* and *P. syringae* were also present in the 3-member community (Fig. S1;
393 panels E and F). *C. subtsugae* and *P. syringae* had minimal effects on each other (Fig.
394 2; panels B and E). Dead cell accumulation of *P. syringae* plateaued in coculture
395 conditions compared to monoculture, suggesting cell lysis (Fig. 2, panels D-F). We note
396 that one doubling occurred in *B. thailandensis* and *P. syringae* monocultures, and in *C.*
397 *subtsugae* in pairwise coculture with *P. syringae.* We elaborated on this finding as the
398 possibility of a reductive cell division in our previous manuscript [36].

399

400 *2. Stationary phase transcript dynamics of microbial community members*

401 Differentially expressed genes were determined by comparing time series
402 transcript trajectories applying an FDR and LFC threshold (see methods: *Quality*
403 *filtering and differential gene expression analysis*). First, we compared each coculture to
404 the monoculture control. A range of 153 to 276 genes were differentially expressed by
405 each member in coculture, irrespective of the identity of neighbors (Fig. S2). In addition,

406 each member also had differential gene expression that was unique to a particular
407 neighbor(s). Summarizing across all cocultures, 1089/5639 (19.3%) coding sequences
408 (CDSs), 1991/4393 CDSs (45.3%), and 3274/5576 CDSs (58.7%) DEGs were
409 determined for *B. thailandensis*, *C. subtsugae*, and *P. syringae*, respectively. Primary
410 drivers of transcriptional response patterns for each member were community
411 membership (PCoA axis 1) and time (PCoA axis 2) (Fig. 3, Table S1). Together, these
412 data suggest that there are both general and specific consequences of neighbors for the
413 transcriptional responses of these bacterial community members.

414 Temporal trajectories in member transcript profiles were generally reproducible
415 across replicates (PROTEST analyses, Table S2). Each member had a distinct
416 transcript profile ($0.480 \leq r2 \leq 0.778$ by Adonis; P value, 0.001; all pairwise false
417 discovery rate [FDR]-adjusted P values, ≤0.01 except for two community memberships,
418 Table S3). For all ordinations, community membership had the most explanatory value
419 (Axis 1), followed by time (Axis 2), with the most variation explained by the interaction
420 between time and membership (Table S1). Membership alone accounted for 60.6% and
421 77.0% of the variation explained in *C. subtsugae* and *P. syringae* analyses, respectively
422 and 46.3% in the *B. thailandensis* analysis (Table S1).

423 When included in the community, *B. thailandensis* strongly determined the
424 transcript profiles of the other two members. For example, the inclusion of *B.*
425 *thailandensis* in a coculture differentiated transcript profiles for both *C. subtsugae* and
426 *P. syringae* (Fig. 3B & 3C, Figs. S3-S5). The transcript profile differences between
427 monoculture and coculture conditions are largest for *C. subtsugae* (Fig. S4) and *P.*
428 *syringae* (Fig. S5) when *B. thailandensis* is included in the coculture. Thus, *B.*

thailandensis appears to have had a dominating influence on the transcriptional response of neighbors, and these responses were dynamic with respect to time.

We analyzed clusters of orthologous groups of proteins (COGs) to infer the responses of members to their neighbors. Differentially expressed genes (DEGs) were categorized as upregulated or downregulated based on temporal patterns and representation in COGs (Fig. S6). We focused on the largest differences between total DEGs upregulated and total DEGs downregulated within a COG, which provides insights into broad biological processes affected by community membership. COGs with large differences toward upregulation in *B. thailandensis* included cell motility [N], secondary metabolites biosynthesis, transport, and catabolism [Q], and signal transduction mechanisms [T] while COGs with large differences toward downregulation included defense mechanisms [V], energy production and conversion [C], translation, and ribosomal structure and biogenesis [J]. These results suggest that *B. thailandensis* responds to neighbors via downregulation of growth and reproduction and upregulation of secondary metabolism. We therefore hypothesized that *B. thailandensis* was producing bioactive exometabolites against *C. subtsugae* and *P. syringae* to competitively inhibit their growth.

Because of the strong transcript response of *C. subtsugae* and *P. syringae* when neighbored with *B. thailandensis* (Fig. 3B & 3C), we focused on COGs within community memberships with *B. thailandensis* (Fig. S6B & S6C, rows 2 & 3). The COG with large differences toward upregulation in both *C. subtsugae* and *P. syringae* were translation, ribosomal structure and biogenesis [J]. COG groups tending toward downregulation in *C. subtsugae* and *P. syringae* were signal transduction mechanisms

[T] and secondary metabolites biosynthesis, transport, and catabolism [Q], respectively. These results suggest that the presence of *B. thailandensis* alters its neighbor's ability to respond to the environment and inhibits secondary metabolism. The effects of *B. thailandensis* on *C. subtsugae* and *P. syringae* were also evident by mapping timeseries LFCs onto KEGG pathways. Various enzymes involved in central metabolism, fatty acid degradation, growth, transport, and response systems were upregulated when *B. thailandensis* was grown with either or both members (https://figshare.com/s/b7f5e559a32cc5c8a61f).

The above analyses focused on DEGs determined by comparing each coculture to the monoculture control. However, we also wanted to understand differences between pairs to determine if the alterations in transcripts were attributed to specific memberships (aka interspecies interactions). A total of 436, 1 762, and 2 962 DEGs were determined when comparing the pairs including *B. thailandensis*, the pairs including *C. subtsugae* , and the pairs including *P. syringae*, respectively. We detected member-specific effects on the COGs that were differentially expressed (Fig. S7). These data suggest that there were transcriptional changes driven by particular members and given their partner. Due to the physical separation of members in our SynCom plate system, these member-specific interspecies interactions were very likely exometabolite-mediated.

3. Stationary phase exometabolite dynamics of microbial communities

Because member populations are physically separated in the SynCom transwell system but allowed to interact chemically, observed transcript responses in different

community memberships are inferred to result from exometabolite interactions. Spent medium from the shared medium reservoir was collected from each transwell plate and analyzed using mass spectrometry to detect exometabolites. Our previous manuscript focused on exometabolite dynamics in monocultures [36]. Here, we focused our analysis on those exometabolites that had maximum accumulation in a coculture (either in pairs or in 3-member community). Consistent with the transcript analysis, we found that both community membership and time explained the exometabolite dynamics, and that the explanatory value of membership and time was maintained across all polarities and ionization modes (Fig. 4, Table S4).

Temporal trajectories in exometabolite profiles were generally reproducible across replicates with some exceptions (PROTEST analyses, Table S5, Supplementary File 1). Exometabolite profiles were distinct by community membership ($0.475 \leq r2 \leq 0.662$ by Adonis; P value, 0.001; all pairwise false discovery rate [FDR]-adjusted P values, ≤0.01 except for two comparisons, Table S6), and also dynamic over time. As observed for the member transcript profiles, the interaction between membership and time had the highest explanatory value for the exometabolite data (Table S4).

We found that the *C. subtsugae-P. syringae* coculture exometabolite profiles were consistently the most distinct from the other coculture memberships (Fig. 4), supporting, again, that the inclusion of *B. thailandensis* was a major driver of exometabolite dynamics, possibly because it provided the largest or most distinctive contributions to the community exometabolite pool. Indeed, we observed that a majority of the most abundant exometabolites were either detected uniquely in the *B. thailandensis* monoculture or accumulated substantially in its included community

memberships (Fig. S8). Some exometabolites detected in *B. thailandensis*-inclusive communities were not detected in its monocultures (Fig. S8D), suggesting that the inclusion of neighbors contributed to the accumulation of these particular exometabolites (e.g. upregulation of biosynthetic gene clusters or lysis products). *C. subtsugae* and *P. syringae* contributed less to the 3-member community exometabolite profile, as exometabolites detected in the *C. subtsugae-P. syringae* coculture were less abundant and had lower accumulation over time in the 3-member community (Fig. S8A). Together, these results suggest that *B. thailandensis* can suppress or overwhelm expected outputs from neighbors.

Exometabolites categorized as primary metabolites were identified according to Metabolomics Standards Initiative (MSI) level 1 criteria [58]. We identified primary metabolites accumulated in the shared medium reservoir over time in each monoculture (Fig. 5; [36]) to compare their dynamics in cocultures. These primary metabolites were detected to decrease in concentration across coculture conditions, suggesting metabolic inhibition or interspecies uptake. In addition, we also found a subset of primary metabolites that accumulate substantially in exponential phase in monocultures (Fig. S9). Taken together, each member contributed a unique set of primary metabolites to the community exometabolite pool. The uptake and metabolism of these primary metabolites by the non-producing members may directly affect the available pool of exometabolites in cocultures, particularly with respect to exometabolites contributed from secondary metabolism.

In summary, we observed both increased accumulation and unique production of exometabolites in pairs and in the 3-member community, with *B. thailandensis*

521 contributing the most to the shared exometabolite pool as determined by comparisons
522 with its monoculture exometabolite profile. Related, the transcriptional responses of *C.*
523 *subtsugae* and *P. syringae* in the 3-member community is most like their respective
524 transcriptional response when neighbored with *B. thailandensis* alone, despite the
525 presence of the third neighbor.

526

527 *4. B. thailandensis increases competition strategies in the presence of neighbors*

528 Given the observed reduction in cell viability (Fig. 2) and that there have been
529 competitive interactions between *B. thailandensis* and *C. subtsugae* previously reported
530 [33], we hypothesized that *B thailandensis* was using competition strategies to influence
531 its neighbors via production of bioactive exometabolites. If true, we would expect
532 transcriptional upregulation in *B. thailandensis* biosynthetic gene clusters (BSGC) that
533 encode bioactive exometabolites. Indeed, when compared to the monoculture control,
534 we found evidence of upregulated BSGCs across various time points in stationary
535 phase in *B. thailandensis* cocultures (Fig. 6, Table S7). Some of these upregulation
536 patterns were associated to particular pairs of members and some upregulation patterns
537 were strongest in the full community (e.g. thailandamide). For example, *B. thailandensis*
538 upregulated an unidentified non-ribosomal peptide synthetase (NRPS) when paired with
539 *P. syringae,* but when paired with *C. subtsugae*, upregulated a different BSGC encoding
540 an unidentified beta-lactone. This suggests that *B. thailandensis* responded to
541 neighbors by upregulating genes involved in the production of bioactive compounds,
542 likely to gain a competitive advantage. However, not all BSGCs in *B. thailandensis* were
543 upregulated. Some BSGCs were unaltered or downregulated (Fig. S10). *C. subtsugae*

upregulated only 1 BSGC, an uncharacterized hybrid nonribosomal peptide synthetase-type I polyketide synthase, in coculture with *B. thailandensis,* while *P. syringae* did not upregulate any BSGC in any coculture (Figs. S11 & S12). Interspecies interactions led to the upregulation of BSGCs in both *B. thailandensis* and *C. subtsugae* and three of these BSGCs encode potentially novel bioactive exometabolites.

Because *B. thailandensis* upregulated the transcription of various BSGCs when grown in cocultures, we asked if this led to the unique production of or increased accumulation of secondary metabolites as compared to when it was grown in monoculture. We identified 6 of the 11 exometabolites from the BSGCs in *B. thailandensis* that were upregulated and quantified their abundances from mass spectrometry data (Fig. 7, Supplementary File 2). We found that each identified exometabolite differentially accumulated between community memberships containing *B. thailandensis* (Table S8), particularly when comparing the *B. thailandensis* monoculture to each coculture (Table S9). As expected, these identified exometabolites were not detected in communities that did not include *B. thailandensis* (data not shown). Bactobolin was the only identified exometabolite that accumulated in monoculture to equivalent levels of accumulation in all coculture conditions. The other identified secondary metabolites were not detected or did not accumulate in monoculture, suggesting interspecies induction of secondary metabolism. Thus, in response to an exometabolite from either *C. subtsugae* or *P. syringae*, *B. thailandensis* increased its competitive strategies through the upregulation and production of many bioactive exometabolites. Of these bioactive exometabolites, three are documented antimicrobials [59, 60, 61], two are siderophores [62, 63], and one is a biosurfactant

567 [64]. We conclude that *B. thailandensis* produced bioactive exometabolites to
568 competitively interact using both interference and exploitative competition strategies
569 [65]. Given that *B. thailandensis* upregulated competitive strategies, and responded
570 more broadly in producing competition-supportive exometabolites when grown with
571 neighbors, we hypothesized that these bioactive exometabolites are responsible for the
572 altered transcriptional responses in *C. subtsugae* and *P. syringae*.

573 In our experimental design, we adjusted glucose concentration depending on
574 plate occupancy. Glucose concentration increased as plate occupancy increased (31
575 wells vs 62 wells vs 93 wells), but a member consistently occupied 31 wells across all
576 experimental conditions. One complication of this design is that population density and
577 resource concentration could contribute to differences in transcripts and exometabolites
578 in a member-agnostic manner. To address this, we performed additional SynCom
579 experiments to affirm confidence that some changes in transcripts and exometabolites
580 are attributable to exometabolite-mediated interspecies interactions. In these
581 experiments, we increased the plate occupancy of *B. thailandensis* in monoculture while
582 subsequently increasing resource concentration. Pairwise cocultures and the 3-member
583 community SynCom experiments were repeated as well (see Supplementary methods).
584 We calculated the relative gene expression of three genes in the thailandamide operon
585 (*thaF*, *thaK*, and *thaQ*) through RT-qPCR by comparing each experimental condition to
586 the monoculture control (*B. thailandensis*, 31 wells in M9-0.067% glucose). Decreased
587 gene expression was observed across all three genes as both plate occupancy and
588 resource concentration increased in *B. thailandensis* monocultures. In fact, *thaF*, *thaK*,
589 and *thaQ* gene expression was further reduced in the 93 well *B. thailandensis*

590 monoculture compared to the 62 well *B. thailandensis* monoculture, suggesting that the
591 thailandamide operon trended towards reduced expression as a function of *B.*
592 *thailandensis* plate occupancy in monoculture conditions. On the contrary, *thaF*, *thaK*,
593 and *thaQ* had increased expression in all coculture memberships, suggesting that
594 exometabolite interspecies interactions were responsible for the increased expression
595 of a BSGC in *B. thailandensis* (Table S10).

596

597 *5. Interspecies co-transcriptional networks reveal coordinated gene expression*
598 *related to competition*

599 We performed interspecies co-expression network analysis to infer interspecies
600 interactions. We used temporal profiles from transcriptional responses to generate co-
601 expression networks for *B. thailandensis*-*C. subtsugae* and *B. thailandensis*-*P. syringae*
602 cocultures, respectively (Table S11). As expected, the majority of nodes in the network
603 had intraspecies edges only, with interspecies edges comprising 1.85% and 1.90% of
604 the total edges in the *B. thailandensis*-*C. subtsugae* and *B. thailandensis*-*P. syringae*
605 networks, respectively. We explored interspecies edges for evidence of interspecies
606 transcriptional co-regulation.

607 We performed two analyses, module analysis and Gene Ontology (GO)
608 enrichment, to validate networks and infer interspecies interactions (Fig. S13). Module
609 analysis validated networks as intraspecies modules enriched for biological processes
610 (Supplementary File 3). To infer interspecies interactions, we filtered genes with
611 interspecies edges and performed enrichment analysis (Supplementary File 4). The top
612 enriched GO term for *B. thailandensis* when paired with *C. subtsugae* was antibiotic

synthesis of thailandamide, supporting the interpretation of interference competition. Though the top enriched GO term in *B. thailandensis* when paired with *P. syringae* was bacterial-type flagellum-dependent cell motility, antibiotic synthesis of malleilactone was also enriched. Both thailandamide genes from the *B. thailandensis*-*C. subtsugae* network (Fig. 8) and malleilactone genes from the *B. thailandensis*-*P. syringae* network (Fig. S14) formed near-complete modules within their respective BSGCs. In addition, genes that were part of the BSGC modules contained interspecies edges with both *C. subtsugae* and *P. syringae.*

At least one gene from each of *B. thailandensis's* upregulated BSGCs (Fig. 6) had an interspecies edge, except for rhamnolipid. Our interpretation of this result is that, generally, *B. thailandensis's* upregulated BSGCs had co-expression patterns with genes from the other members. In the thailandamide and malleilactone modules, some of these interspecies genes were related to stress, transport, and iron-scavenging (Supplementary File 5). The top GO term for both *C. subtsugae* and *P. syringae* genes that had edges shared with *B. thailandensis* was bacterial-type flagellum-dependent motility. Other notable enriched GO processes were efflux activity for *C. subtsugae* and signal transduction for *P. syringae*. Specifically, a DNA starvation/stationary phase gene (CLV04_2968, Fig. 8), *dspA*, was within the network module that also contained thailandamide genes from the *B. thailandensis*-*C. subtsugae* network and a TonB-dependent siderophore receptor gene (PSPTO_1206, Fig. S14) was within the network module that also contained malleilactone genes from the *B. thailandensis*-*P. syringae* network. Interestingly, both CLV04_2968 and PSPTO_1206 were DEGs and downregulated when cocultured with *B. thailandensis* (Figs. S15A & S16A,

636 respectively). Additionally, the closest homolog for *dspA* in *B. thailandensis* was
637 unaltered (BTH_I1284, Supplementary File 6) when cocultured with *C. subtsugae* (Fig.
638 S15B) and the closest homolog to the TonB-dependent receptor in *B. thailandensis*
639 (BTH_I2415, Supplementary File 7) was a DEG and upregulated when cocultured with
640 *P. syrinage* (Fig. S16B). Taken together, these co-expression networks revealed
641 interspecies coordinated expression patterns. Specifically, we detected interspecies co-
642 expression patterns related to antibiotic upregulation in *B. thailandensis*, suggesting *C.*
643 *subtsugae* and *P. syringae* were sensing and responding directly to these competition
644 strategies of *B. thailandensis.*

645

646 Discussion

647 Here, we used a synthetic community system to understand how
648 exometabolomic interactions determine members transcriptional responses and
649 exometabolite outputs. Our experiment used a systems approach to compare the seven
650 possible community memberships of three members, and their dynamics in member
651 transcripts and community exometabolites over stationary phase. Differential gene
652 expression across community memberships and over time show that the
653 exometabolites released by a member were sensed and responded to by its neighbors.
654 Furthermore, members' ouputs in monocultures changed because of coculturing, as
655 evidenced by differential exometabolite production. The largest transcriptional
656 alterations in *C. subtsugae* and *P. syringae* occurred when cocultured with *B.*
657 *thailandensis*. Global expression patterns in *C. subtsugae* and *P. syringae* when in the

658 3-member community still resembled expression patterns in pairwise cocultures with *B.*
659 *thailandensis.* These transcriptional alterations in *C. subtsugae* and *P. syringae* were
660 coordinated with increases in *B. thailandensis* competitive strategies (evaluated by
661 BSGC transcript upregulation and exometabolite abundance). That interactions within a
662 relatively simple community altered the transcriptional responses and exometabolite
663 outputs of each member is important because these kinds of alterations could, in turn,
664 drive changes in community structure and/or function in an environmental setting. For
665 example, it was shown that interspecies interactions more strongly influenced the
666 assembly of *C. elegans* gut communities than host-associated factors [66]. Therefore,
667 mechanistic and ecological characterization of interspecies interactions will inform as to
668 the principles that govern emergent properties of microbial communities.

669 Overall, competitive interactions predominated in this synthetic community. This
670 was first evidenced by reductions in viable cell counts in both *C. subtsugae* and *P.*
671 *syringae* when cocultured with *B. thailandensis*. Interestingly, *P .syringae* was the only
672 member to have an exponential increase in dead cell counts in monoculture. *P.*
673 *syringae* dead cell count accumulation ceased in coculture conditions. We attribute this
674 finding to the overall reduction of cell viability and/or lysis of dead cells when cocultured.

675 Our previous study found that, over stationary phase in monocultures, each
676 member released and accumulated at least one exometabolite documented to be
677 involved in either interference or exploitative competition [36]. This suggests that entry
678 into stationary phase primed members for competitive interactions, regardless of
679 heterospecific neighbors present. We interpret this strategy of preemptive aggression to
680 be especially advantageous to *B. thailandensis,* as it successfully used competitive

681 strategies against both *C. subtsugae* and *P. syringae*. *B. thailandensis's* success was
682 supported by decreased viable *P. syringae* cells when cocultured with *B. thailandensis*.
683 Though *C. subtsugae* viable cell counts were not as affected directly by the coculture
684 with *B. thailandensis*, *B. thailandensis*-produced bactobolin [67] was detected in the
685 shared medium reservoir. Bactobolin is a bacteriostatic antibiotic previously shown to be
686 bioactive against *C. subtsugae* [33] through ribosome binding [59]. But, *C. subtsugae*
687 can resist bactobolin through upregulation of an RND-type efflux pump [68]. This finding
688 also is supported by our data, as all genes coding for the CdeAB-OprM RND-type efflux
689 system were DEGs and upregulated in *C. subtsugae* cocultures with *B. thailandensis*
690 (CLV04_2413-CLV04_2415).

691 When cocultured with *B. thailandensis*, we observed COG groups such as
692 translation, ribosomal structure and biogenesis [J] had large differences toward
693 upregulation in both *C. subtsugae* and *P. syringae*. At first glance, this seems at odds
694 with our interpretation of *B. thailandensis* competitiveness toward *C. subtsugae* and *P.*
695 *syringae*. In other words, how is *B. thailandensis* effectively competing via interference
696 competition if both *C. subtsugae* and *P. syringae* are upregulating machinery for
697 growth? There is both theoretical [69] and experimental [70] evidence that show how
698 cells treated with antibiotics stimulate ribosomal production to maintain a sufficient
699 number of active ribosomes. As previously mentioned, *B. thailandensis*-produced
700 bactobolin binds to the ribosome and can inhibit *C. subtsugae* [33, 59]. We also have
701 evidence that bactobolin inhibits *P. syringae* (data not shown). It could be that
702 bactobolin is stimulating ribosomal production in *C. subtsugae* and *P. syringae* as a
703 survival mechanism to maintain protein production by maintaining enough active

ribosomes. There also was evidence of *B. thailandensis* antibiotic efficacy against *C. subtsugae* and *P. syringae*, including general loss of cell viability and upregulation of various enzymes involved in central metabolism by both members when they were cocultured with *B. thailandensis* (https://figshare.com/s/b7f5e559a32cc5c8a61f). These patterns are consistent with antibiotic treatments in *Escherichia coli* and *Staphylococcus aureus* where the upregulation of oxidative phosphorylation due to drug treatment contributes to antibiotic efficacy [71, 72]. A barrage of *B. thailandensis*-produced antibiotics (Figs. 6 & 7) likely drove the transcriptional patterns in *C. subtsugae* and *P. syringae*.

Coculturing can induce secondary metabolism [73, 74, 75] because an exometabolite produced by one microbe can prompt secondary metabolism in a neighbor [31]. We found that coculturing led to the upregulation of numerous BSGCs in *B. thailandensis*. These exometabolites included bactobolin, malleilactone [62, 76; siderophore and cytotoxin], malleobactin [77, 78; siderophore], capistruin [79; lasso peptide], thailandamide [80; polyketide], pyochelin [63; siderophore], rhamnolipids [64; biosurfactants], and two uncharacterized BSGCs encoding nonribosomal peptide synthetases. Of these exometabolites, bactobolin, capistruin, and thailandamide have documented antimicrobial activities through translation inhibition [59], transcription inhibition [60], and inhibition of fatty acid synthesis [61], respectively. For those exometabolites we were able to identify with mass spectrometry, their accumulation in cocultures was correlated with the upregulation of their BSGCs. Furthermore, up/downregulated patterns across all *B. thailandensis* BSGCs was consistent with ScmR global regulatory patterns of secondary metabolism [81].

We acknowledge that this study is limited in its ability to pinpoint the underlying mechanisms driving the activation of secondary metabolism, particularly in *B. thailandensis*. Aside from self-activating mechanisms documented in *B. thailandensis* (e.g. quorum-sensing driven bactobolin production) and/or sensing antibiotics and competitively responding [82], we note two major patterns in exometabolite production in the monocultures that may have contributed to activation of secondary metabolism in the cocultures. First, each member released and accumulated a unique set of primary metabolites over their time series. These exometabolites had relatively reduced concentrations in their coculture conditions. Second, because our experimental design included a comparative time point taken during exponential growth, we also identified a unique set of primary metabolites that had substantially accumulated by 12.5 h. Indeed, primary metabolites [83] have been documented to induce secondary metabolism in *B. thailandensis.* Thus, it is possible that the dynamics observed over stationary phase could be attributed also to the uptake of exometabolites that were produced earlier in exponential phase, or to the uptake of accumulated primary metabolites. Instead of pinpointing single molecule elicitors of secondary metabolism, our systems-level approach is better used to improve understanding of the environmental and ecological factors that contribute to member or community success.

C. subtsugae can inhibit *B. thailandensis* [33] but we did not observe *B. thailandensis* inhibition based on cell counts. However, we did find that in stationary phase *C. subtsugae-B. thailandensis* cocultures, *C. subtsugae* upregulated an uncharacterized hybrid nonribosomal peptide synthetase-type I polyketide synthase. *P. syringae* was the least competitive of the three neighbors, as evidenced by a reduction

750 in live cell counts when cocultured with *B. thailandensis*. Also, *P. syringae* did not
751 increase competitive strategies when cocultured, as no BSGCs were upregulated
752 across all coculture conditions. In summary, though all three neighbors had potential to
753 use competitive strategies and maintained competitive strategies in monoculture [36], *B.*
754 *thailandensis* was most successful in cocultures over stationary phase through
755 increased production of exometabolites involved in interference and exploitative
756 competition strategies.

757 Given the upregulation of BSGCs in *B. thailandensis* and the strong
758 transcriptional responses of *C. subtsugae* and *P. syringae* to the presence of *B.*
759 *thailandensis*, we hypothesized that competitive exometabolites were contributing to
760 their community dynamics. Thus, we used a co-expression network analysis with our
761 longitudinal transcriptome series to infer interspecies interactions [84]. The use of this
762 approach was first demonstrated to infer coregulation between a phototroph-heterotroph
763 commensal pair [85]. Our network confirmed that *B. thailandensis* BSGCs had
764 coordinated gene expression patterns with both *C. subtsugae* and *P. syringae*.
765 Interspecies nodes in both networks contained various genes involved in the
766 upregulated *B. thailandensis* BSGCs. We focused on interspecies edges within
767 thailandamide nodes for the *B. thailandensis*-*C. subtsugae* network and interspecies
768 edges within malleilactone nodes for the *B. thailandensis*-*P. syringae* network because
769 these were significantly enriched as interspecies nodes. A *C. subtsugae* gene of
770 interest, CLV04_2968, was contained within the thailandamide cluster of interspecies
771 nodes. This gene codes for a DNA starvation/stationary phase protection protein and
772 had the highest homology to the Dps protein in *Escherichia coli* across all *C. subtsugae*

773 protein coding genes. Dps mediates tolerance to multiple stressors and *dps* knockouts
774 are more susceptible to thermal, oxidative, antibiotic, iron toxicity, osmotic, and
775 starvation stressors [86]. Interestingly, CLV04_2968 was downregulated when
776 cocultured with *B. thailandensis*, suggesting that *B. thailandensis* attenuates *C.*
777 *subtsugae* stress tolerance over stationary phase. While we observed a slight decrease
778 in viable *C. subtsugae* cells when cocultured with *B. thailandensis*, one may expect *C.*
779 *subtsugae* to have increased sensitivity to a subsequent stress [e.g. pH stress; 87]
780 resulting from CLV04_2968 downregulation in the presence of *B. thailandensis*.

781 In the *B. thailandensis-P. syringae* co-expression network, a *P. syringae* gene of
782 interest, PSPTO_1206, was contained within the malleilactone cluster of interspecies
783 nodes. PSPTO_1206 is annotated as a TonB-dependent siderophore receptor. A *P.*
784 *syringae* iron-acquistion receptor had coordinated expression with malleilactone, which
785 has been characterized as a siderophore with antimicrobial properties [62]. Interestingly,
786 this gene was downregulated when in coculture with *B. thailandensis*. In contrast, the
787 closest TonB-dependent siderophore receptor homolog to PSPTO_1206 in *B.*
788 *thailandensis*, BTH_I2415, was upregulated in coculture conditions with *P. syringae*. To
789 summarize, co-expression network analysis revealed interspecies coordinated gene
790 expression patterns. Though determining directionality was beyond the scope of this
791 analysis, we observed *B. thailandensis*-increased competition strategies were
792 coordinated with a potential decrease in competition strategies in *C. subtsugae* via
793 reduced stress tolerance and in *P. syringae* with reduced iron acquisition ability.

794 One feature of our study is that we adjusted glucose concentration depending on
795 plate occupancy. Glucose concentration increased as membership increased, but a

796 member consistently occupied 31 wells across all experimental conditions. One could
797 argue that resource concentration contributed to differences in transcripts and
798 exometabolites and not interspecies interactions. However, DEGs were present when
799 comparing pairwise coculture conditions and these were attributed to differences in
800 temporal regulation of COG categories (Fig. S7). More specifically, regarding BSGCs,
801 an unidentified NRPS was upregulated in *B. thailandensis* when cocultured with *P.*
802 *syringae* but not when cocultured with *C. subtsugae* (Fig. 6) and, an unidentified NRPS-
803 Type I polyketide synthase was upregulated in *C. subtsugae* when cocultured with *B.*
804 *thailandensis* but not when cocultured with *P. syringae* (Fig. S11). These differences
805 occurred in experimental conditions where the glucose concentration was the same.
806 Furthermore, we performed additional SynCom experiments where we increased the
807 plate occupancy of *B. thailandensis* in monoculture while subsequently increasing
808 resource concentration. Decreased gene expression was observed across all three RT-
809 qPCR tested thailandamide genes as both plate occupancy and resource concentration
810 increased in *B. thailandensis* monocultures. These same three genes had increased
811 gene expression across all cocultures. These findings show that some undefined
812 exometabolite interspecies interactions were responsible for the increased expression
813 of a BSGC in *B. thailandensis*. Overall, we acknowledge that resource concentration
814 and exometabolite output are intertwined, and subsequent work could test how initial
815 resource availability determines SynCom outcomes.

816 A major goal in microbial ecology is to predict community dynamics for purposes
817 of modulating and/or maintaining ecosystem function [88, 89]. At its core, microbial
818 functional properties emerge, in part, from the concerted interactions of multi-species

819 assemblages. The SynCom system provides a tractable experimental system to
820 understand the relationships between exometabolite interactions and environmental
821 stimuli to inform higher-order community interactions. Higher-order interactions are
822 those that are unexpected based on interactions observed in simpler situations (e.g., of
823 member pairs) [90, 91, 92]. Therefore, integrating different system variables, like
824 transcriptome and metabolome dynamics, within controlled microbial communities will
825 inform how unexpected phenomena arise and how they contribute to deviations in
826 predictive models of community outcomes.

827 Our results indicated that competition strategies were maintained despite
828 stagnant population growth. *B. thailandensis* upregulated various bioactive
829 exometabolites involved in both interference and exploitative competition when with
830 neighbors. An effective competitor is often defined as by its ability to outcompete
831 neighbors via growth advantage that stems from efficient nutrient uptake and/or
832 biomass conversion rates [93, 94]. We add to this that a competitor can also have a
833 fitness advantage through effective maintenance, which can similarly employ
834 interference or exploitative competitive strategies despite no net growth. Maintenance
835 may ensure survival in some environments that impose a stationary phase lifestyle,
836 where long periods of nutrient depletion are punctuated with short periods of nutrient
837 flux. In these scenarios, it warrants to understand how competitive strategies are
838 deployed in the interim of growth and the extent to which these interactions contribute to
839 long-term community outcomes. Though population levels remain constant, sub-
840 populations of growing cells have been observed in stationary phase [95], and
841 continued production of competitive exometabolites may serve as an advantageous

842 strategy to hinder growth of competitors. In addition, some antibiotics remain effective in
843 non-replicating bacteria [96]. The ability for continued maintenance via effective
844 competition strategies during stationary phase may provide spatiotemporal maintenance
845 of population levels before growth resumption [97]. Alternatively, both growth and non-
846 growth strategies may be occurring simultaneously (e.g. as can occur in biofilms). The
847 heterogeneity of biofilms may provide an environment where a bacterial population
848 contains both stationary cells in the center of the colony with growing cells at the
849 periphery of the colony that compete and alter developmental patterns of neighboring
850 populations [98, 99]. Thus, we expect that insights into the long-term consequences of
851 competition for microbial community outcomes will be gained by considering
852 competition in both active growth and maintenance scenarios.

853

854 **Code availability**

855 Computing code, workflows, and data sets are available at
856 [https://github.com/ShadeLab/Paper_Chodkowski_3member_SynCom_2021]. R
857 packages used during computing analyses included DEseq2 [41], ImpulseDE2 [42],
858 VennDiagram [43], ggplot2 [44], vegan 2.5-4 [45], RVAideMemoire [46], Minet [50],
859 rtracklayer [100], viridis [101], and helper functions [102, 103, 104, 105].

860

861 **Data availability**

862 Genomes for *B. thailandensis*, *C. subtsugae*, and *P. syringae* are available at the
863 National Center for Biotechnology Information (NCBI) under accession
864 numbers NC_007651 (Chromosome I)/NC_007650 (Chromosome

II), NZ_PKBZ01000001, and NC_004578 (Chromosome)/NC_004633 (Plasmid A)/NC_004632 (Plasmid B), respectively. An improved annotated draft genome of *C. subtsugae* is available under NCBI BioProject accession number PRJNA402426 (GenBank accession number PKBZ00000000). Data for resequencing efforts for *B. thailandensis* and *P. syringae* are under NCBI BioProject accession numbers PRJNA402425 and PRJNA402424, respectively. Metabolomics data and transcriptomics data are also available at the JGI Genome Portal [106] under JGI proposal identifier 502921. MZmine XML parameter files for all analyses can be viewed at and downloaded from GitHub (see Dataset 7 at https://github.com/ShadeLab/Paper_Chodkowski_MonocultureExometabolites_2020/tree/master/Datasets). Large data files (e.g., MZmine project files) are available upon request. Supplementary files are also available on GitHub (https://github.com/ShadeLab/Paper_Chodkowski_3member_SynCom_2021/tree/master/Supplemental_Files).

Acknowledgements

This material is based upon work supported by the National Science Foundation under grant DEB 1749544 and by Michigan State University. In addition, metabolite analysis and transcript sequencing were provided by a DOE-JGI Community Science Program award (proposal identifier 502921). The work conducted by the U.S. Department of Energy Joint Genome Institute, a DOE Office of Science User Facility, is supported under contract number DE-AC02-05CH11231. J.L.C. was supported by the Eleanor L. Gilmore Fellowship from the Department of Microbiology and Molecular Genetics.

We thank Katherine B. Louie and Benjamin P. Bowen for support in mass spectral analysis.

Competing Interests

The authors declare no competing financial interests.

Author contributions

J.L.C. and A.S. conceived of and designed the study. J.L.C. performed the research and analyses. J.L.C. and A.S. wrote the manuscript.

References

1. Stock, A. M., Robinson, V. L., & Goudreau, P. N. (2000). Two-component signal transduction. Annual Review of Biochemistry, 69, 183–215. https://doi.org/10.1146/annurev.biochem.69.1.183

2. Browning, D. F., & Busby, S. J. W. (2004). The regulation of bacterial transcription initiation. Nature Reviews Microbiology, 2(1), 57–65. https://doi.org/10.1038/nrmicro787

3. Pietschke, C., Treitz, C., Forêt, S., Schultze, A., Künzel, S., Tholey, A., … Fraune, S. (2017). Host modification of a bacterial quorum-sensing signal induces a phenotypic switch in bacterial symbionts. Proceedings of the National Academy of Sciences of the United States of America, 114(40), E8488–E8497. https://doi.org/10.1073/pnas.1706879114

4. Garren, M., Son, K., Tout, J., Seymour, J. R., & Stocker, R. (2016). Temperature-induced behavioral switches in a bacterial coral pathogen. ISME Journal, 10(6), 1363–1372. https://doi.org/10.1038/ismej.2015.216

5. Kato, S., Haruta, S., Cui, Z. J., Ishii, M., & Igarashi, Y. (2005). Stable coexistence of five bacterial strains as a cellulose-degrading community. Applied and Environmental Microbiology, 71(11), 7099–7106. https://doi.org/10.1128/AEM.71.11.7099-7106.2005

6. Megan Steinweg, J., Dukes, J. S., Paul, E. A., & Wallenstein, M. D. (2013). Microbial responses to multi-factor climate change: Effects on soil enzymes. Frontiers in Microbiology, 4, 146. https://doi.org/10.3389/fmicb.2013.00146

7. Aziz, F. A. A., Suzuki, K., Ohtaki, A., Sagegami, K., Hirai, H., Seno, J., … Futamata, H. (2015). Interspecies interactions are an integral determinant of microbial community dynamics. Frontiers in Microbiology, 6, 1148. https://doi.org/10.3389/fmicb.2015.01148

8. Orr, J. A., Vinebrooke, R. D., Jackson, M. C., Kroeker, K. J., Kordas, R. L., Mantyka-Pringle, C., … Piggott, J. J. (2020). Towards a unified study of multiple stressors: Divisions and common goals across research disciplines. Proceedings of the Royal Society B: Biological Sciences, 287(1926), 20200421. https://doi.org/10.1098/rspb.2020.0421

9. Little, A. E. F., Robinson, C. J., Peterson, S. B., Raffa, K. F., & Handelsman, J. (2008). Rules of engagement: Interspecies interactions that regulate microbial communities. Annual Review of Microbiology, 62, 375–401. https://doi.org/10.1146/annurev.micro.030608.101423

10. Phelan, V. V, Liu, W.-T., Pogliano, K., & Dorrestein, P. C. (2011). Microbial metabolic exchange--the chemotype-to-phenotype link. Nature Chemical Biology, 8(1), 26–35. https://doi.org/10.1038/nchembio.739

11. Kell, D. B., Brown, M., Davey, H. M., Dunn, W. B., Spasic, I., & Oliver, S. G. (2005). Metabolic footprinting and systems biology: The medium is the message. Nature Reviews Microbiology, 3(7), 557–565. https://doi.org/10.1038/nrmicro1177

12. Pinu, F. R., & Villas-Boas, S. G. (2017). Extracellular microbial metabolomics: The state of the art. Metabolites, 7(3), 43. https://doi.org/10.3390/metabo7030043

13. Silva, L. P., & Northen, T. R. (2015). Exometabolomics and MSI: Deconstructing how cells interact to transform their small molecule environment. Current Opinion in Biotechnology, 34, 209–216. https://doi.org/10.1016/j.copbio.2015.03.015

14. Großkopf, T., & Soyer, O. S. (2014). Synthetic microbial communities. Current Opinion in Microbiology, 18(1), 72–77. https://doi.org/10.1016/j.mib.2014.02.002

15. Foster, K. R., & Bell, T. (2012). Competition, not cooperation, dominates interactions among culturable microbial species. Current Biology, 22(19), 1845–1850. https://doi.org/10.1016/j.cub.2012.08.005

16. Coyte, K. Z., Schluter, J., & Foster, K. R. (2015). The ecology of the microbiome: Networks, competition, and stability. Science, 350(6261), 663–666. https://doi.org/10.1126/science.aad2602

17. Hibbing, M. E., Fuqua, C., Parsek, M. R., & Peterson, S. B. (2010). Bacterial competition: Surviving and thriving in the microbial jungle. Nature Reviews Microbiology, 8(1), 15–25. https://doi.org/10.1038/nrmicro2259

18. Tilman, D. (1982). Resource Competition and Community Structure. Princeton, NJ, U.S.A.: Princeton University Press.

19. Stewart, F. M., & Levin, B. R. (1973). Partitioning of Resources and the Outcome of Interspecific Competition: A Model and Some General Considerations. The American Naturalist, 107(954), 171–198. https://doi.org/10.1086/282825

20. Smith, H. L. (2011). Bacterial competition in serial transfer culture. Mathematical Biosciences, 229(2), 149–159. https://doi.org/10.1016/j.mbs.2010.12.001

21. Pekkonen, M., Korhonen, J., & Laakso, J. T. (2011). Increased survival during famine improves fitness of bacteria in a pulsed-resource environment. Evolutionary Ecology Research (Vol. 13). Evolutionary Ecology, Ltd.

22. Holt, R. D. (2008). Theoretical perspectives on resource pulses. Ecology, 89(3), 671–681. https://doi.org/10.1890/07-0348.1

23. Schimel, J. P. (2018). Life in dry soils: Effects of drought on soil microbial communities and processes. Annual Review of Ecology, Evolution, and Systematics, 49, 409–432. https://doi.org/10.1146/annurev-ecolsys-110617-062614

24. Chiesa, S. C., Irvine, R. L., & Manning, J. F. (1985). Feast/famine growth environments and activated sludge population selection. Biotechnology and Bioengineering, 27(5), 562–568. https://doi.org/10.1002/bit.260270503

25. Fetissov, S. O. (2017). Role of the gut microbiota in host appetite control: Bacterial growth to animal feeding behaviour. Nature Reviews Endocrinology, 13(1), 11–25. https://doi.org/10.1038/nrendo.2016.150

26. Hiltunen, T., Laakso, J., Kaitala, V., Suomalainen, L. R., & Pekkonen, M. (2008). Temporal variability in detritus resource maintains diversity of bacterial communities. Acta Oecologica, 33(3), 291–299. https://doi.org/10.1016/j.actao.2007.12.002

27. Navarro Llorens, J. M., Tormo, A., & Martínez-García, E. (2010). Stationary phase in gram-negative bacteria. FEMS Microbiology Reviews, 34(4), 476–495. https://doi.org/10.1111/j.1574-6976.2010.00213.x

28. Čihák, M., Kameník, Z., Šmídová, K., Bergman, N., Benada, O., Kofronová, O., … Bobek, J. (2017). Secondary metabolites produced during the germination of Streptomyces coelicolor. Frontiers in Microbiology, 8, 2495. https://doi.org/10.3389/fmicb.2017.02495

29. Medema, M. H., Kottmann, R., Yilmaz, P., Cummings, M., Biggins, J. B., Blin, K., … Glöckner, F. O. (2015). Minimum Information about a Biosynthetic Gene cluster. Nature Chemical Biology, 11(9), 625–631. https://doi.org/10.1038/nchembio.1890

30. Cornforth, D. M., & Foster, K. R. (2013). Competition sensing: The social side of bacterial stress responses. Nature Reviews Microbiology, 11(4), 285–293. https://doi.org/10.1038/nrmicro2977

31. Okada, B. K., & Seyedsayamdost, M. R. (2017). Antibiotic dialogues: Induction of silent biosynthetic gene clusters by exogenous small molecules. FEMS Microbiology Reviews, 41(1), 19–33. https://doi.org/10.1093/femsre/fuw035

32. Goh, E. B., Yim, G., Tsui, W., McClure, J. A., Surette, M. G., & Davies, J. (2002). Transcriptional modulation of bacterial gene expression by subinhibitory concentrations of antibiotics. Proceedings of the National Academy of Sciences of the United States of America, 99(26), 17025–17030. https://doi.org/10.1073/pnas.252607699

33. Chandler, J. R., Heilmann, S., Mittler, J. E., & Greenberg, E. P. (2012). Acyl-homoserine lactone-dependent eavesdropping promotes competition in a laboratory co-culture model. ISME Journal, 6(12), 2219–2228. https://doi.org/10.1038/ismej.2012.69

34. De Roy, K., Marzorati, M., Van den Abbeele, P., Van de Wiele, T., & Boon, N. (2014). Synthetic microbial ecosystems: an exciting tool to understand and apply microbial communities. Environmental Microbiology, 16(6), 1472–1481. https://doi.org/10.1111/1462-2920.12343

35. Chodkowski, J. L., & Shade, A. (2017). A Synthetic Community System for Probing Microbial Interactions Driven by Exometabolites. MSystems, 2(6), e00129-17. https://doi.org/10.1128/msystems.00129-17

36. Chodkowski, J. L., & Shade, A. (2020). Exometabolite Dynamics over Stationary Phase Reveal Strain-Specific Responses. MSystems, 5(6), e00493-20. https://doi.org/10.1128/msystems.00493-20

37. Brett, P. J., DeShazer, D., & Woods, D. E. (1998). Burkholderia thailandensis sp. nov., a Burkholderia pseudomallei-like species. International Journal of Systematic Bacteriology, 48 Pt 1(1), 317–320. https://doi.org/10.1099/00207713-48-1-317

38. Wells, J. S., Trejo, W. H., Principe, P. A., Bush, K., Georgopapadakou, N., Bonner, D. P., & Sykes, R. B. (1982). SQ 26,180, a novel monobactam. I Taxonomy, fermentation and biological properties. The Journal of Antibiotics, 35(2), 184–188. https://doi.org/10.7164/ANTIBIOTICS.35.184

39. Buell, C. R., Joardar, V., Lindeberg, M., Selengut, J., Paulsen, I. T., Gwinn, M. L., … Collmer, A. (2003). The complete genome sequence of the Arabidopsis and tomato pathogen Pseudomonas syringae pv. tomato DC3000. Proceedings of the National Academy of Sciences, 100(18), 10181–10186. https://doi.org/10.1073/PNAS.1731982100

40. Harrison, A. M., & Soby, S. D. (2020). Reclassification of Chromobacterium violaceum ATCC 31532 and its quorum biosensor mutant CV026 to Chromobacterium subtsugae. *AMB Express*, *10*(1), 202. https://doi.org/10.1186/S13568-020-01140-1

41. Love, M. I., Huber, W., & Anders, S. (2014). Moderated estimation of fold change and dispersion for RNA-seq data with DESeq2. Genome Biology, 15, 550. https://doi.org/10.1186/s13059-014-0550-8

42. Fischer, D. S., Theis, F. J., & Yosef, N. (2018). Impulse model-based differential expression analysis of time course sequencing data. Nucleic Acids Research, 46(20), 119. https://doi.org/10.1093/nar/gky675

43. Chen, H. (2018). VennDiagram: Generate High-Resolution Venn and Euler Plots. R package version 1.6.20.

44. Wickham, H. (2016). ggplot2: Elegant Graphics for Data Analysis. Springer-Verlag New York.

45. Oksanen, J., Blanchet, F. G., Friendly, M., Kindt, R., Legendre, P., McGlinn, D., … Wagner, H. (2019). vegan: Community Ecology Package. R package version 2.5-4.

46. Herve M. (2020). RVAideMemoire: testing and plotting procedures for biostatistics. R Packag version 09-77.

47. Blin, K., Shaw, S., Kloosterman, A. M., Charlop-Powers, Z., van Wezel, G. P., Medema, M. H., & Weber, T. (2021). antiSMASH 6.0: improving cluster detection and comparison capabilities. Nucleic Acids Research, 49(W1), W29–W35. https://doi.org/10.1093/NAR/GKAB335

48. Kautsar, S. A., Blin, K., Shaw, S., Navarro-Muñoz, J. C., Terlouw, B. R., van der Hooft, J. J. J., … Medema, M. H. (2020). MIBiG 2.0: a repository for biosynthetic gene clusters of known function. Nucleic Acids Research, 48(D1), D454–D458. https://doi.org/10.1093/NAR/GKZ882

49. Faith, J. J., Hayete, B., Thaden, J. T., Mogno, I., Wierzbowski, J., Cottarel, G., … Gardner, T. S. (2007). Large-scale mapping and validation of Escherichia coli transcriptional regulation from a compendium of expression profiles. PLoS Biology, 5(1), e8. https://doi.org/10.1371/journal.pbio.0050008

50. Meyer, P. E., Lafitte, F., & Bontempi, G. (2008). Minet: A r/bioconductor package for inferring large transcriptional networks using mutual information. BMC Bioinformatics, 9(1), 461. https://doi.org/10.1186/1471-2105-9-461

51. McClure, R. S., Overall, C. C., Mcdermott, J. E., Hill, E. A., Markillie, L. M., Mccue, L. A., … Beliaev, A. S. (2016). Network analysis of transcriptomics expands regulatory landscapes in Synechococcus sp. PCC 7002. Nucleic Acids Research, 44(18), 8810–8825. https://doi.org/10.1093/nar/gkw737

52. Shannon, P., Markiel, A., Ozier, O., Baliga, N. S., Wang, J. T., Ramage, D., … Ideker, T. (2003). Cytoscape: A software Environment for integrated models of biomolecular interaction networks. Genome Research, 13(11), 2498–2504. https://doi.org/10.1101/gr.1239303

53. Götz, S., García-Gómez, J. M., Terol, J., Williams, T. D., Nagaraj, S. H., Nueda, M. J., … Conesa, A. (2008). High-throughput functional annotation and data mining with the Blast2GO suite. Nucleic Acids Research, 36(10), 3420–3435. https://doi.org/10.1093/nar/gkn176

54. Zdobnov, E. M., & Apweiler, R. (2001). InterProScan - An integration platform for the signature-recognition methods in InterPro. Bioinformatics, 17(9), 847–848. https://doi.org/10.1093/bioinformatics/17.9.847

55. Maere, S., Heymans, K., & Kuiper, M. (2005). BiNGO: a Cytoscape plugin to assess overrepresentation of gene ontology categories in biological networks. Bioinformatics (Oxford, England), 21(16), 3448–3449. https://doi.org/10.1093/BIOINFORMATICS/BTI551

56. Pluskal, T., Castillo, S., Villar-Briones, A., & Orešič, M. (2010). MZmine 2: Modular framework for processing, visualizing, and analyzing mass spectrometry-based molecular profile data. BMC Bioinformatics, 11, 395. https://doi.org/10.1186/1471-2105-11-395

57. Pang, Z., Chong, J., Zhou, G., de Lima Morais, D. A., Chang, L., Barrette, M., … Xia, J. (2021). MetaboAnalyst 5.0: narrowing the gap between raw spectra and functional insights. Nucleic Acids Research, (1), gkab382. https://doi.org/10.1093/nar/gkab382

58. Schymanski, E.L., Jeon, J., Gulde, R., Fenner, K., Ruff, M., Singer, H.P., & Hollender, J. (2014). Identifying small molecules via high resolution mass spectrometry: communicating confidence. Environmental Science & Technology, 48, 2097–2098. https://doi.org/10.1021/es5002105

59. Amunts, A., Fiedorczuk, K., Truong, T. T., Chandler, J., Peter Greenberg, E., & Ramakrishnan, V. (2015). Bactobolin A binds to a site on the 70S ribosome distinct from previously seen

antibiotics. Journal of Molecular Biology, 427(4), 753–755. https://doi.org/10.1016/j.jmb.2014.12.018

60. Kuznedelov, K., Semenova, E., Knappe, T. A., Mukhamedyarov, D., Srivastava, A., Chatterjee, S., … Severinov, K. (2011). The antibacterial threaded-lasso peptide capistruin inhibits bacterial RNA polymerase. Journal of Molecular Biology, 412(5), 842–848. https://doi.org/10.1016/j.jmb.2011.02.060

61. Wozniak, C. E., Lin, Z., Schmidt, E. W., Hughes, K. T., & Liou, T. G. (2018). Thailandamide, a fatty acid synthesis antibiotic that is coexpressed with a resistant target gene. Antimicrobial Agents and Chemotherapy, 62(9), e00463-18. https://doi.org/10.1128/AAC.00463-18

62. Biggins, J. B., Ternei, M. A., & Brady, S. F. (2012). Malleilactone, a polyketide synthase-derived virulence factor encoded by the cryptic secondary metabolome of Burkholderia pseudomallei group pathogens. Journal of the American Chemical Society, 134(32), 13192–13195. https://doi.org/10.1021/ja3052156

63. Butt, A. T., & Thomas, M. S. (2017). Iron acquisition mechanisms and their role in the virulence of Burkholderia species. Frontiers in Cellular and Infection Microbiology, 7, 460. https://doi.org/10.3389/fcimb.2017.00460

64. Dubeau, D., Déziel, E., Woods, D. E., & Lépine, F. (2009). Burkholderia thailandensis harbors two identical rhl gene clusters responsible for the biosynthesis of rhamnolipids. BMC Microbiology, 9(1), 1–12. https://doi.org/10.1186/1471-2180-9-263

65. Ghoul, M., & Mitri, S. (2016). The Ecology and Evolution of Microbial Competition. Trends in Microbiology, 24(10), 833–845. https://doi.org/10.1016/j.tim.2016.06.011

66. Ortiz, A., Vega, N. M., Ratzke, C., & Gore, J. (2021). Interspecies bacterial competition regulates community assembly in the C. elegans intestine. ISME J, 1–15. https://doi.org/10.1038/s41396-021-00910-4

67. Duerkop, B. A., Varga, J., Chandler, J. R., Peterson, S. B., Herman, J. P., Churchill, M. E. A., … Greenberg, E. P. (2009). Quorum-sensing control of antibiotic synthesis in Burkholderia thailandensis. Journal of Bacteriology, 191(12), 3909–3918. https://doi.org/10.1128/JB.00200-09

68. Evans, K. C., Benomar, S., Camuy-Vélez, L. A., Nasseri, E. B., Wang, X., Neuenswander, B., & Chandler, J. R. (2018). Quorum-sensing control of antibiotic resistance stabilizes cooperation in Chromobacterium *subtsugae*. ISME J, 12(5), 1263–1272. https://doi.org/10.1038/s41396-018-0047-7

69. Maitra, A., & Dill, K. A. (2016). Modeling the Overproduction of Ribosomes when Antibacterial Drugs Act on Cells. Biophysical Journal, 110(3), 743–748. https://doi.org/10.1016/J.BPJ.2015.12.016

70. Dennis, P. P. (1976). Effects of chloramphenicol on the transcriptional activities of ribosomal RNA and ribosomal protein genes in Escherichia coli. Journal of Molecular Biology, 108(3), 535–546. https://doi.org/10.1016/S0022-2836(76)80135-0

71. Dwyer, D. J., Kohanski, M. A., Hayete, B., & Collins, J. J. (2007). Gyrase inhibitors induce an oxidative damage cellular death pathway in Escherichia coli. Molecular systems biology, 3, 91. https://doi.org/10.1038/msb4100135

72. Kohanski, M. A., Dwyer, D. J., Hayete, B., Lawrence, C. A., & Collins, J. J. (2007). A common mechanism of cellular death induced by bactericidal antibiotics. Cell, 130(5), 797–810. https://doi.org/10.1016/j.cell.2007.06.049

73. Pettit, R. K. (2009). Mixed fermentation for natural product drug discovery. Applied Microbiology and Biotechnology, 83(1), 19–25. https://doi.org/10.1007/s00253-009-1916-9

74. Netzker, T., Fischer, J., Weber, J., Mattern, D. J., König, C. C., Valiante, V., … Brakhage, A. A. (2015). Microbial communication leading to the activation of silent fungal secondary metabolite gene clusters. Frontiers in Microbiology. Frontiers Media S.A. https://doi.org/10.3389/fmicb.2015.00299

75. Zhu, H., Sandiford, S. K., & Van Wezel, G. P. (2014). Triggers and cues that activate antibiotic production by actinomycetes. Journal of Industrial Microbiology and Biotechnology, 41(2), 371–386. https://doi.org/10.1007/s10295-013-1309

76. Truong, T. T., Seyedsayamdost, M., Greenberg, E. P., & Chandler, J. R. (2015). A Burkholderia thailandensis acyl-homoserine lactone-independent orphan LuxR homolog that activates production of the cytotoxin malleilactone. Journal of Bacteriology, 197(21), 3456–3462. https://doi.org/10.1128/JB.00425-15

77. Alice, A. F., López, C. S., Lowe, C. A., Ledesma, M. A., & Crosa, J. H. (2006). Genetic and transcriptional analysis of the siderophore malleobactin biosynthesis and transport genes in the human pathogen Burkholderia pseudomallei K96243. Journal of Bacteriology, 188(4), 1551–1566. https://doi.org/10.1128/JB.188.4.1551-1566.2006

78. Gupta, A., Bedre, R., Thapa, S. S., Sabrin, A., Wang, G., Dassanayake, M., & Grove, A. (2017). Global Awakening of Cryptic Biosynthetic Gene Clusters in Burkholderia thailandensis. ACS Chemical Biology, 12(12), 3012–3021. https://doi.org/10.1021/acschembio.7b00681

79. Knappe, T. A., Linne, U., Zirah, S., Rebuffat, S., Xie, X., & Marahiel, M. A. (2008). Isolation and structural characterization of capistruin, a lasso peptide predicted from the genome sequence of Burkholderia thailandensis E264. Journal of the American Chemical Society, 130(34), 11446–11454. https://doi.org/10.1021/ja802966g

80. Ishida, K., Lincke, T., Behnken, S., & Hertweck, C. (2010). Induced biosynthesis of cryptic polyketide metabolites in a Burkholderia thailandensis quorum sensing mutant. Journal of the American Chemical Society, 132(40), 13966–13968. https://doi.org/10.1021/ja105003g

81. Mao, D., Bushin, L. B., Moon, K., Wu, Y., & Seyedsayamdost, M. R. (2017). Discovery of scmR as a global regulator of secondary metabolism and virulence in Burkholderia thailandensis E264. Proceedings of the National Academy of Sciences of the United States of America, 114(14), E2920–E2928. https://doi.org/10.1073/pnas.1619529114

82. Okada, B. K., Wu, Y., Mao, D., Bushin, L. B., & Seyedsayamdost, M. R. (2016). Mapping the Trimethoprim-Induced Secondary Metabolome of Burkholderia thailandensis. ACS Chemical Biology, 11(8), 2124–2130. https://doi.org/10.1021/acschembio.6b00447

83. Li, A., Mao, D., Yoshimura, A., Rosen, P. C., Martin, W. L., Gallant, É., … Seyedsayamdost, M. R. (2020). Multi-omic analyses provide links between low-dose antibiotic treatment and induction of secondary metabolism in Burkholderia thailandensis. mBio, 11(1), e03210-19. https://doi.org/10.1128/mBio.03210-19

84. McClure, R. S. (2019). Toward a Better Understanding of Species Interactions through Network Biology. MSystems, 4(3), e00114-19. https://doi.org/10.1128/msystems.00114-19

85. McClure, R. S., Overall, C. C., Hill, E. A., Song, H.-S., Charania, M., Bernstein, H. C., … Beliaev, A. S. (2018). Species-specific transcriptomic network inference of interspecies interactions. ISME J, 12(8), 2011–2023. https://doi.org/10.1038/s41396-018-0145-6

86. Karas, V. O., Westerlaken, I., & Meyer, A. S. (2015). The DNA-binding protein from starved cells (Dps) utilizes dual functions to defend cells against multiple stresses. Journal of Bacteriology, 197(19), 3206–3215. https://doi.org/10.1128/JB.00475-15

87. Nair, S., & Finkel, S. E. (2004). Dps protects cells against multiple stresses during stationary phase. Journal of Bacteriology, 186(13), 4192–4198. https://doi.org/10.1128/JB.186.13.4192-4198.2004

88. Antwis, R. E., Griffiths, S. M., Harrison, X. A., Aranega-Bou, P., Arce, A., Bettridge, A. S., … Sutherland, W. J. (2017). Fifty important research questions in microbial ecology. FEMS Microbiology Ecology, 93(5), fix044. https://doi.org/10.1093/femsec/fix044

89. Konopka, A. (2009). What is microbial community ecology. ISME J, 3(11), 1223–1230. https://doi.org/10.1038/ismej.2009.88

90. Sanchez-Gorostiaga, A., Bajić, D., Osborne, M. L., Poyatos, J. F., & Sanchez, A. (2019). High-order interactions distort the functional landscape of microbial consortia. PLoS Biology, 17(12), e3000550. https://doi.org/10.1371/journal.pbio.3000550

91. Mickalide, H., & Kuehn, S. (2019). Higher-Order Interaction between Species Inhibits Bacterial Invasion of a Phototroph-Predator Microbial Community. Cell Systems, 9(6), 521-533.e10. https://doi.org/10.1016/j.cels.2019.11.004

92. D'hoe, K., Vet, S., Faust, K., Moens, F., Falony, G., Gonze, D., … Raes, J. (2018). Integrated culturing, modeling and transcriptomics uncovers complex interactions and emergent behavior in a three-species synthetic gut community. ELife, 7, e37090. https://doi.org/10.7554/eLife.37090

93. Miller, T. E., Burns, J. H., Munguia, P., Walters, E. L., Kneitel, J. M., Richards, P. M., … Buckley, H. L. (2005). A critical review of twenty years' use of the resource-ratio theory. American Naturalist, 165(4), 439–448. https://doi.org/10.1086/428681

94. De Jong, H., Casagranda, S., Giordano, N., Cinquemani, E., Ropers, D., Geiselmann, J., & Gouzé, J. L. (2017). Mathematical modelling of microbes: Metabolism, gene expression and growth. Journal of the Royal Society Interface, 14(136), 20170502. https://doi.org/10.1098/rsif.2017.0502

95. Jõers, A., Liske, E., & Tenson, T. (2020). Dividing subpopulation of Escherichia coli in stationary phase. Research in Microbiology, 171(3–4), 153–157. https://doi.org/10.1016/j.resmic.2020.02.002

96. McCall, I. C., Shah, N., Govindan, A., Baquero, F., & Levin, B. R. (2019). Antibiotic killing of diversely generated populations of nonreplicating bacteria. Antimicrobial Agents and Chemotherapy, 63(7), e02360-18. https://doi.org/10.1128/AAC.02360-18

97. Chesson, P. L. (1983). Coexistence of Competitors in a Stochastic Environment: The Storage Effect. Lecture Notes in Biomathematics, 52, 188–198. https://doi.org/10.1007/978-3-642-87893-0_25

98. Stewart, P. S., & Franklin, M. J. (2008). Physiological heterogeneity in biofilms. Nature Reviews Microbiology 2008 6:3, 6(3), 199–210. https://doi.org/10.1038/nrmicro1838

99. Traxler, M. F., Seyedsayamdost, M. R., Clardy, J., & Kolter, R. (2012). Interspecies modulation of bacterial development through iron competition and siderophore piracy. Molecular Microbiology, 86(3), 628. https://doi.org/10.1111/MMI.12008

100. Lawrence, M., Gentleman, R., & Carey, V. (2009). rtracklayer: An R package for interfacing with genome browsers. Bioinformatics, 25(14), 1841–1842. https://doi.org/10.1093/bioinformatics/btp328

101. Garnier, S., Ross, N., Rudis, R., Camargo, P. A., Sciaini, M., & Scherer, C. (2021). viridis - Colorblind-Friendly Color Maps for R, R package, https://sjmgarnier.github.io/viridis/. https://doi.org/10.5281/zenodo.4679424

102. Wickham, H. (2007). Reshaping data with the reshape package. Journal of Statistical Software, 21(12), 1–20. https://doi.org/10.18637/jss.v021.i12

103. Wickham, H. (2019). stringr: Simple, Consistent Wrappers for Common String Operations. R package version 1.4.0.

104. Wickham, H., Averick, M., Bryan, J., Chang, W., McGowan, L., François, R., … Yutani, H. (2019). Welcome to the Tidyverse. Journal of Open Source Software, 4(43), 1686. https://doi.org/10.21105/joss.01686

105. Wickham, H., François, R., Henry, L., & Müller, K. (2019). dplyr: A Grammar of Data Manipulation. R package version 0.8.3.

106. Nordberg, H., Cantor, M., Dusheyko, S., Hua, S., Poliakov, A., Shabalov, I., … Dubchak, I. (2014). The genome portal of the Department of Energy Joint Genome Institute: 2014 updates. Nucleic Acids Research, 42, D26-31. https://doi.org/10.1093/nar/gkt1069

Figure legends

Figure 1. Experimental design and destructive sampling procedure of transwell plates. There were seven conditions, six time points/condition, and four independent replicates/condition (168 total transwell plates). Each member occupied 31 wells/condition to maintain member-specific population density across all conditions (A). The SynCom transwell plate maintains physical separation of members in individual wells while permitting exometabolite exchange through a 0.22-μm-pore filter bottom. Exometabolite exchange occurs via a bottom-fitted shared medium reservoir (B; [35]). Six replicate transwell plates were prepared for a time course experiment. The time course experiment included one exponential phase time point and five stationary phase time points. At specified time points, a transwell plate was destructively sampled (C). Note that all members were diluted to different starting ODs to allow for all members to achieve stationary phase within a two-hour window of each other. This figure was created with BioRender.com.

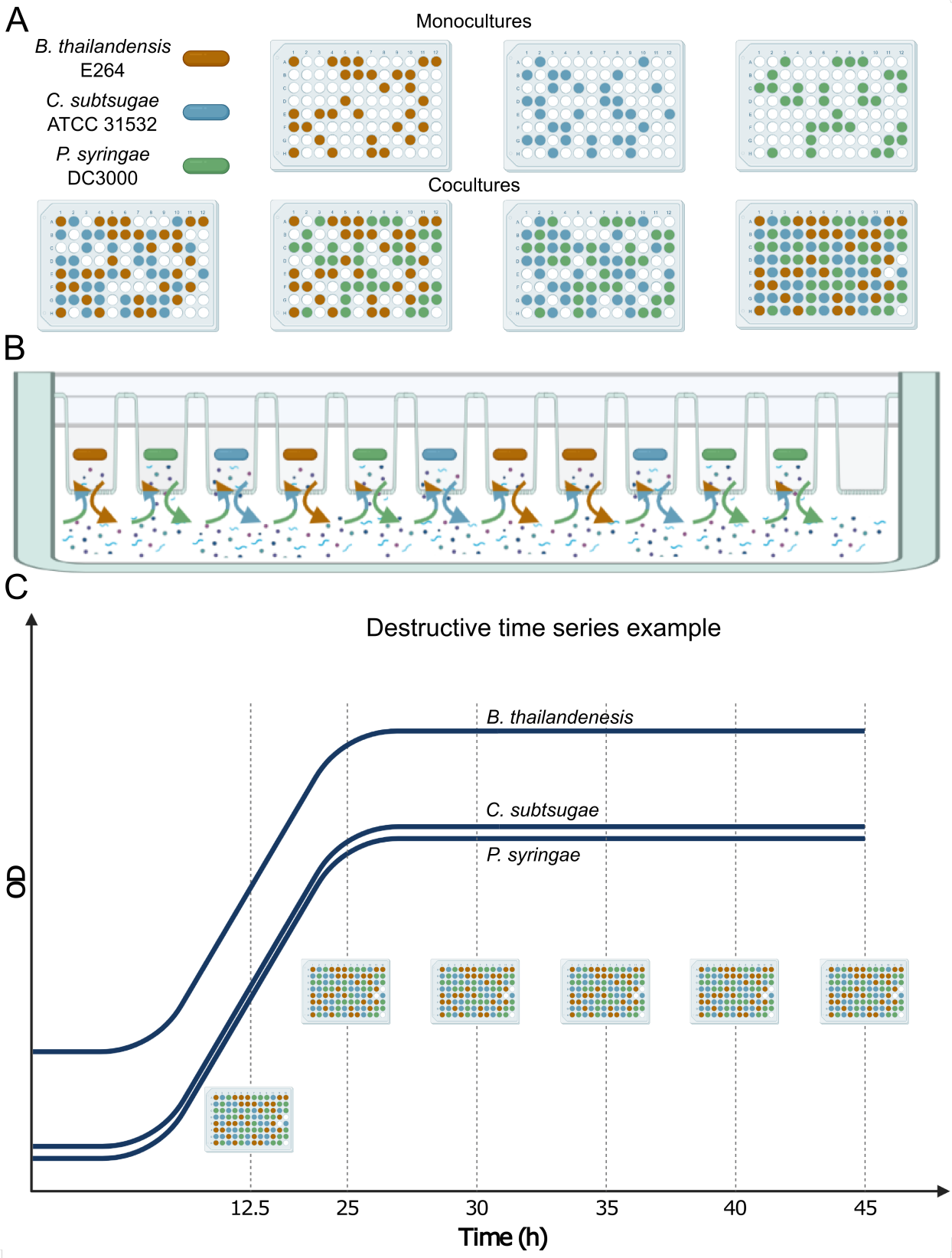
A
Monocultures
B. thailandensis
E264
C. subtsugae
ATCC 31532
P. syringae
DC3000
Cocultures
B
C
Destructive time series example
B. thailandenesis
C. subtsugae
P. syringae
OD
12.5
25
30
35
40
45
Time (h)

1345

1346

Figure 2. Loss of cell viability in *B. thailandensis* cocultures. Live (green) and dead (blue) flow cytometry cell counts for *C. subtsugae* (Top row, panels A-C) and *P. syringae* (Bottom row, panels D-F) from Syto9- and propidium iodide-stained cells (n = 4 to 5 technical replicates/time point/community membership/transwell plate and n = 4 independent replicates/time point/community membership). Cell counts are from monocultures (panels A & D), cocultures with *P. syringae* (panel B) or *C. subtsugae* (panel E), and cocultures with *B. thailandensis* (panels C & F). The bottom and top of the box are the first (Q1) and third (Q3) quartiles, respectively, and the line inside the box is the median. The whiskers extend from their respective hinges to the largest value (top), and smallest value (bottom) was no further away than 1.5× the interquartile range. Points represent outliers that are less than 1.5x the interquartile range of Q1 or greater than 1.5x the interquartile range of Q3.

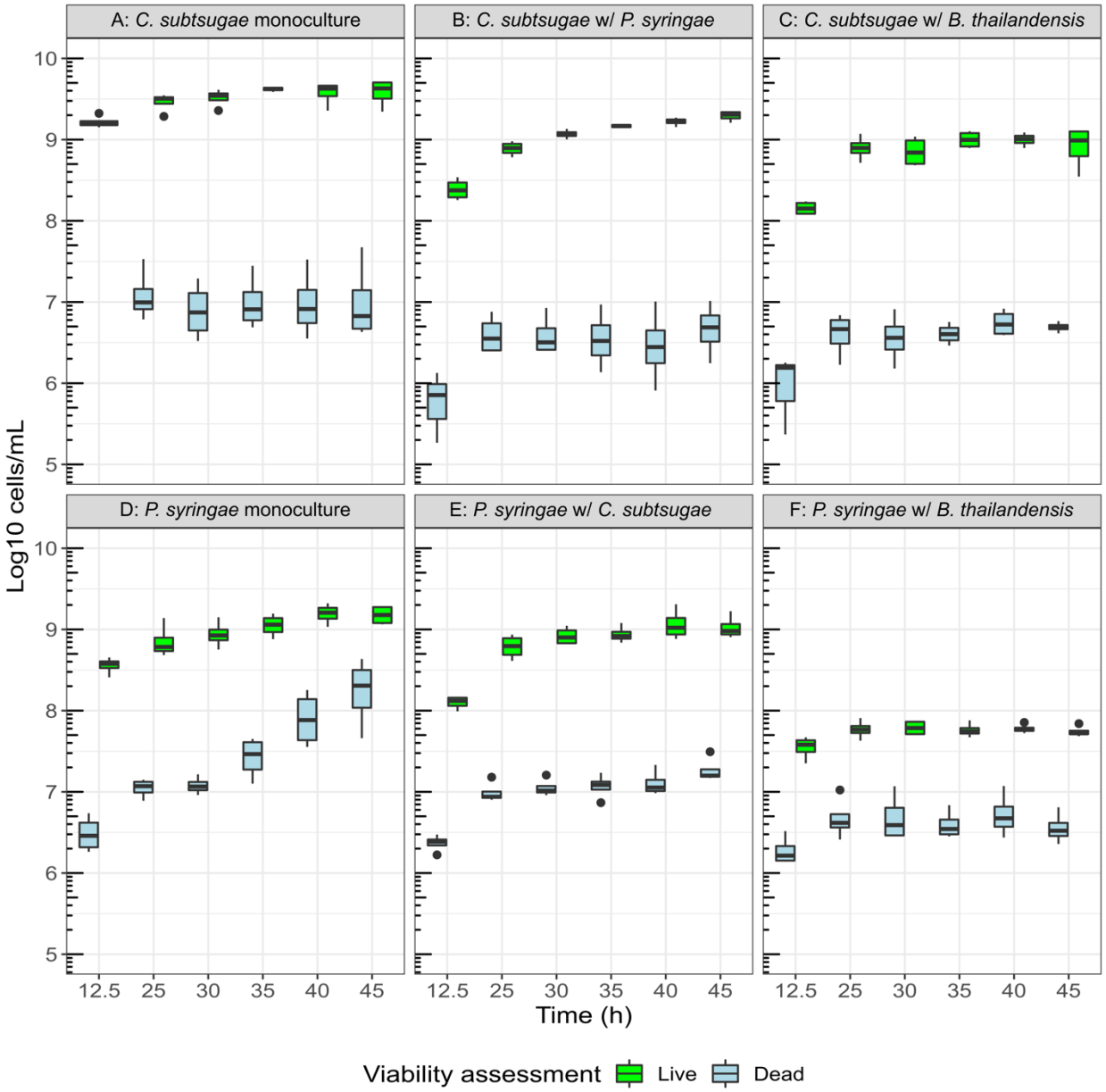

1359

1360

1361

Figure 3. Transcriptional responses are driven by community membership and time. Shown are principal coordinates analysis (PCoA) plots for *B. thailandensis* (A), *C. subtsugae* (B), and *P. syringae* (C). Each PCoA sub-panel presents the time series of transcriptional patterns of the focal member given each of its 4 growth conditions (one monoculture condition, two pairs, and one three-member). Each point represents a mean transcript profile for a community member given a particular condition (indicated by symbol color) and sampled at a given time point over exponential and stationary phases (in hours since inoculation, h, indicated by symbol size, n = 3 to 4 replicates per time point/community membership). The Bray-Curtis distance metric was used to calculate dissimilarities between transcript profiles. Error bars are 1 standard deviation around the mean axis scores. Note that transcriptional responses are driven by community membership on PCoA axis 1 and time on PCoA axis 2 across all plots.

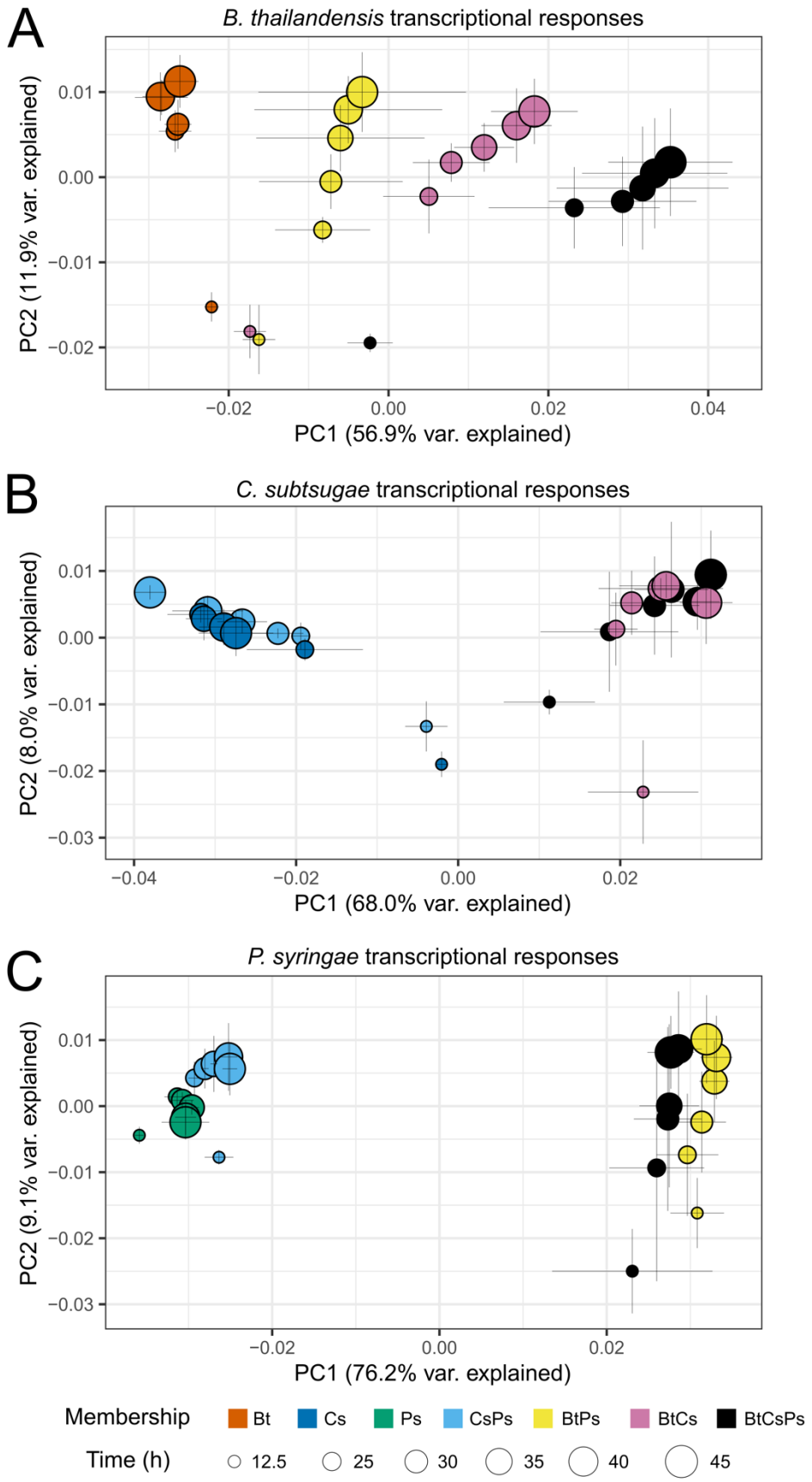
A
B. thailandensis transcriptional responses
PC2 (11.9% var. explained)
PC1 (56.9% var. explained)
B
C. subtsugae transcriptional responses
PC2 (8.0% var. explained)
PC1 (68.0% var. explained)
C
P. syringae transcriptional responses
PC2 (9.1% var. explained)
PC1 (76.2% var. explained)
Membership
Bt
Cs
Ps
CsPs
BtPs
BtCs
BtCsPs
Time (h)
12.5
25
30
35
40
45

1374

Figure 4. Bacterial community exometabolite profiles differ by community membership and time. Shown are PCoA plots for exometabolite profiles from the following mass spectrometry modes: polar positive (A), polar negative (B), nonpolar positive (C), and nonpolar negative (D). Each point represents the mean exometabolite profile (relative contributions by peak area) given a particular community membership (indicated by symbol color) at a particular time point (indicated by symbol size). The Bray-Curtis distance metric was used to calculate dissimilarities between exometabolite profiles. Error bars are 1 standard deviation around the mean axis scores (n = 2 to 4 replicates). Bt is *B. thailandensis*, Cs is *C. subtsugae*, and Ps is *P. syringae*.

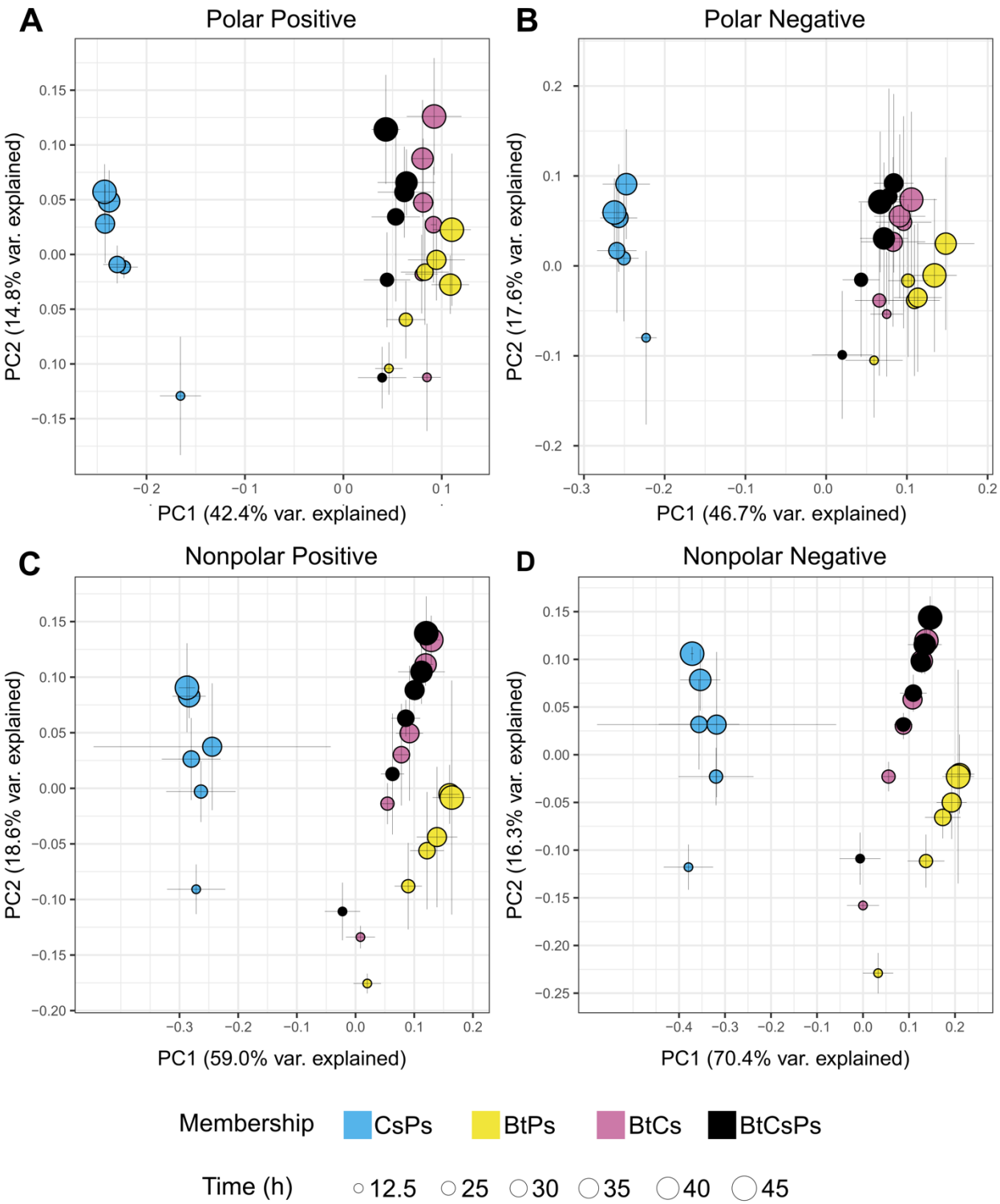
A
Polar Positive
PC2 (14.8% var. explained)
PC1 (42.4% var. explained)
B
Polar Negative
PC2 (17.6% var. explained)
PC1 (46.7% var. explained)
C
Nonpolar Positive
PC2 (18.6% var. explained)
PC1 (59.0% var. explained)
D
Nonpolar Negative
PC2 (16.3% var. explained)
PC1 (70.4% var. explained)
Membership
CsPs
BtPs
BtCs
BtCsPs
Time (h)
12.5
25
30
35
40
45

1384

1385

Figure 5. Primary metabolites accumulated in monocultures have altered dynamics in cocultures. A heat map of identified, primary metabolites is shown for *C. subtsugae* monoculture (Cs), *P. syringae* monoculture (Ps), *B. thailandensis* monoculture (Bt), *C. subtsugae-P. syringae* coculture (CsPs)*, B. thailandensis-P. syringae* coculture (BtPs)*, B. thailandensis-C. subtsugae* coculture (BtCs), and the 3-member community (BtCsPs), where samples are in columns and exometabolites are in rows. These exometabolites were filtered based on their time series accumulation in monocultures (See supplementary methods for details). Data for each sample are the averages from independent time point replicates (n = 3 to 4). Euclidean distance was calculated from Z-scored mass spectral profiles. Features with similar dynamics were clustered by Ward's method.

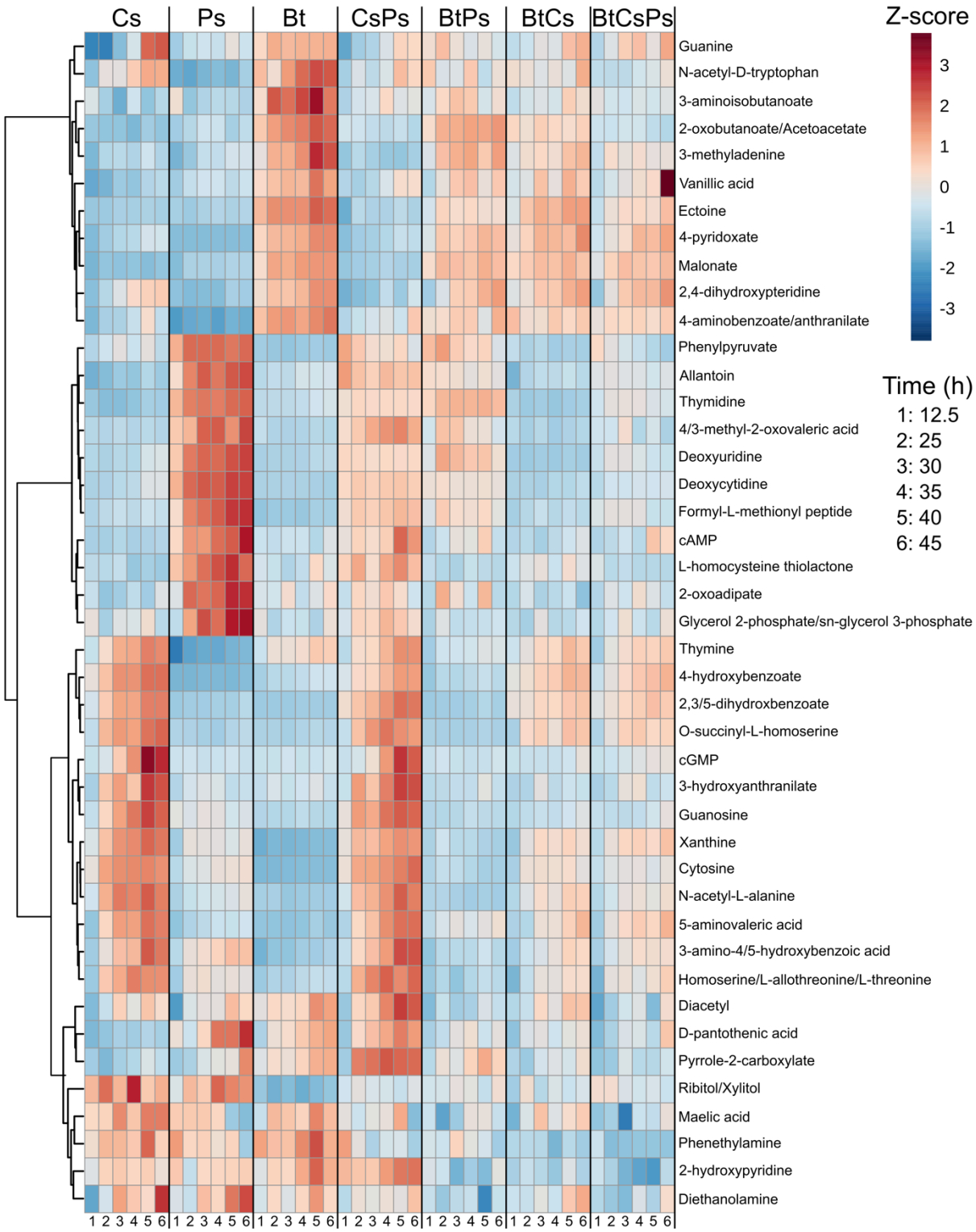
Cs
Ps
Bt
CsPs
BtPs
BtCs
BtCsPs
Guanine
N-acetyl-D-tryptophan
3-aminoisobutanoate
2-oxobutanoate/Acetoacetate
3-methyladenine
Vanillic acid
Ectoine
4-pyridoxate
Malonate
2,4-dihydroxypteridine
4-aminobenzoate/anthranilate
Phenylpyruvate
Allantoin
Thymidine
4/3-methyl-2-oxovaleric acid
Deoxyuridine
Deoxycytidine
Formyl-L-methionyl peptide
cAMP
L-homocysteine thiolactone
2-oxoadipate
Glycerol 2-phosphate/sn-glycerol 3-phosphate
Thymine
4-hydroxybenzoate
2,3/5-dihydroxbenzoate
O-succinyl-L-homoserine
cGMP
3-hydroxyanthranilate
Guanosine
Xanthine
Cytosine
N-acetyl-L-alanine
5-aminovaleric acid
3-amino-4/5-hydroxybenzoic acid
Homoserine/L-allothreonine/L-threonine
Diacetyl
D-pantothenic acid
Pyrrole-2-carboxylate
Ribitol/Xylitol
Maelic acid
Phenethylamine
2-hydroxypyridine
Diethanolamine
1 2 3 4 5 6
Z-score
3
2
1
0
-1
-2
-3
Time (h)
1: 12.5
2: 25
3: 30
4: 35
5: 40
6: 45

1397

1398

Figure 6. *B. thailandensis* upregulates biosynthetic gene clusters (BSGC) in cocultures. Columns represent community membership for *B. thailandensis* cocultures and rows represent BSGCs in *B. thailandensis* that were determined to be upregulated compared to the monoculture control. Genes part of a BSGC were curated from antiSMASH predictions and literature-based evidence. Within each BSGC at each time point, the log2 fold-change (LFC) was calculated by comparing gene counts from a coculture to the monoculture control (n = 3 to 4 LFC calculations/community membership/time point). Log2 fold-changes were then averaged from all biosynthetic genes within the BSGC at each time point. Error bars indicate standard deviations. We defined an upregulated BSGC as a BSGC that had at least two consecutive stationary phase time points with a LFCs > 1 (indicated by the horizontal red dashed line). Note that plots for each BSGC have separate scales for the Y-axis.

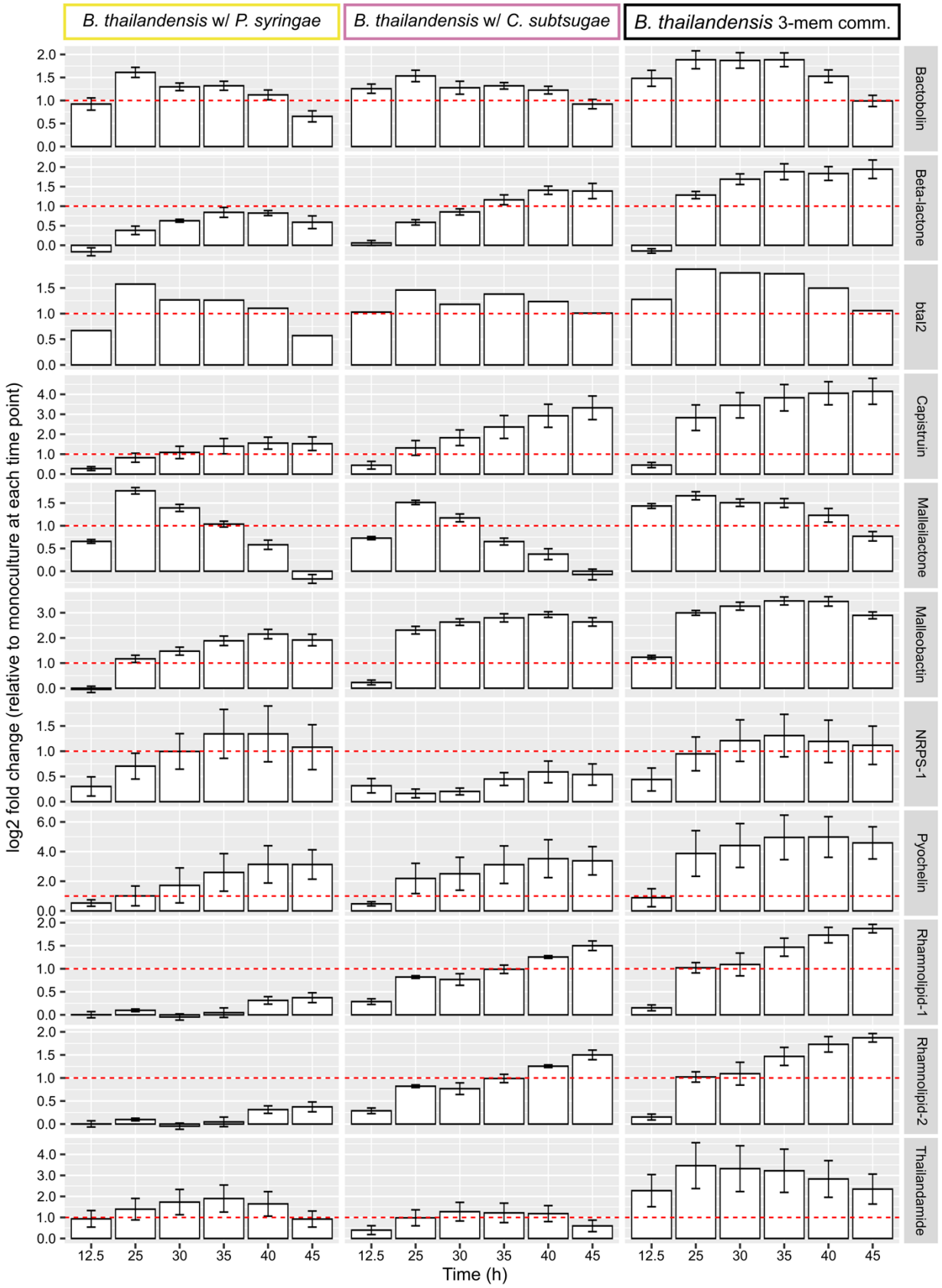
B. thailandensis w/ P. syringae
B. thailandensis w/ C. subtsugae
B. thailandensis 3-mem comm.
Bactobolin
Beta-lactone
btal2
Capistruin
Malleilactone
Malleobactin
NRPS-1
Pyochelin
Rhamnolipid-1
Rhamnolipid-2
Thailandamide
log2 fold change (relative to monoculture at each time point)
Time (h)
12.5
25
30
35
40
45

1411

Figure 7. Coculture upregulation of BSGCs from *B. thailandensis* translates to temporally accumulated secondary metabolites. Columns represent community membership and rows represent identified secondary metabolites in *B. thailandensis*. Known bioactive secondary metabolites produced by *B. thailandensis* were identified in MZmine 2 through the observation of MS and MS/MS data. The accumulation of each exometabolite was quantified through time (n = 2 to 4 integrated peak areas per time point). The bottom and top of the box are the first (Q1) and third (Q3) quartiles, respectively, and the line inside the box is the median. The whiskers extend from their respective hinges to the largest value (top), and smallest value (bottom) was no further away than 1.5× the interquartile range. Points represent outliers that are less than 1.5x the interquartile range of Q1 or greater than 1.5x the interquartile range of Q3.

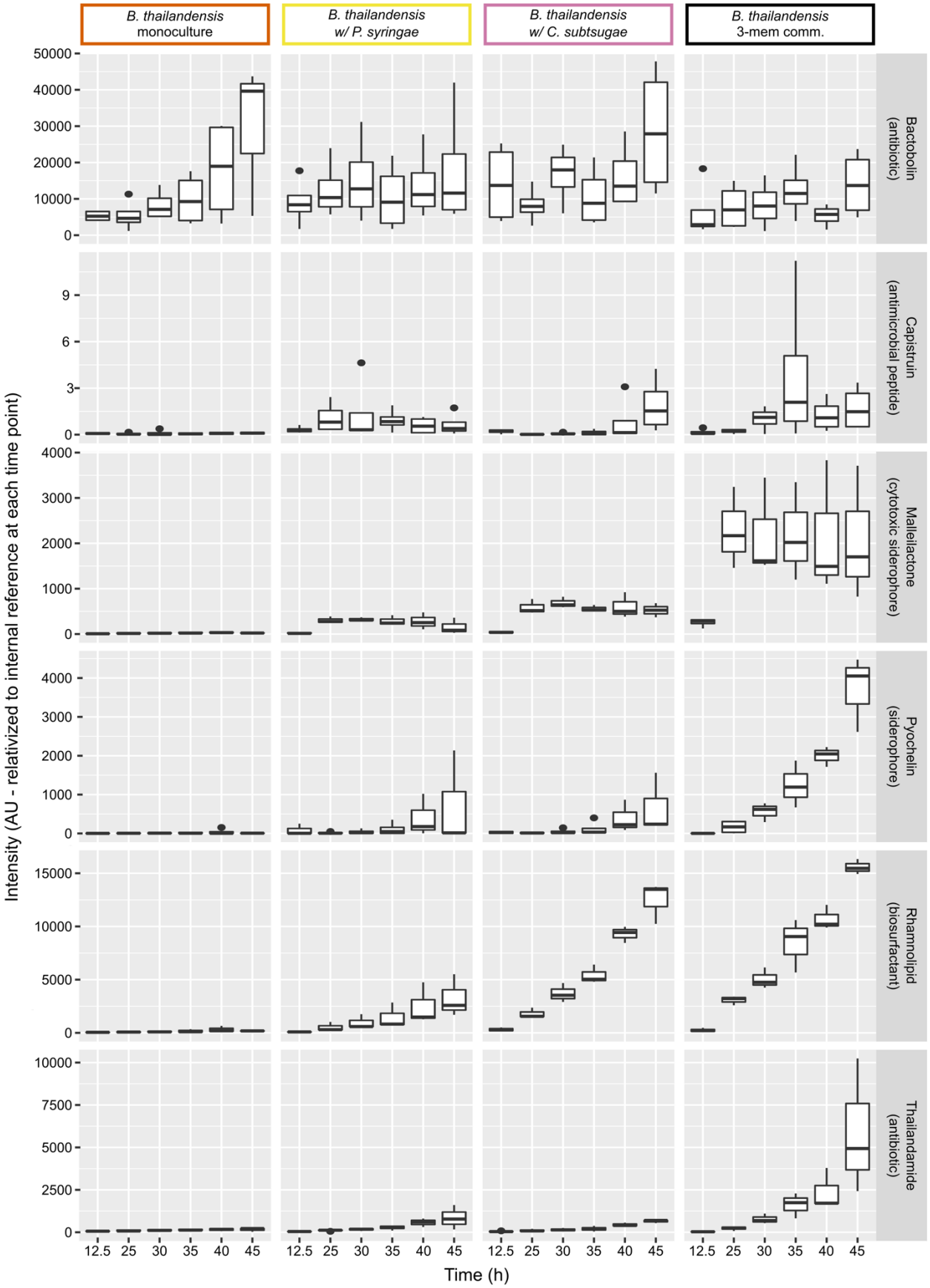
B. thailandensis monoculture
B. thailandensis w/ P. syringae
B. thailandensis w/ C. subtsugae
B. thailandensis 3-mem comm.
Bactobolin (antibiotic)
Capistruin (antimicrobial peptide)
Malleilactone (cytotoxic siderophore)
Pyochelin (siderophore)
Rhamnolipid (biosurfactant)
Thailandamide (antibiotic)
Intensity (AU - relativized to internal reference at each time point)
Time (h)
12.5 25 30 35 40 45

Figure 8. *B. thailandensis* genes involved in thailandamide production are co-expressed with *C. subtsugae* genes. A network module containing the thailandamide BSGC is shown (A). The network module nodes are color coded by according to the following criteria: thailandamide biosynthetic genes that had interspecies edges (magenta), thailandamide biosynthetic genes that did not have interspecies edges (orange), other *B. thailandensis* genes that were not part of the BSGC (yellow), and genes that were from *C. subtsugae* (blue). The chromosomal organization of the thailandamide BSGC is shown below the network module (B). The same colors are applied to the BSGC operon. The operon also depicts genes that were not detected within the interspecies network, shown in gray. Asterisks indicate core biosynthetic genes in the BSGCs, as predicted from antiSMASH. The table (C) shows upregulated *B. thailandensis* BSGCs (Fig. 6) and whether interspecies edges were detected (check is yes, x is no).

A

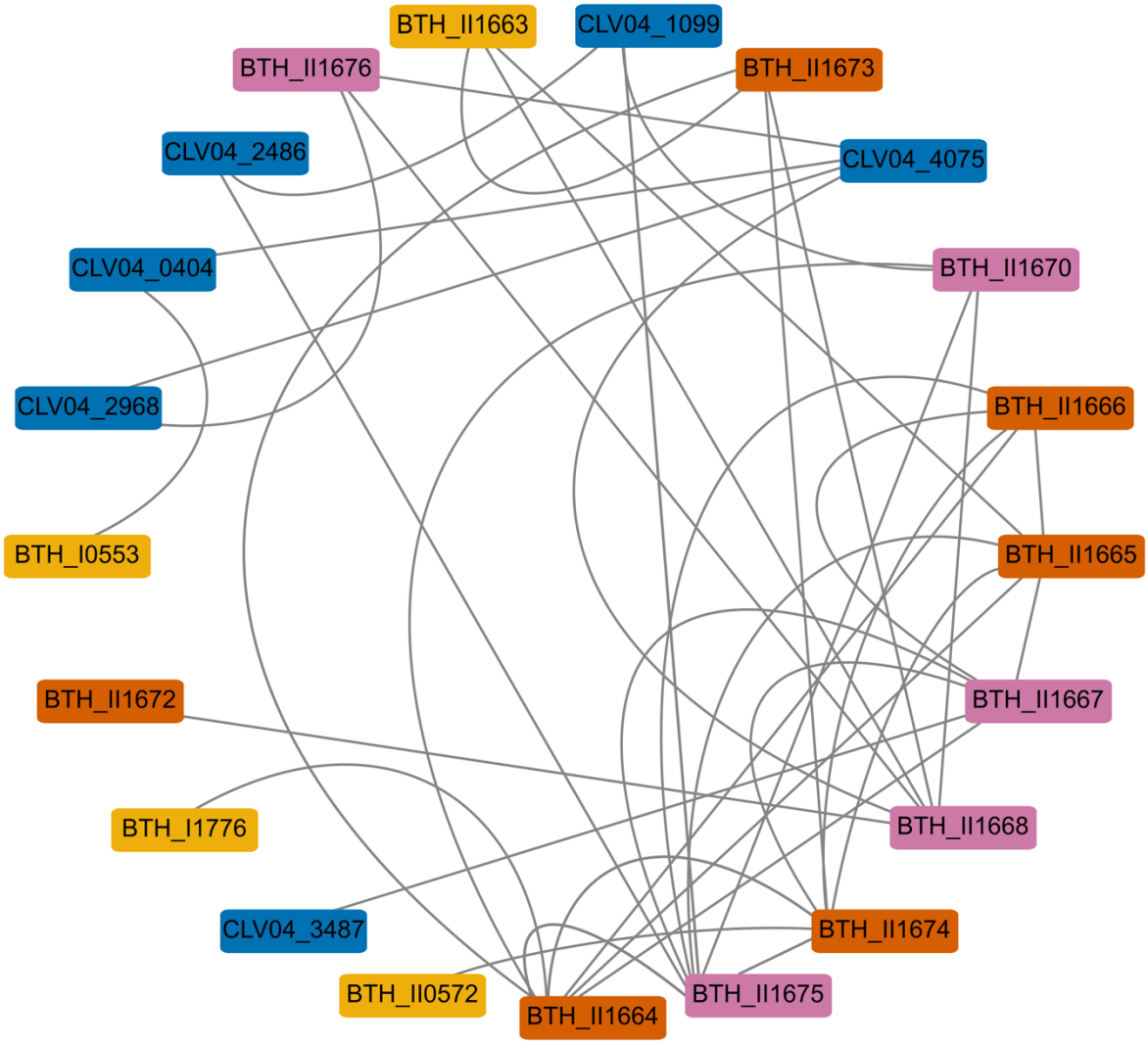

B

C

	B. thailandensis-C. subtsugae interspecies network	*B. thailandensis-P. syringae* interspecies network
Bactobolin	✓	✓
Beta-lactone	✓	×
Capistruin	✓	✓
Malleilactone	✓	✓
Malleobactin	✓	✓
NRPS-1	×	✓
Pyochelin	✓	✓
Rhamnolipid	×	×
Thailandamide	✓	✓

1437

1438

Supplemental Materials for

Bioactive exometabolites drive maintenance competition in simple bacterial communities.

Chodkowski JL and A Shade.

Code and data:

https://github.com/ShadeLab/Paper_Chodkowski_3member_SynCom_2021

Supplementary Methods

This supplementary information contains expanded Materials and Methods.

RNA-seq

RNA extraction

RNA was extracted using the E.Z.N.A. Bacterial RNA kit (Omega Bio-tek, Inc.). An in-tube DNase I (Ambion, Inc AM2222, 2U) digestion was performed to remove DNA from RNA samples. RNA samples were purified and concentrated using the Qiagen RNAeasy MinElute Clean up Kit (Qiagen, Inc). Ten random samples were chosen to assess RNA integrity (RIN > 7) on an Agilent 2100 Bioanalyzer. Standard operating protocols were performed at the Department of Energy Joint Genome Institute as previously described [1].

RNA sample prep, sequencing, QC, read preprocessing, and filtering

Standard operating protocols were performed at the Department of Energy Joint Genome Institute as previously described [1].

Pseudoalignment and counting

Reads from each library were pseudoaligned to the transcriptome of each member with kallisto [2]. Raw counts from each library were combined into a gene count matrix for each member. The gene count matrix was used for downstream analyses.

KEGG pathway analysis

Log-2 fold changes (LFC) were extracted from DESeq analysis by comparing each condition at each time point to the exponential-phase time point (12.5 h) in monoculture. We then mapped longitudinal LFCs onto KEGG pathways for each strain using the pathview package in R. First, K numbers were assigned to genes for both *C. subtsugae* and *P. syringae* using BlastKOALA (version 2.2). K numbers were not assigned to *B. thailandensis* because KEGG identifiers were available. KEGG identifiers for *B. thailandensis* and K numbers assigned to *C. subtsugae* and *P. syringae* were used to map longitudinal LFCs onto KEGG pathways. Pathways of interest were uploaded to FigShare.

Flow cytometry

Diluted cultures were stained with the Thermo Scientific LIVE/DEAD BacLight bacterial viability kit at final concentrations of 1.5 µM Syto9 (live stain) and 2.5 µM propidium iodide (dead stain). Two hundred microliters of stained cultures were transferred to a 96-well microtiter U-bottom microplate (Thermo Scientific). Twenty microliters of sample were analyzed on a BD Accuri C6 flow cytometer (BD Biosciences) at a fluidics rate of 66 µl/min and a threshold of 500 on an FL2 gate. The instrument contained the following optical filters: FL1-533, 30 nm; FL2-585, 40 nm; and FL3, 670-nm longpass. The counting accuracy of the flow cytometer was checked with green fluorescent protein beads (Thermo Scientific). Data were analyzed using BD Accuri C6 software version 1.0.264.21 (BD Biosciences).

Metabolomics

Normalization and heatmap analysis

Features were normalized by an ITSD reference feature (see Dataset 5 at https://github.com/ShadeLab/Paper_Chodkowski_MonocultureExometabolites_2020/tree/master/Datasets) and cube root transformed. Reference features for polar analyses in positive ([^{13}C,^{15}N]proline) and negative ([^{13}C,^{15}N]alanine) modes were determined by the ITSD with the lowest CV value across all samples. The reference feature for nonpolar data sets was the ITSD ABMBA. Heat maps were generated in MetaboAnalyst using Ward's clustering algorithm with Euclidean distances from Z-scored data. Data for each sample are the averages from independent time point replicates (n = 2 to 4). The heatmaps were exported and edited in InkScape for labelling purposes. The normalized and transformed data sets were exported from MetaboAnalyst to generate principal-coordinate analysis (PCoA) plots in R (see main methods).

Selection of Metabolomics Standards Initiative (MSI) level 1 primary metabolites for heatmap analysis

DOE-JGI provided a feature table containing MSI level 1 identified primary metabolites from their in-house curated reference database. The metabolites were only identified from polar positive and polar negative analyses. The m/z and retention times (RT) provided by DOE-JGI were used to identify these metabolites from our feature table after MZmine 2 analysis. Internal standards, [^{13}C,^{15}N]proline and [^{13}C,^{15}N]alanine were added to the polar positive feature table and polar negative feature table, respectively. Each feature table, containing all 7 conditions, was uploaded to

MetaboAnalyst. Features were normalized by ITSD and cube root transformed. Each feature table was exported and combined. Then, the feature table was split by each member, meaning 3 feature tables were created containing 4 conditions each (1 monoculture, 2 pairwise cocultures, and 1, 3-member community). These normalized and log transformed feature tables were re-uploaded to MetaboAnalyst for heatmap analysis.

Heat maps were generated in MetaboAnalyst using Ward's clustering algorithm with Euclidean distances from Z-scored data. The dendrograms from each analysis were manually inspected to select clusters of primary metabolites that met the following criteria for each member: 1) accumulated over the time series in monoculture or 2) accumulated substantially in the exponential phase time point in monoculture compared to the stationary phase time points in monoculture. Primary metabolites that met criteria 1 were filtered from the normalized and log transformed MSI level 1 feature table and primary metabolites that met criteria 2 were filtered from the normalized and log transformed MSI level 1 feature table, separately. These filtered feature tables, containing all 7 conditions, were re-uploaded to MetaboAnalyst for heatmap analysis.

Heat maps were generated in MetaboAnalyst using Ward's clustering algorithm with Euclidean distances from Z-scored data. The heatmaps were exported and edited in InkScape for labeling purposes.

Effects of plate occupancy and resource concentration on gene expression

SynCom experiments

We designed an additional experiment to determine whether the observed dynamics in exometabolites and transcription could be attributed solely to population density given resource availability, rather than to interspecies interactions. Additional SynCom experiments (6 conditions, 3 replicates/condition), were prepared as described (see methods section: Bacterial strains and culture conditions and Synthetic Community Experiments). The conditions varied based on plate occupancy (# of wells occupied by each member) and resources (% glucose) in the transwell plate. The conditions were as follows: *B. thailandensis* (31 wells) in M9-0.067% glucose, *B. thailandensis* (62 wells) in M9-0.13% glucose, *B. thailandensis* (93 wells) in M9-0.2% glucose, *B. thailandensis-C. subtsugae* (31 wells/member) in M9-0.13% glucose, *B. thailandensis- P. syringae* (31 wells/member) in M9-0.13% glucose, and *B. thailandensis-C. subtsugae- P. syringae* (31 wells/member) in M9-0.2% glucose. Plates were destructed after 45 h incubation and the following procedures were performed: 1) Wells containing spent culture from each member were separately pooled into 15 mL conical tubes, flash frozen in liquid nitrogen, and stored at -80 until further processing. 2) Spent medium (~31 ml) from the shared reservoir was transferred to 50 mL conical tubes, flash-frozen in liquid nitrogen and stored at −80 °C.

RNA extraction, QC, and cDNA synthesis

RNA was extracted using the E.Z.N.A. Bacterial RNA kit (Omega Bio-tek, Inc.). An in-tube DNase I (Ambion, Inc. AM2222, 2U) digestion was performed to remove DNA from RNA samples. RNA samples were purified and concentrated using the Qiagen RNAeasy MinElute Clean up Kit (Qiagen, Inc.). RNA samples were quantified

on a Qubit using the RNA High Sensitivity Assay Kit (Thermo Fisher Scientific, Inc.). RNA samples were then sent to the RTSF Genomics Core at Michigan State University for high sensitivity RNA ScreenTape analysis on an Agilent 4200 TapeStation. TapeStation analysis confirmed successful digestion of DNA. Total RNA (150 ng/sample) was synthesized to cDNA using the Invitrogen SuperScript III First-Strand Synthesis kit (Thermo Fisher Scientific, Inc.). cDNA samples were quantified by Qubit in preparation of target genes for RT-qPCR.

Three genes from the *B. thailandensis* thailandamide operon were targeted for relative quantification normalized to the *rpoD* reference gene. Primers used for RT-qPCR are shown in Table S12. We first confirmed amplification of intended targets. Each of these genes were amplified from *B. thailandensis* gDNA (100 ng) using the Phusion High-Fidelity DNA Polymerase (New England Biolabs, Inc.) with the following conditions: 98 ^{o}C (30 s), 30 cycles of 98 ^{o}C (10 s), 59 ^{o}C (10 s), and 72 ^{o}C (10 s), and a final extension at 72 ^{o}C (5 min). PCR products were run on gel (100 V for 50 min) and gel extracted and purified using the Wizard SV Gel and PCR Clean-Up System (Promega Corporation). PCR amplified and purified products of *rpoD*, *thaF*, *thaK*, and *thaQ* were sent to the RTSF Genomics Core at Michigan State University for Sanger sequencing.

RT-qPCR assays were performed using the SsoAdvanced Universal SYBR Green Supermix (Bio-Rad Laboratories, Inc.). SYBR reactions were placed into Hard-Shell PCR Plates 96-well, thin wall (Bio-Rad Laboratories, Inc. HSP9601) and analyzed using a CFX Connect Real-Time System (Bio-Rad Laboratories, Inc.). First, the dynamic range of each primer set was determined by making a 10-fold dilution series

from 10 ng-0.1 pg of cDNA. The following mixture was used for each RT-qPCR assay: 10 µL SsoAdvanced universal SYBR Green supermix (2x), 0.5 µL each of forward and reverse primers, 1 µL water, and 8 µL cDNA sample (6 serially diluted samples concentrated between 1.25E-5 and 1.25 ng/uL). The RT-qPCR reaction was run with the following conditions: 95 °C (3 min), 40 cycles of 95 °C (10 s), 59 °C (10 s), and 72 °C (10 s). Following the last extension step, the melt curve was run with the following conditions: 95 °C (10 s), then 65 °C to 95 °C in 0.5 °C increments. Each primer set had a 5-fold dynamic range (10 ng-10 pg) with efficiencies between 90-110% (Table S13) The Δslope between the reference gene and each target gene were all ≤0.1, confirming that relative gene expression math models were a viable option for comparing gene expression across conditions.

cDNA concentrations across all conditions were diluted to a stock concentration of 0.0125 ng/uL. RT-qPCR reactions and conditions were prepared and run as previously described. Controls for the assay included a gDNA positive control, a no template negative control, and a no amplification (no-RT) negative control. The Livak method ($2^{-\Delta\Delta C_T}$) was used to calculate relative gene expression in each test condition compared to the reference condition (*B. thailandensis*, 31 wells in M9-0.067% glucose) where target genes were *thaF*, *thaK*, and *thaQ* and the reference gene was *rpoD*.

References

1. Chodkowski, J. L., & Shade, A. (2020). Exometabolite Dynamics over Stationary Phase Reveal Strain-Specific Responses. MSystems, 5(6), e00493-20. https://doi.org/10.1128/msystems.00493-20

2. Bray, N. L., Pimentel, H., Melsted, P., & Pachter, L. (2016). Near-optimal probabilistic RNA-seq quantification. Nature Biotechnology, 34, 525–527. https://doi.org/10.1038/nbt.3519

3. Funston SJ, Tsaousi K, Rudden M, Smyth TJ, Stevenson PS, Marchant R, Banat IM. (2016). Characterising rhamnolipid production in Burkholderia thailandensis E264, a non-pathogenic producer. Appl Microbiol Biotechnol.,100(18), 7945-56. https://doi.org/10.1007/s00253-016-7564-y

Supplementary Files/Datasets

Supplementary File 1: Pairwise PROTEST analyses comparing the reproducibility of exometabolome profiles across biological replicate time series. Coordinates of the first two PCoA axes were used to perform PROTEST analysis in vegan. File type: .xlsx

Supplementary File 2: Identification of *B. thailandensis* bioactive exometabolites of interest through observation of mass spectrometry data. File type: .xlsx

Supplementary File 3: Genes part of the interspecies network, their corresponding modules, and GO enrichment analysis of modules. File type: .xlsx

Supplementary File 4: GO enrichment analysis on genes with interspecies edges from network analysis. File type: .xlsx

Supplementary File 5: Gene annotations for *C. subtsugae* and *P. syringae* that contained interspecies edges with *B. thailandensis* thailandamide and malleilactone biosynthetic genes, respectively. File type: .xlsx

Supplementary File 6: Protein alignment of the DNA starvation/stationary phase protein from *C. subtsugae* and the closest homolog in *B. thailandensis.* File type: .txt

Supplementary File 7: Protein alignment of the TonB-dependent siderophore receptor family protein from *P. syringae* and the closest homolog in *B. thailandensis*. File type: .txt

198

199

200

201

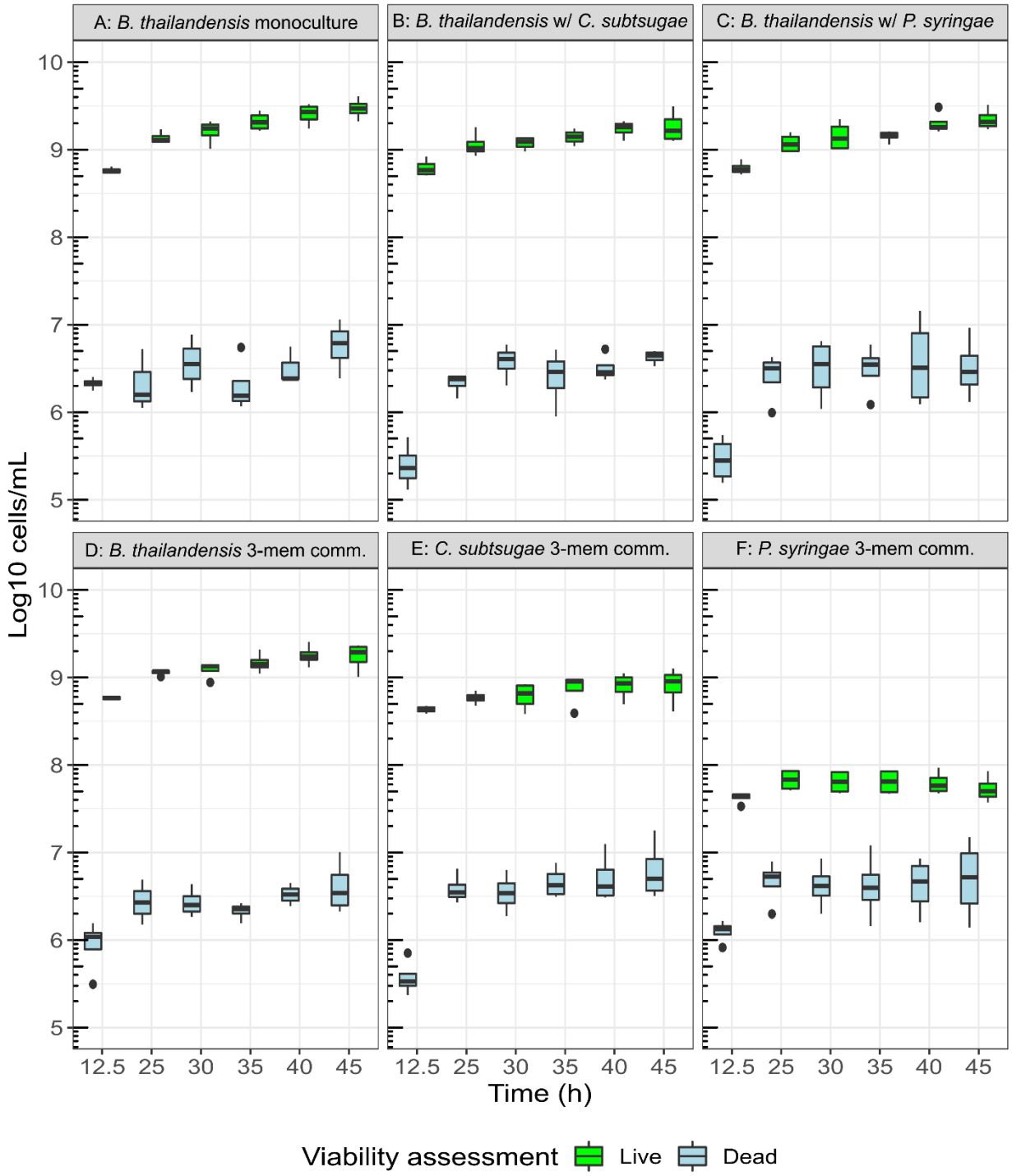

Figure S1. Cell viability of SynCom members. Live (green) and dead (blue) flow cytometry cell counts for *B. thailandensis* in monoculture and pairwise cocultures (Top row, panels A-C) and for each member in the 3-member community (Bottom row, panel D; *B. thailandensis*, panel E; *C. subtsugae*, panel F; *P. syringae*). Cells were stained with Syto9- and propdium iodide (n = 4 to 5 wells/time point/community membsership/transwell plate and n=4 independent replicates/time point/community membership). The bottom and top of the box are the first (Q1) and third (Q3) quartiles, respectively, and the line inside the box is the median. The whiskers extend from their respective hinges to the largest value (top), and

smallest value (bottom) was no further away than 1.5× the interquartile range. Points represent outliers that are less than 1.5x the interquartile range of Q1 or greater than 1.5x the interquartile range of Q3.

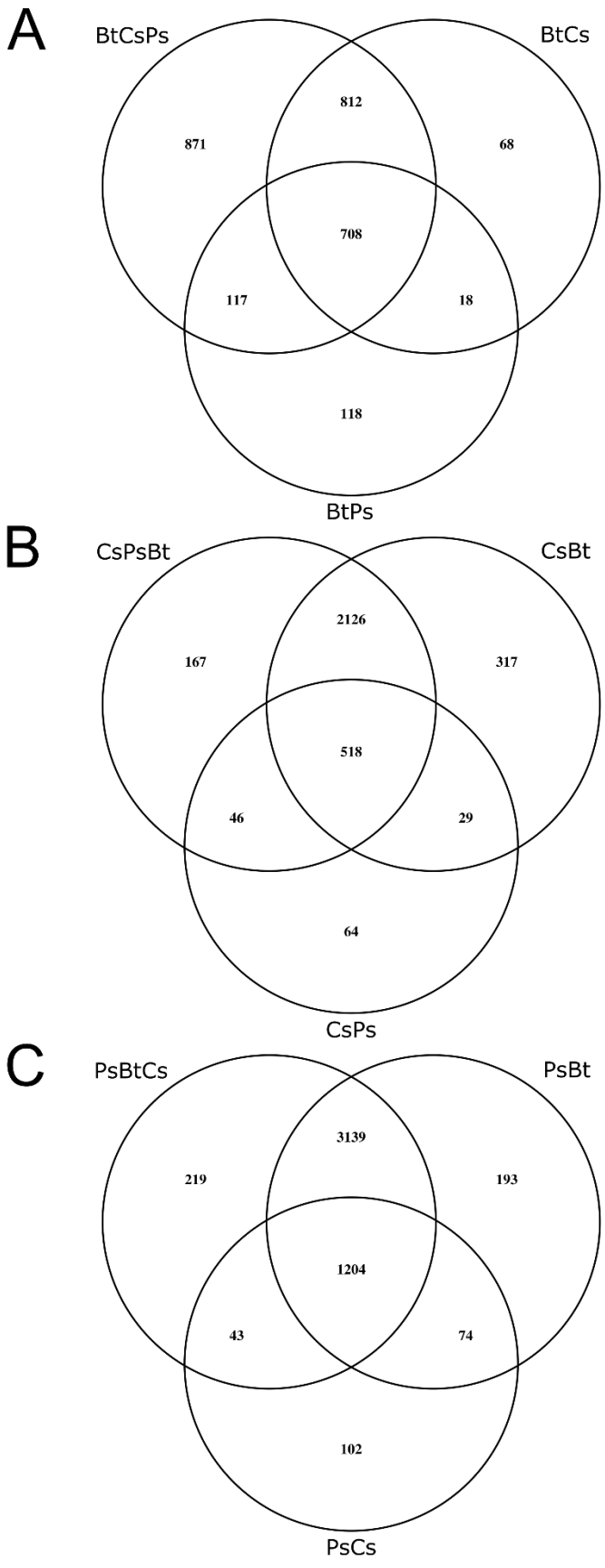
A
BtCsPs
BtCs
812
871
68
708
117
18
118
BtPs
B
CsPsBt
CsBt
2126
167
317
518
46
29
64
CsPs
C
PsBtCs
PsBt
3139
219
193
1204
43
74
102
PsCs

Figure S2. Differential gene expression patterns across community memberships. Venn diagram plots of differentially expressed genes in A) *B. thailandensis* B) *C. subtsugae* and C) *P. syringae*. Differential gene expression was determined using ImpulseDE2 comparing longitudinal gene expression to a monoculture control (FDR-corrected cutoff of 0.01). Bt- *B. thailandensis*, Cs- *C.subtsugae*, and Ps – *P. syringae*.

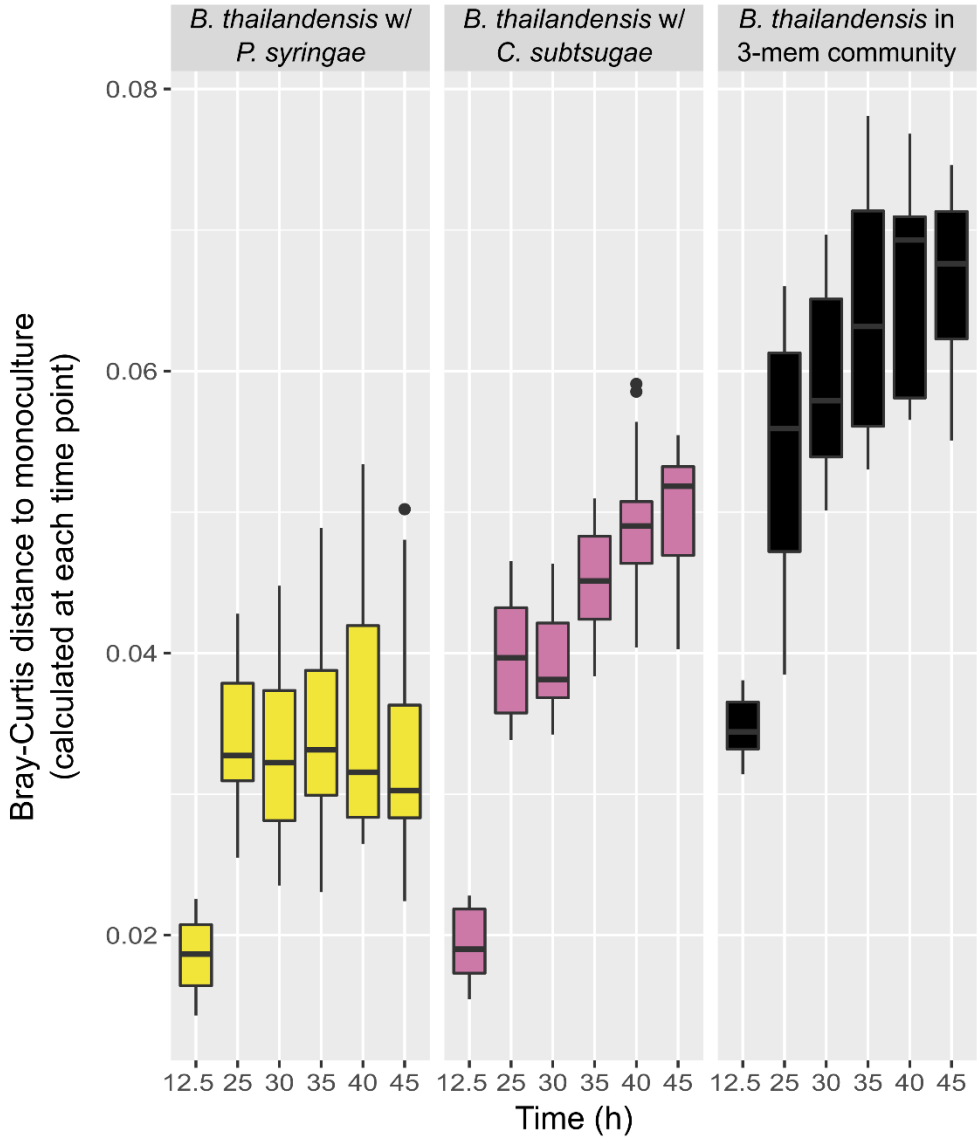

Figure S3. *B. thailandensis* RNA-seq transcript dissimilarity through time. Bray-Curtis dissimilarities were calculated for each coculture condition compared to the monoculture condition at each time point (n= 3-4 replicates/condition/time point). The bottom and top of the box are the first (Q1) and third (Q3) quartiles, respectively, and the line inside the box is the median. The whiskers extend from their respective hinges to the largest value (top), and smallest value (bottom) was no further away than 1.5× the interquartile range. Points represent outliers that are less than 1.5x the interquartile range of Q1 or greater than 1.5x the interquartile range of Q3.

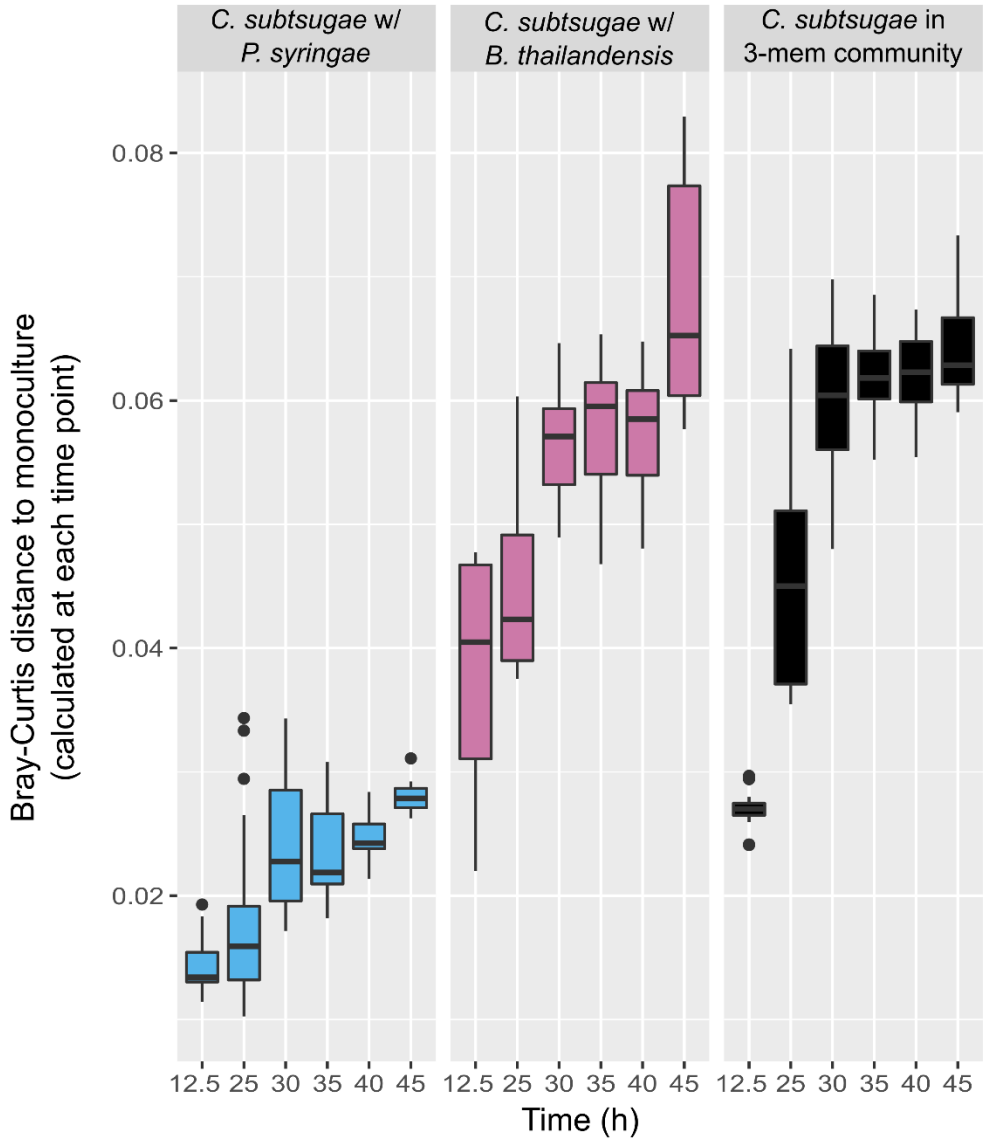

Figure S4. *C. subtsugae* RNA-seq transcript dissimilarity through time. Bray-Curtis dissimilarities were calculated for each coculture condition compared to the monoculture condition at each time point (n= 3-4 replicates/condition/time point). The bottom and top of the box are the first (Q1) and third (Q3) quartiles, respectively, and the line inside the box is the median. The whiskers extend from their respective hinges to the largest value (top), and smallest value (bottom) was no further away than 1.5× the interquartile range. Points represent outliers that are less than 1.5x the interquartile range of Q1 or greater than 1.5x the interquartile range of Q3.

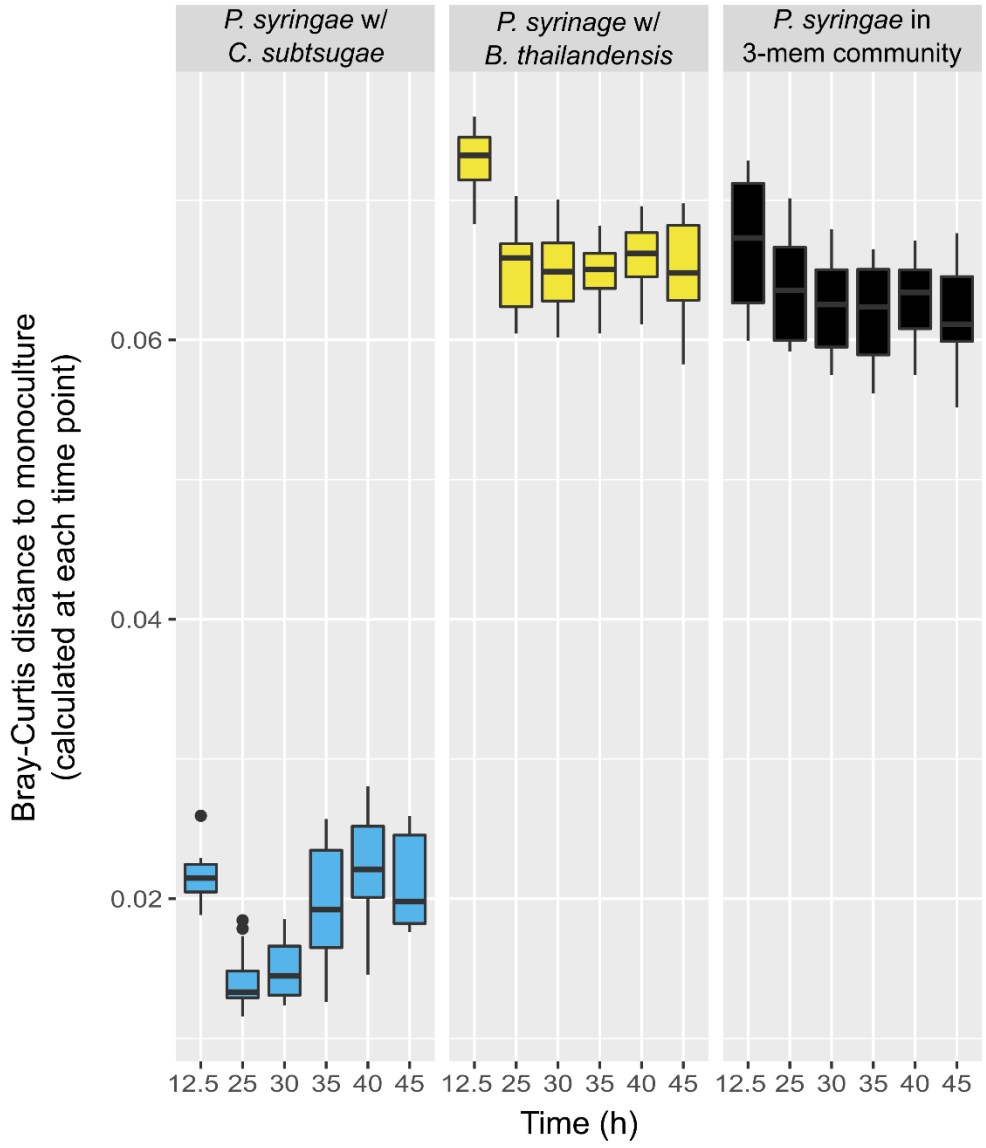

Figure S5. *P. syringae* RNA-seq transcript dissimilarity through time. Bray-Curtis dissimilarities were calculated for each coculture condition compared to the monoculture condition at each time point (n= 3-4 replicates/condition/time point). The bottom and top of the box are the first (Q1) and third (Q3) quartiles, respectively, and the line inside the box is the median. The whiskers extend from their respective hinges to the largest value (top), and smallest value (bottom) was no further away than 1.5× the interquartile range. Points represent outliers that are less than 1.5x the interquartile range of Q1 or greater than 1.5x the interquartile range of Q3.

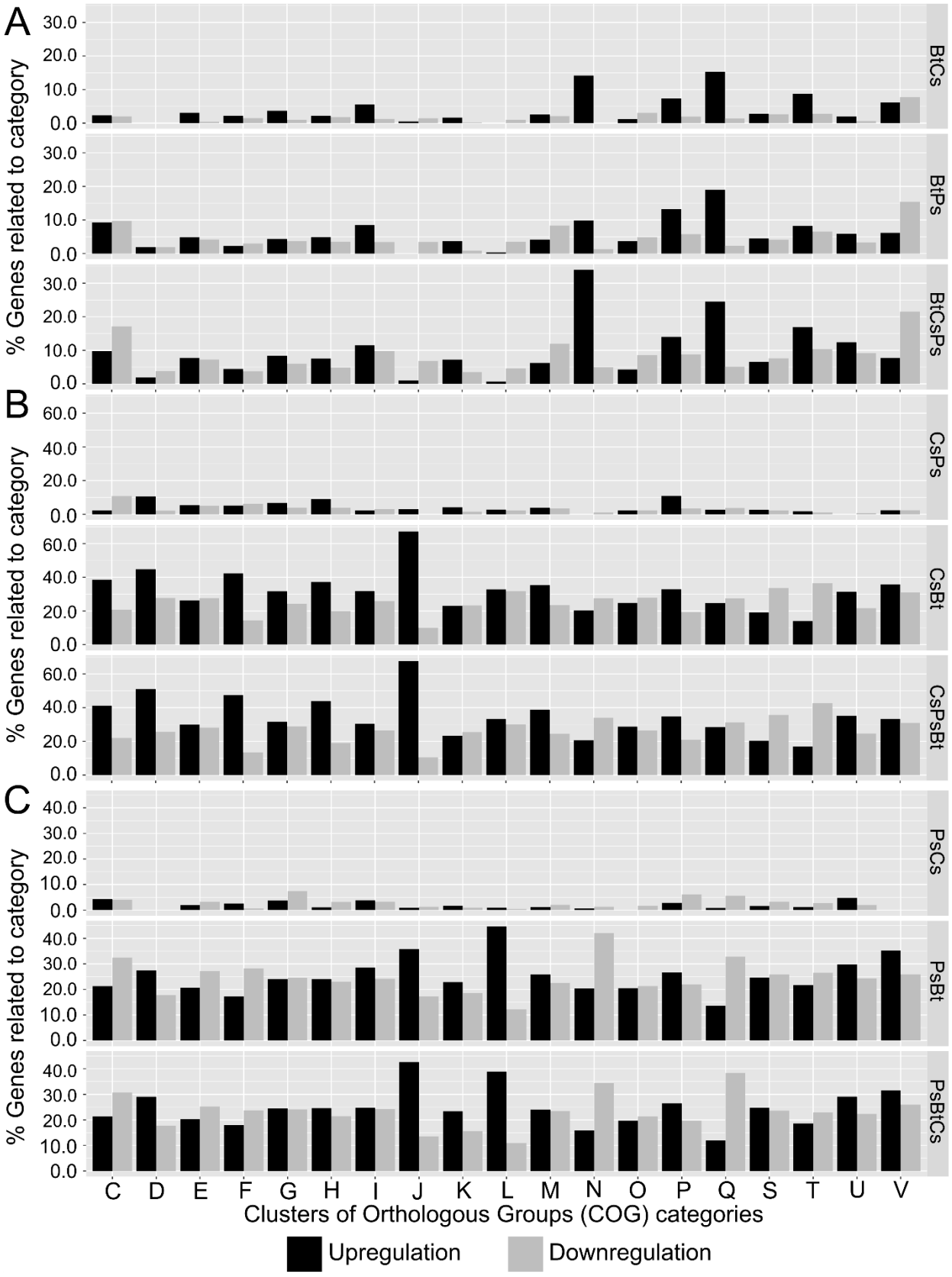
A
B
C
% Genes related to category
BtCs
BtPs
BtCsPs
CsPs
CsBt
CsPsBt
PsCs
PsBt
PsBtCs
C D E F G H I J K L M N O P Q S T U V
Clusters of Orthologous Groups (COG) categories
Upregulation
Downregulation

Figure S6. Patterns of transcriptional regulation reveal biological responses of community members to different community memberships. Differentially expressed genes categorized by COG categories in A) *B. thailandensis* B) *C. subtsugae* and C) *P. syringae*. These DEGs were determined by comparing each coculture conditions to the monoculture control. COG categories include: [C] Energy production and conversion, [D] Cell cycle control, cell division, chromosome partitioning, [E] Amino acid transport and metabolism, [F] Nucleotide transport and metabolism, [G] Carbohydrate transport and metabolism, [H] Coenzyme transport and metabolism, [I] Lipid transport and metabolism, [J] Translation, ribosomal structure and biogenesis, [K] Transcription, [L] Replication, recombination and repair, [M] Cell wall/membrane/envelope biogenesis, [N] Cell motility, [O] Post-translational modification, protein turnover, and chaperones, [P] Inorganic ion transport and metabolism, [Q] Secondary metabolites biosynthesis, transport, and catabolism, [S] Function unknown, [T] Signal transduction mechanisms, [U] Intracellular trafficking, secretion, and vesicular transport, and [V] Defense mechanisms. Community memberships are as follows: *B. thailandensis*-*P. syringae* coculture (BtPs/PsBt), *B. thailandensis*-*C. subtsugae* coculture (BtCs/CsBt), *C. subtsugae*-*P. syringae* coculture (CsPs/PsCs), and the 3-member community (BtCsPs/CsPsBt/PsBtCs).

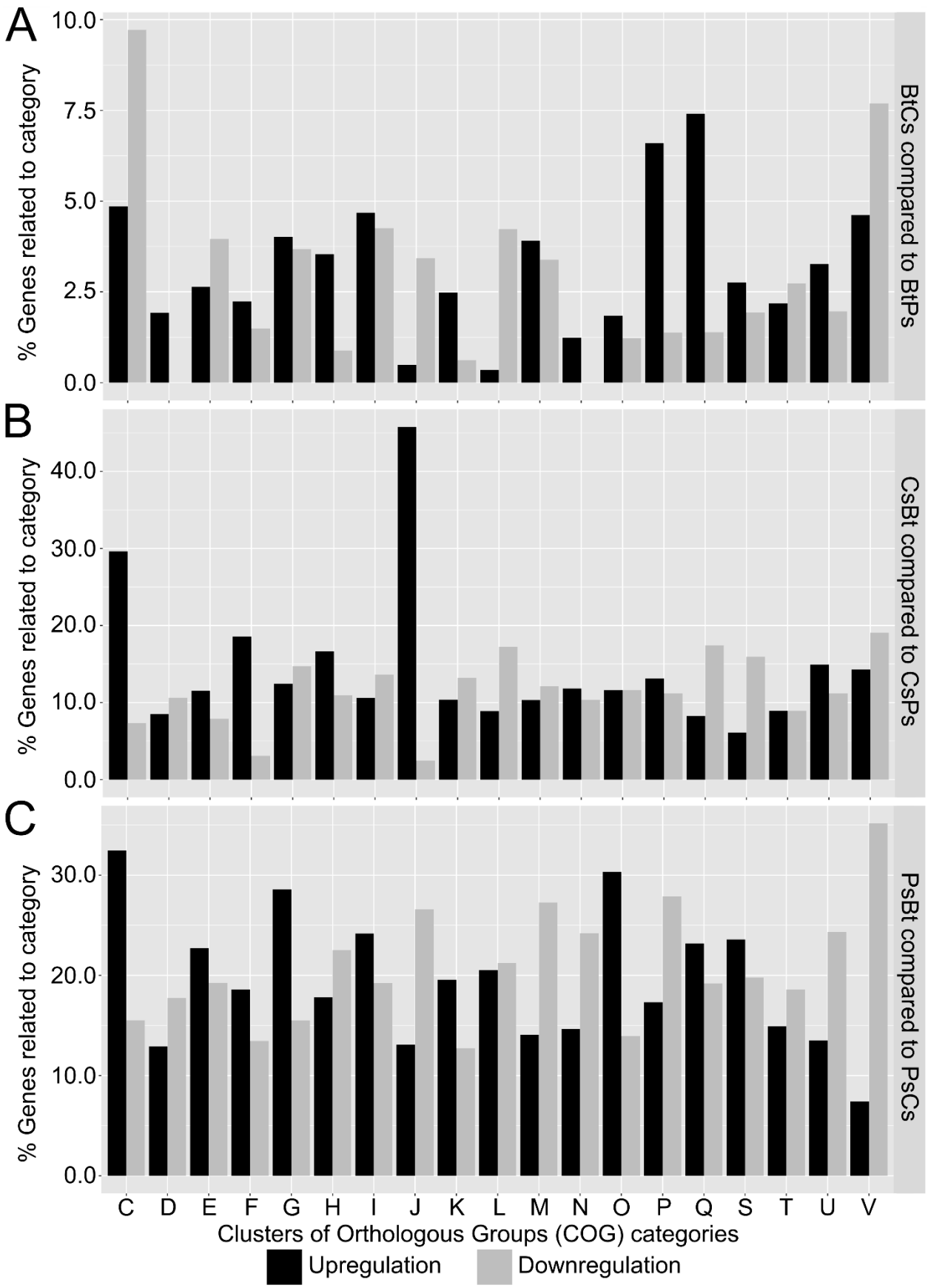
A
B
C
% Genes related to category
BtCs compared to BtPs
CsBt compared to CsPs
PsBt compared to PsCs
10.0
7.5
5.0
2.5
0.0
40.0
30.0
20.0
10.0
0.0
C D E F G H I J K L M N O P Q S T U V
Clusters of Orthologous Groups (COG) categories
Upregulation
Downregulation

272

Figure S7. Patterns of transcriptional regulation reveal pairwise coculture-specific differences. Differentially expressed genes categorized by COG categories in A) *B. thailandensis* B) *C. subtsugae* and C) *P. syringae*. These DEGs were determined by comparing gene expression between pairwise cocultures for each member. Analyses were as follows: BtCs-BtPs; *B. thailandensis* coculture with *C. subtsugae* (case) was compared to *B. thailandensis* coculture with *P. syringae* (control), CsBt-CsPs; *C. subtsugae* coculture with *B. thailandensis* (case) was compared to *C. subtsugae* coculture with *P. syringae* (control), and PsBt-PsCs; *P. syringae* coculture with *B. thailandensis* (case) was compared to *P. syringae* coculture with *C, subtsugae* (control). COG categories are labeled in the Figure S6 legend.

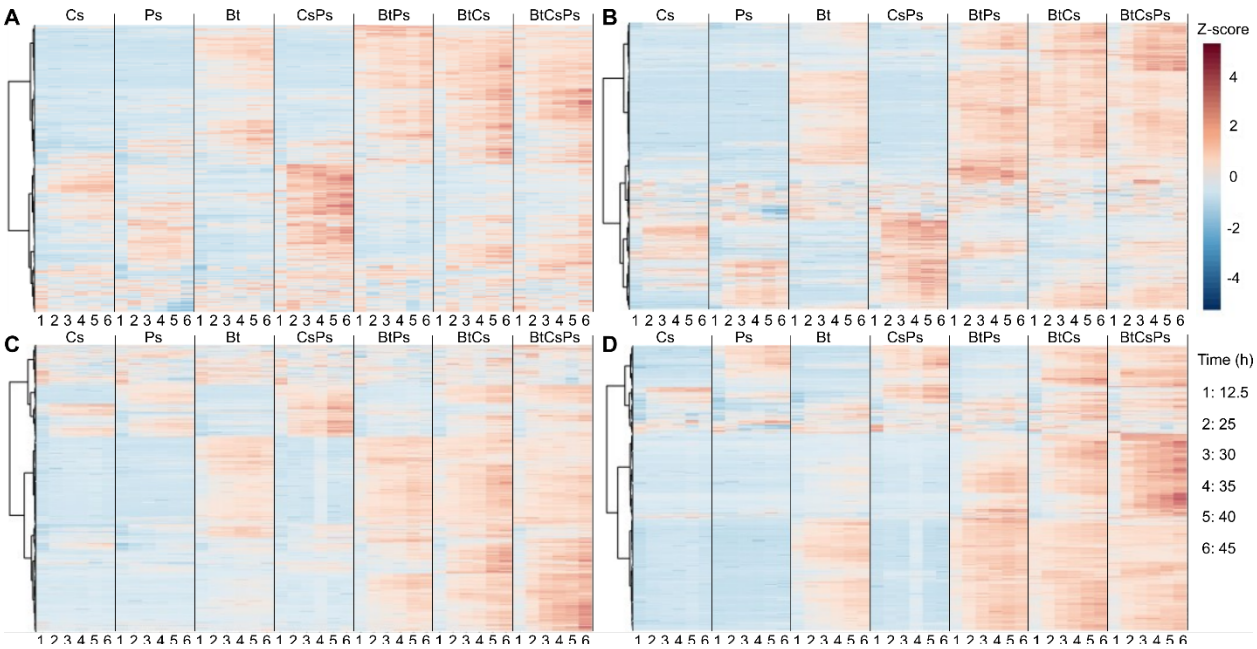

Figure S8. Exometabolites have membership-specific production and temporal accumulation. A heat map of coculture accumulated exometabolites is shown for polar positive (A), polar negative (B), nonpolar positive (C), and nonpolar negative (D) modes, for *C. subtsugae* monoculture (Cs), *P. syringae* monoculture (Ps), *B. thailandensis* monoculture (Bt), *C. subtsugae-P. syringae* coculture (CsPs), *B. thailandensis-P. syringae* coculture (BtPs), *B. thailandensis-C. subtsugae* coculture (BtCs), and the 3-member community (BtCsPs), where samples are in columns and exometabolites are in rows. Data for each sample are the averages from independent time point replicates (n = 2 to 4). Euclidean distance was calculated from Z-scored mass spectral profiles. Features with similar dynamics were clustered by Ward's method.

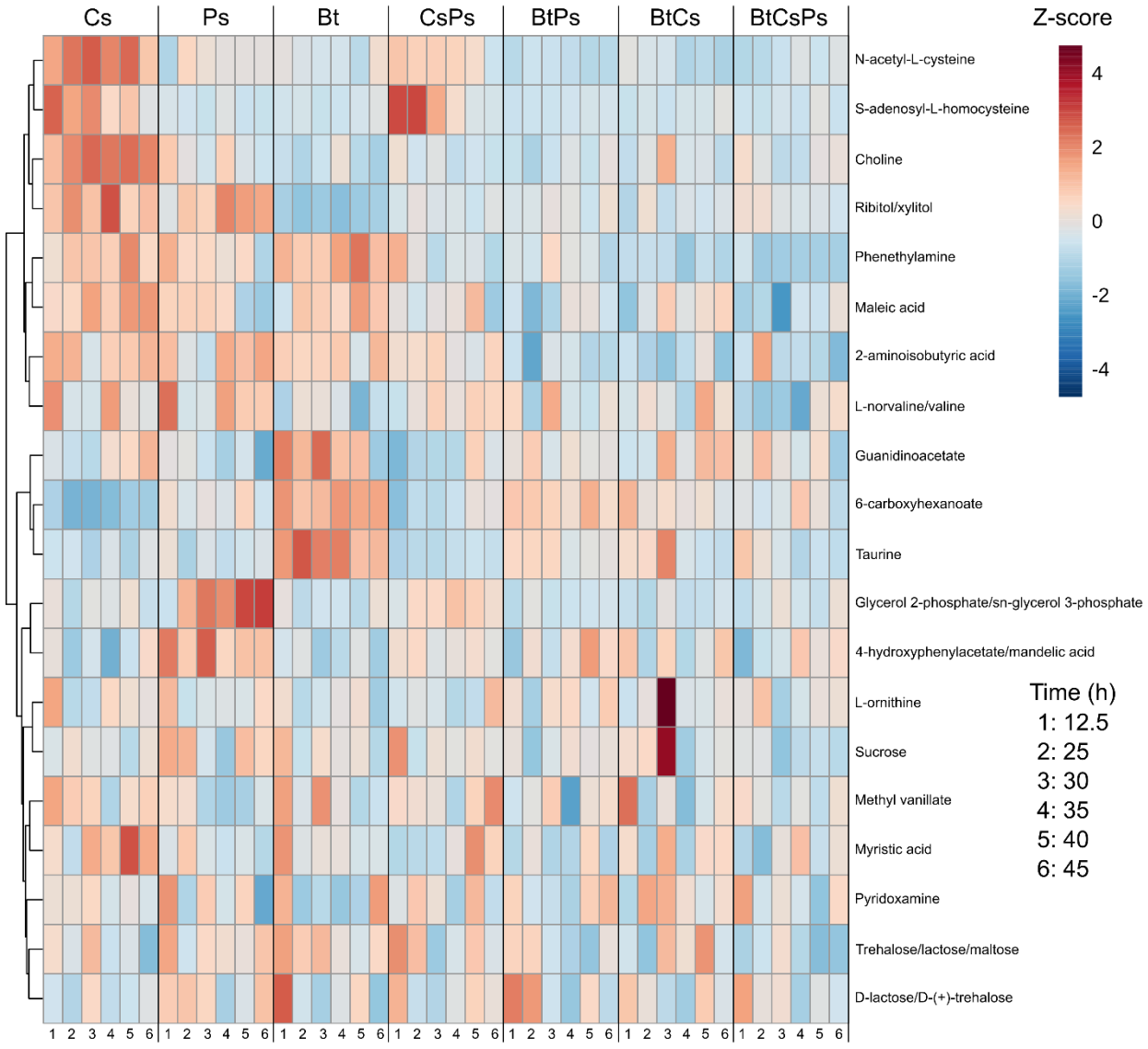

Figure S9. Identified exometabolites with exponential phase accumulation. A heat map of exometabolite dynamics is shown for identified metabolites with exponential phase accumulation (time point 12.5 h) determined from *C. subtsugae* monoculture (Cs), *P. syringae* monoculture (Ps), and *B. thailandensis* monoculture (Bt), Temporal dynamics for these exometabolites were then plotted for *C. subtsugae-P. syringae* coculture (CsPs), *B. thailandensis-P. syringae* coculture (BtPs), *B. thailandensis-C. subtsugae* coculture (BtCs), and the 3-member community (BtCsPs), where samples are in columns and exometabolites are in rows. Data for each sample are the averages from independent time point replicates (n = 2 to 4). Euclidean distance was calculated from Z-scored mass spectral profiles. Features with similar dynamics were clustered by Ward's method.

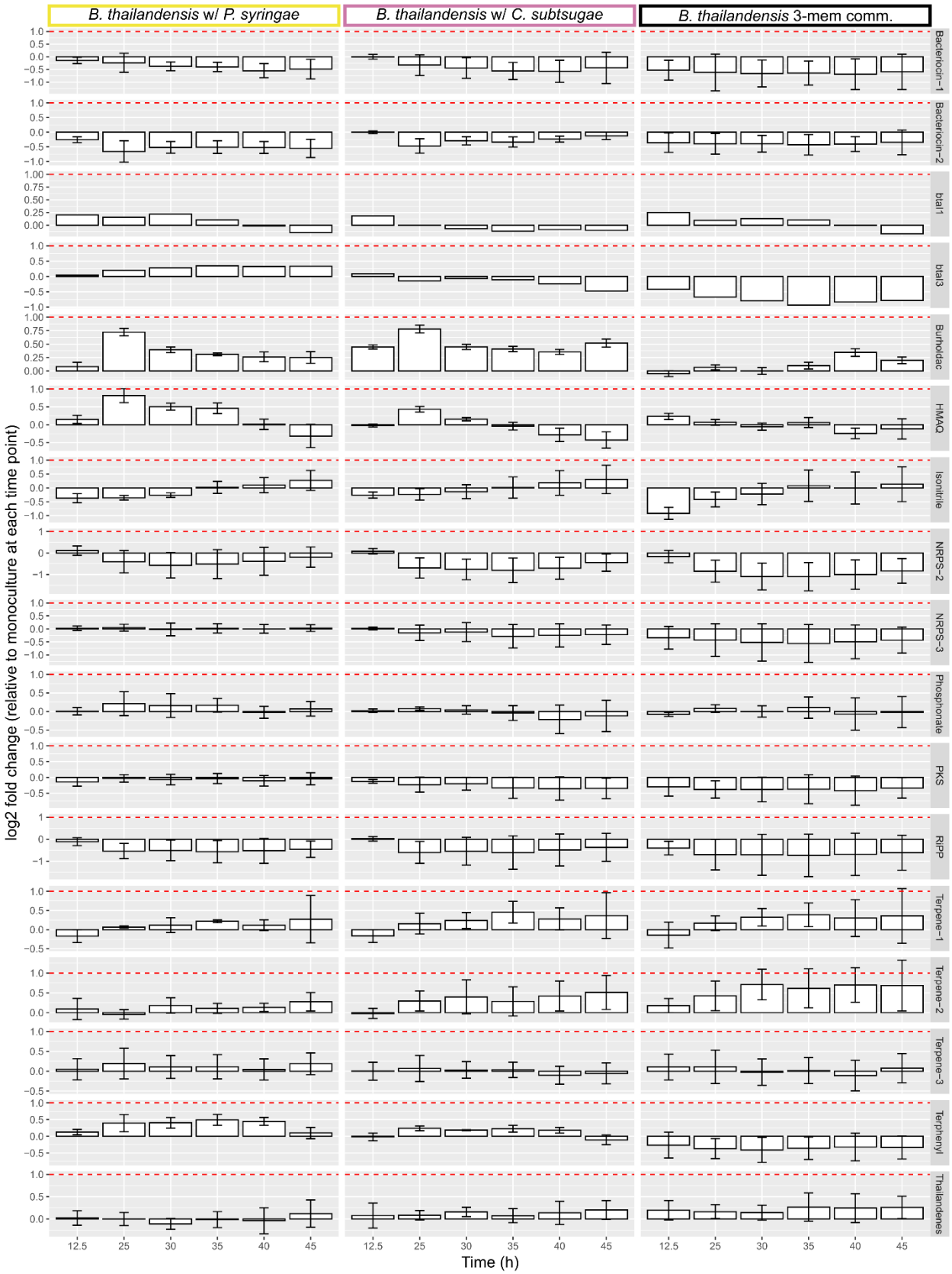

313
314 **Figure S10. BSGC downregulated or unaltered in *B. thailandensis*.** Biosynthetic genes involved in

each BSGC were determined with antiSMASH and evidence from literature. At each time point, the average log2 fold-change (LFC) was determined across all biosynthetic genes for each BSGC. The horizontal line represents a LFC threshold of 1. Note that plots for each BSGC have separate scales for the Y-axis.

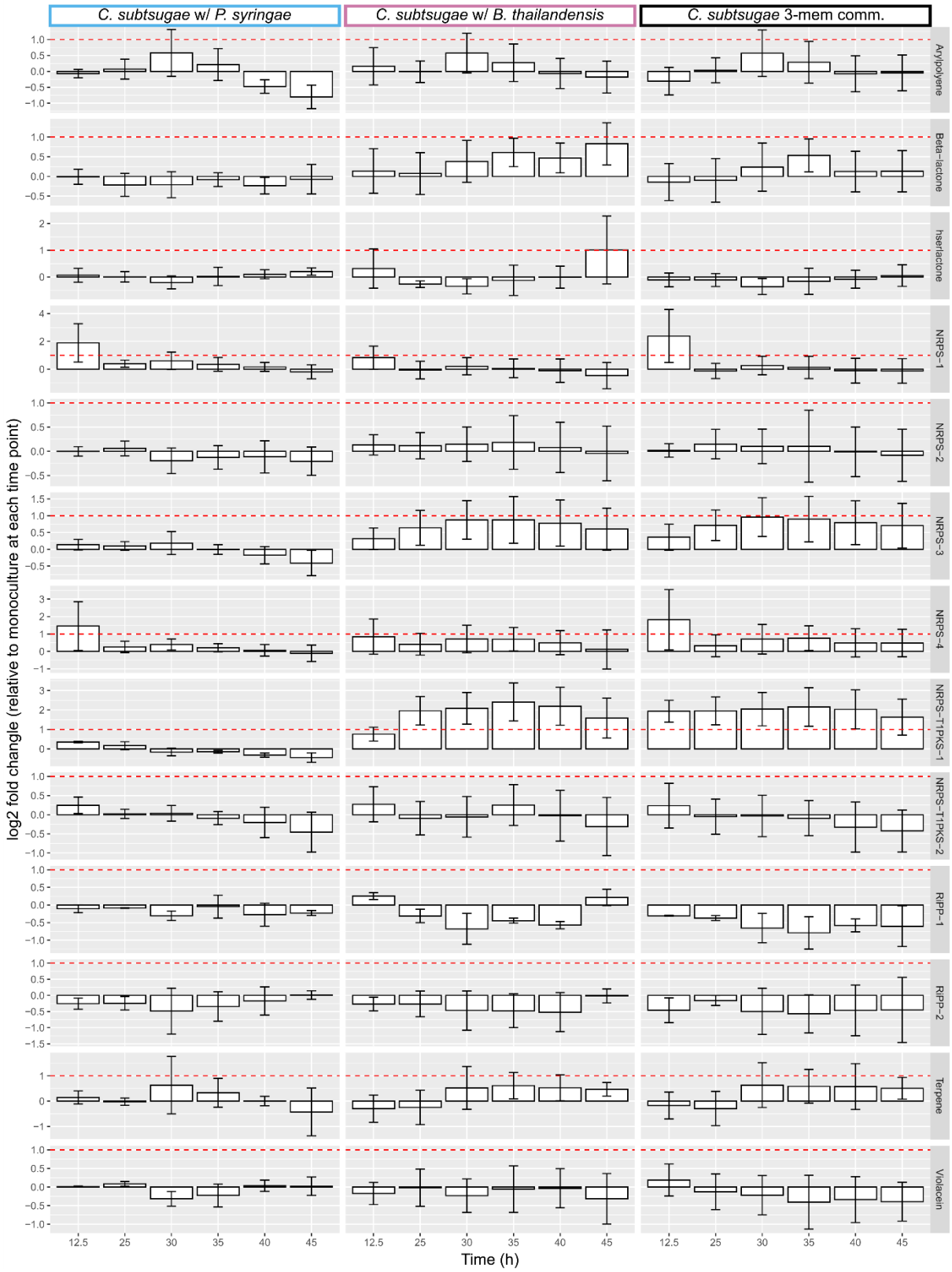

Figure S11. Patterns of transcriptional regulation for BSGC in *C. subtsugae*. Biosynthetic genes involved in each BSGC were determined with antiSMASH and evidence from literature. At each time point, the average log2 fold-change (LFC) was determined across all biosynthetic genes for each BSGC.

The horizontal line represents a LFC threshold of 1. Note that plots for each BSGC have separate scales for the Y-axis.

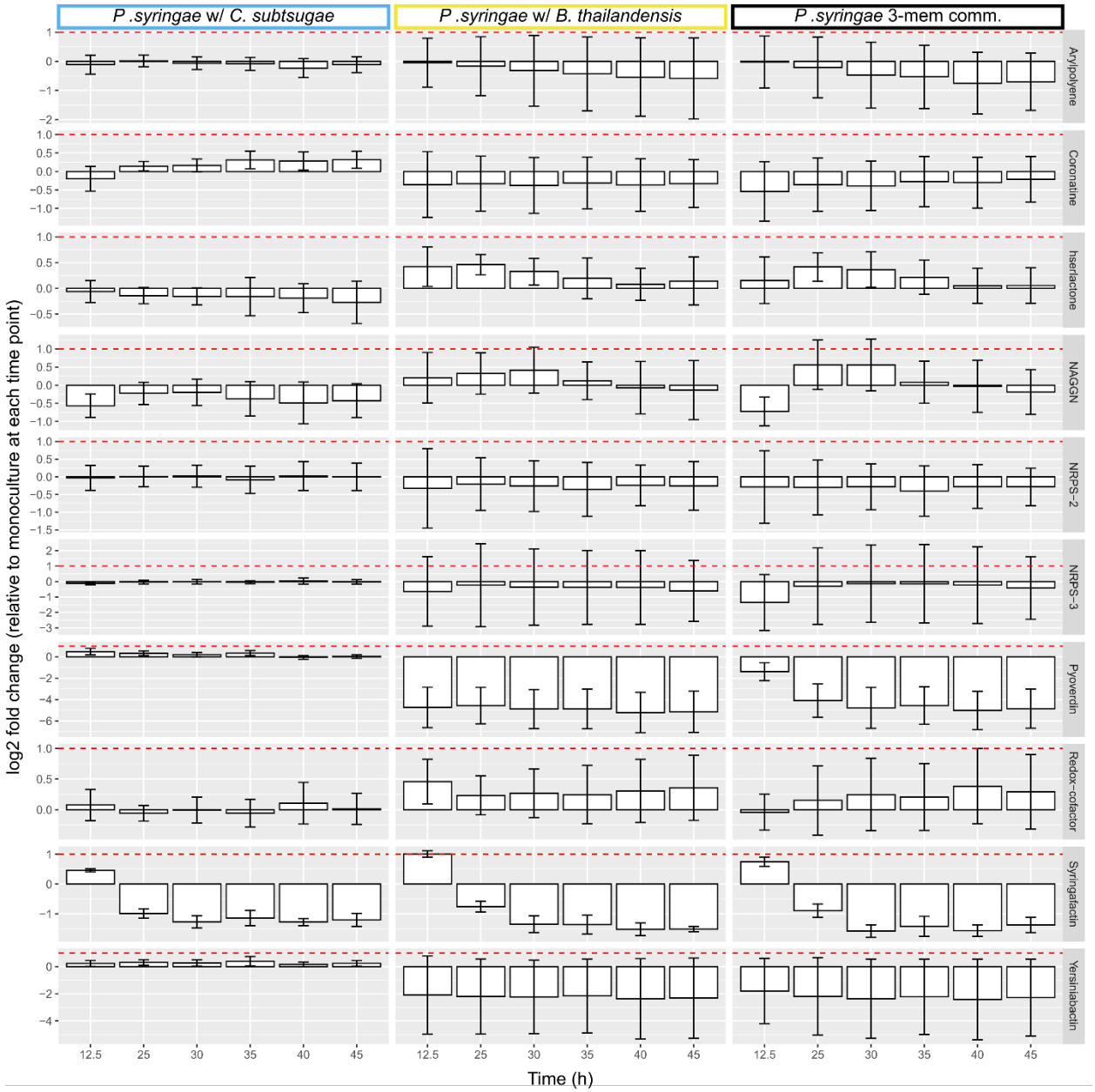

Figure S12. Patterns of transcriptional regulation for BSGC in *P. syringae*. Biosynthetic genes involved in each BSGC were determined with antiSMASH and evidence from literature. At each time point, the average log2 fold-change (LFC) was determined across all biosynthetic genes for each BSGC. The horizontal line represents a LFC threshold of 1. Note that plots for each BSGC have separate scales for the Y-axis.

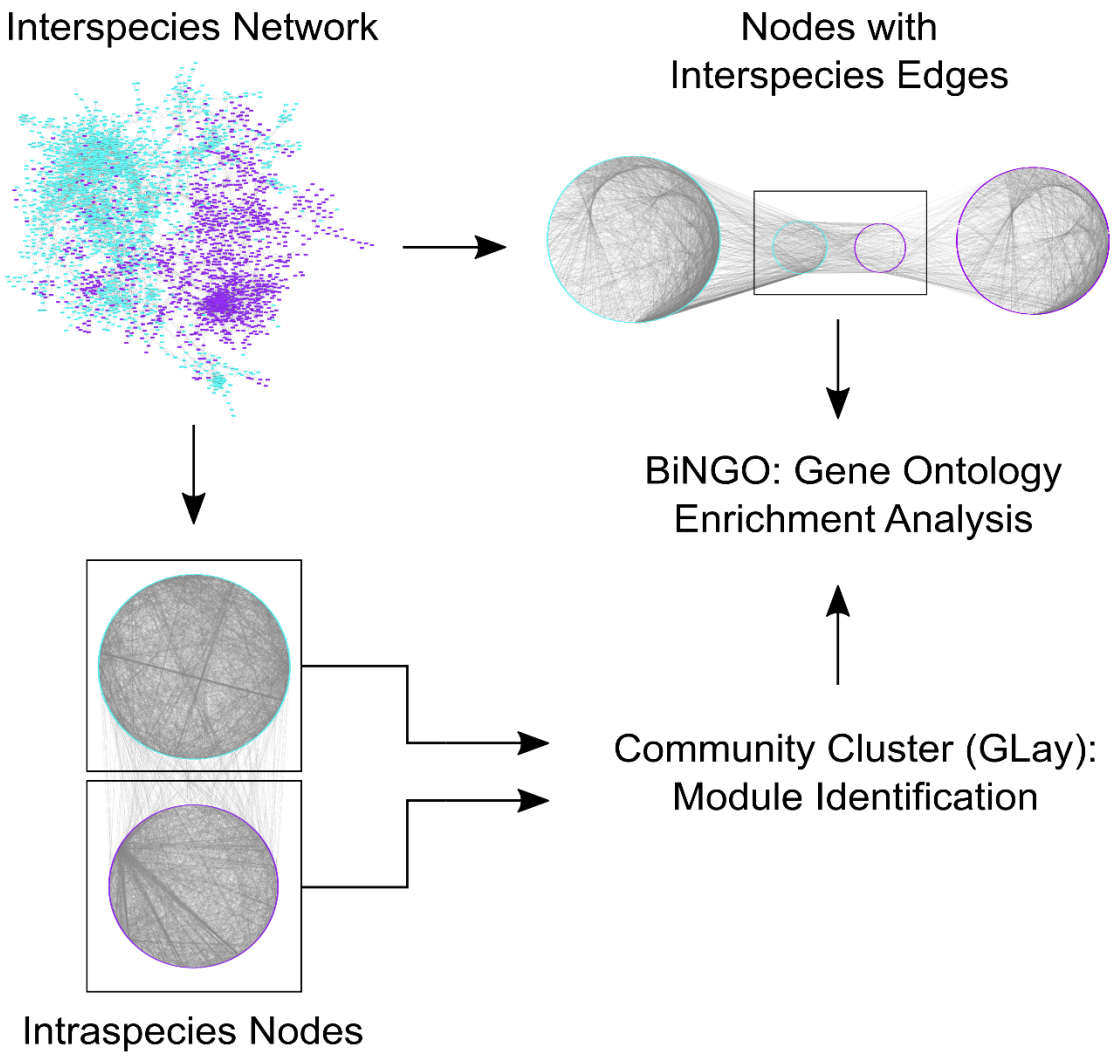

Figure S13. Flow diagram for interspecies co-expression network analysis. An interspecies coexpression network was created based on transcript counts from *B. thailandensis-C. subtsugae* and *B. thailandensis-P. syringae* cocultures. All genes that passed initial quality filtering were included in the analysis to generate networks. Unweighted gene coexpression networks were generated with a Z-score cutoff of 4.5. Intraspecies genes were used to identify network modules. Gene ontology enrichment analysis was performed on nodes with interspecies edges.

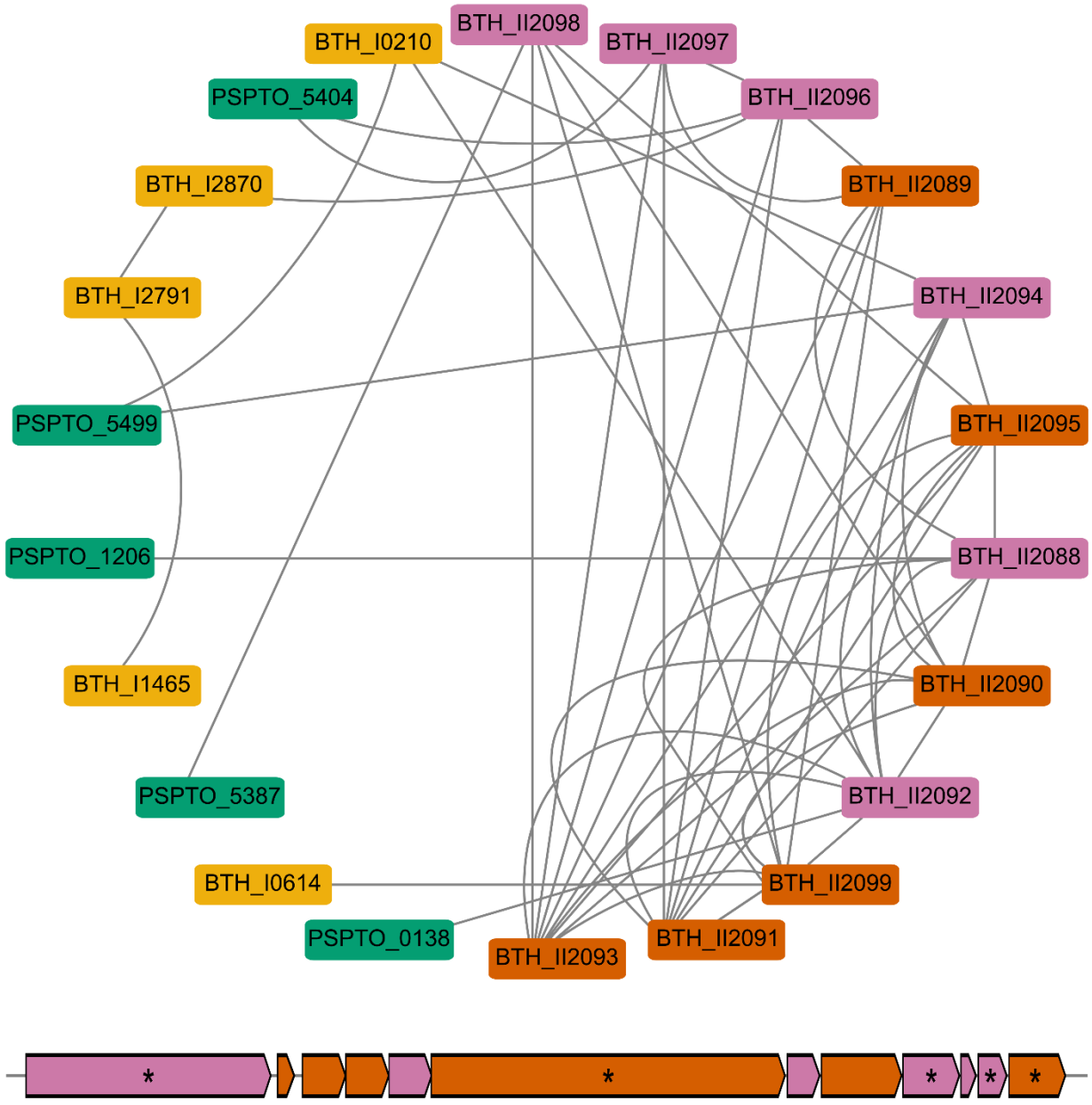

Figure S14. *B. thailandensis* genes involved in malleilactone production are detected as interspecies edges in the *B. thailandensis-P. syringae* coexpression network and biosynthetic genes organize into network modules. A network module containing the malleilactone BSGC is shown. The network module nodes are color coded by *B. thailandensis* gene type (BSGC or not) and type of connections (interspecies or not): malleilactone biosynthetic genes that had interspecies edges (magenta), malleilactone biosynthetic genes that did not have interspecies edges (orange), or other genes that were not part of the BSGC (yellow); as well as genes that were from *P. syringae* (green). The chromosomal organization of the malleilactone BSGC is shown below the network module. The same colors are applied to the BSGC operons. Asterisks indicate core biosynthetic genes in the BSGCs, as predicted from antiSMASH.

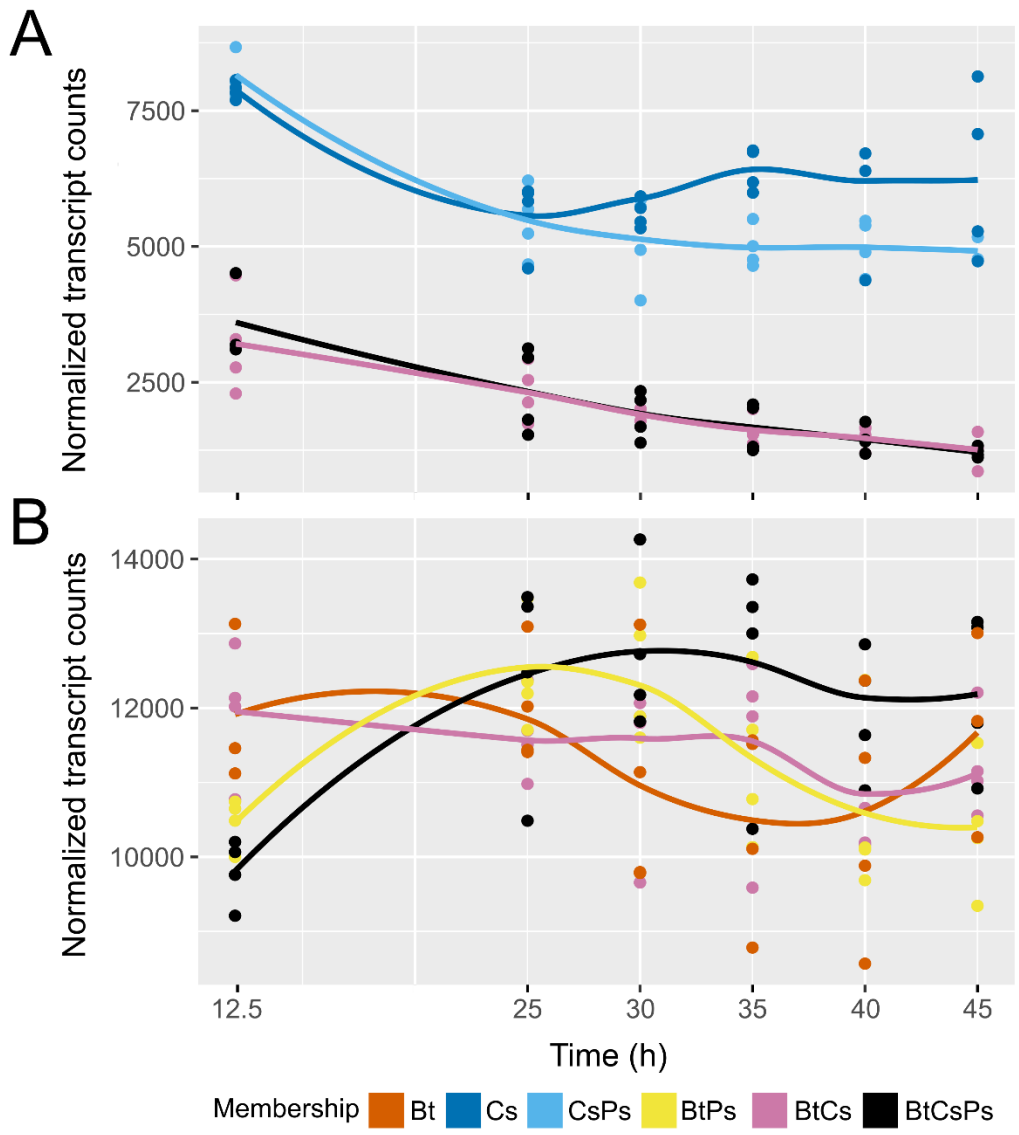

Figure S15. The DNA starvation/stationary phase protection gene, *dpsA*, in downregulated in *C. subtsugae* when cocultured with *B. thailandensis* while unaltered in *B. thailandensis*. Transcript abundance trajectories of *dpsA* are plotted for *C. subtsugae* (A) and *B. thailandensis* (B). Time course scatter plots were smooth curve fitted by loess (n=3-4 replicates/condition/time point). Community memberships are as follows: *B. thailandensis* monoculture (Bt; orange), *C. subtsugae* monoculture (Cs; blue), *C. subtsugae-P. syringae* coculture (CsPs; light blue), *B. thailandensis-P. syringae* coculture (BtPs; yellow), *B. thailandensis-C. subtsugae* coculture (BtCs; purple), and the 3-member community (BtCsPs; black).

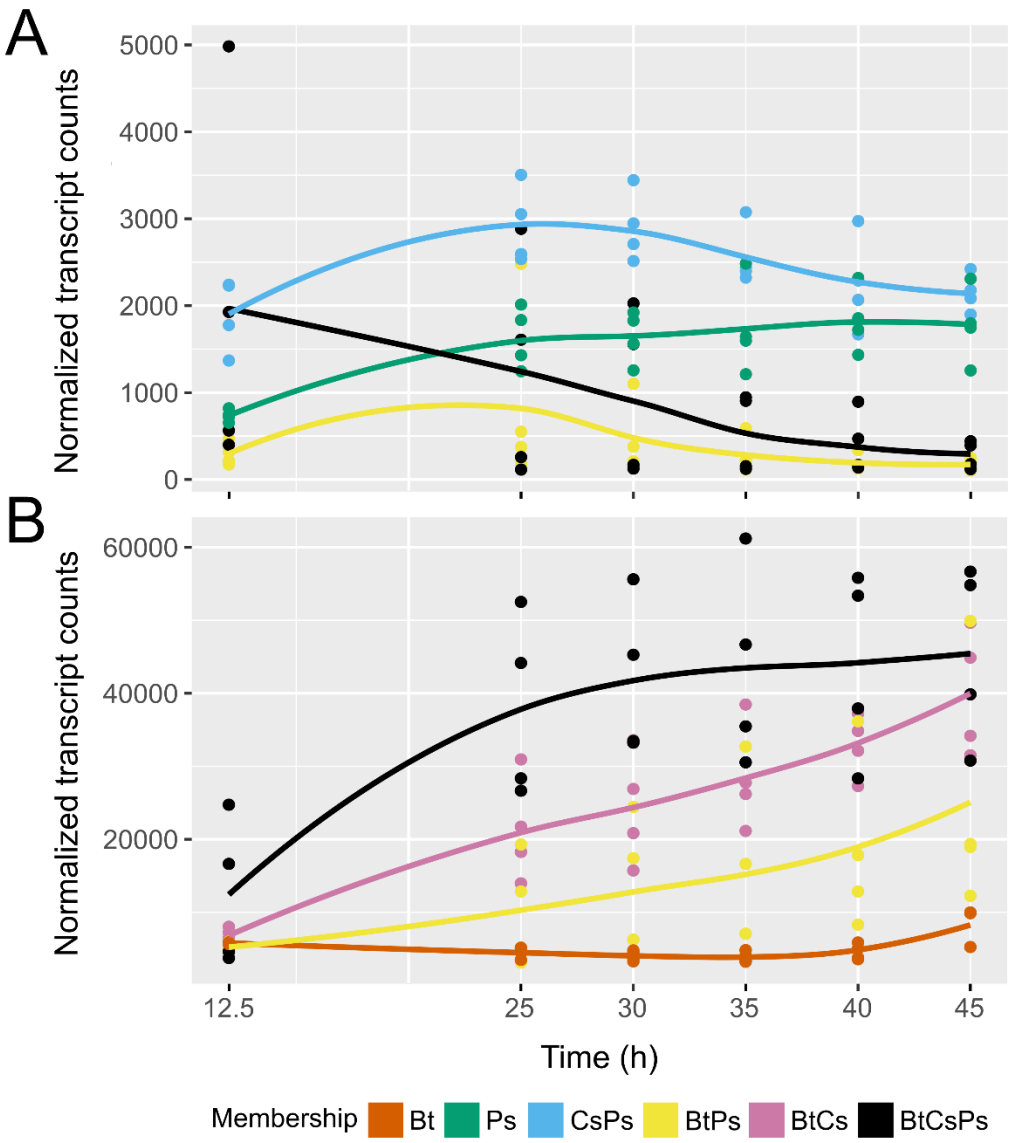

Figure S16. The gene encoding a TonB-dependent siderophore receptor is downregulated in *P. syringae* when cocultured with *B. thailandensis* while upregulated in *B. thailandensis*. Transcript abundance trajectories of *tonB* are plotted for *P. syringae* (A) and *B. thailandensis* (B). Time course scatter plots were smooth curve fitted by loess (n = 3-4 replicates/condition/time point). Community memberships are as follows: *B. thailandensis* monoculture (Bt; orange), *P. syringae* monoculture (Ps; green), *C. subtsugae-P. syringae* coculture (CsPs; light blue), *B. thailandensis-P. syringae* coculture (BtPs; yellow), *B. thailandensis-C. subtsugae* coculture (BtCs; purple), and the 3-member community (BtCsPs; black).

382 **Supplementary Table S1.** Percent variation explained on the effect of membership,

383 time, and their interaction on transcriptomic profiles.

	Membership	Time	Membership x Time
B. thailandensis	46.26	13.24	63.11
C. *subtsugae*	60.60	3.88	68.29
P. syringae	77.03	0.00	81.40

384

385

Supplementary Table S2. Summary of Protest analyses comparing transcriptional profiles through time across independent replicates. Coordinates of the first two PCA axes were used to perform Protest analyses. Ranges reflect separate Protest analyses performed between all replicates in a community membership. Values in parenthesis represent the median *P* value.

	m12	R	*P*
B. thailandensis			
Monoculture	0.048 – 0.820	0.424 – 0.976	0.010 – 0.867 (0.200)
P. syringae coculture	0.018 – 0.049	0.975 – 0.991	0.001 – 0.001 (0.001)
C. subtsugae coculture	0.010 – 0.112	0.943 – 0.995	0.001 – 0.003 (0.001)
3-member	0.013 – 0.162	0.916 – 0.994	0.001 – 0.006 (0.001)
C. subtsugae			
Monoculture	0.011 – 0.140	0.927 – 0.995	0.004 – 0.067 (0.039)
P. syringae coculture	0.045 – 0.206	0.891 – 0.977	0.003 – 0.042 (0.008)
B. thailandensis coculture	0.091 – 0.182	0.905 – 0.954	0.001 – 0.108 (0.019)
3-member	0.190 – 0.543	0.676 – 0.900	0.001 – 0.208 (0.013)
P. syringae			
Monoculture	0.178 – 0.538	0.680 – 0.907	0.008 – 0.136 (0.054)
C. subtsugae coculture	0.035 – 0.251	0.865 – 0.982	0.001 – 0.083 (0.021)
B. thailandensis coculture	0.021 – 0.290	0.843 – 0.990	0.001 – 0.001 (0.001)
3-member	0.034 – 0.687	0.560 – 0.983	0.007 – 0.317 (0.038)

Supplementary Table S3. PERMANOVA results calculated on independently replicated time series within members across all community memberships. PERMANOVA results are presented as *P* values, R^2 values, and pseudo-F statistic results in the first row. Post-hoc pairwise PERMANOVA results are presented below the first row.

	B. thailandensis	*C. subtsugae*	*P. syringae*
adonis	*P* = 0.001, R^2 = 0.480, F = 27.686	*P* = 0.001, R^2 = 0.619, F= 47.15	*P* = 0.001, R^2 = 0.778, F= 107.21
Monoculture vs *B. thailandensis* coculture	-	0.002	0.001
Monoculture vs *C. subtsugae* coculture	0.001	-	0.001
Monoculture vs *P. syringae* coculture	0.001	0.010	-
Monoculture vs 3-member	0.001	0.002	0.001
B. thailandensis coculture vs *C. subtsugae* coculture	-	-	0.001
B. thailandensis coculture vs *P. syringae* coculture	-	0.002	-
C. subtsugae coculture vs *P. syringae* coculture	0.001	-	-
B. thailandensis coculture vs 3-member	-	0.248	0.068
C. subtsugae coculture vs 3-member	0.001	-	0.001
P. syringae coculture vs 3-member	0.001	0.002	-

Supplementary Table S4. Percent variation explained on the effect of membership, time, and their interaction on exometabolite profiles.

	Membership	Time	Membership x Time
Polar Positive	45.76	7.26	55.89
Polar Negative	51.61	4.12	58.83
Nonpolar Positive	56.92	9.49	71.88
Nonpolar Negative	64.77	7.94	79.38

Supplementary Table S5. Summary of Protest analyses comparing exometabolite composition through time across independent replicates. Coordinates of the first two PCoA axes were used to perform Protest analyses. Ranges reflect separate Protest analyses performed for each polarity (polar/nonpolar) and ionization mode (positive/negative).

	m12	R	*P*
C. subtsugae-P. syringae coculture	0.022 – 0.906	0.307 – 0.989	0.001 – 0.849 (0.025)
B. thailandensis-P. syringae coculture	0.015 – 0.592	0.638 – 0.992	0.001 – 0.667 (0.050)
B. thailandensis-C. subtsugae coculture	0.003 – 0.456	0.738 – 0.995	0.001 – 0.250 (0.003)
3-member community	0.021 – 0.556	0.667 – 0.990	0.001 – 0.133 (0.003)

Supplementary Table 6. PERMANOVA results calculated on independently replicated time series across coculture community memberships. PERMANOVA results are presented as *P* values, R^2 values, and pseudo-F statistic results in the first row. Post-hoc pairwise PERMANOVA results are presented below the first row.

	Polar Positive	Polar Negative	Nonpolar Positive	Nonpolar Negative
adonis	*P* = 0.001, R^2 = 0.475, F = 27.711	*P* = 0.001, R^2 = 0.531, F = 34.773	*P* = 0.001 R^2 = 0.585, F = 37.549	*P* = 0.001, R^2 = 0.662, F = 45.743
B. thailandensis-C. subtsugae coculture vs *C. subtsugae-P. syringae* coculture	0.001	0.001	0.001	0.001
B. thailandensis-C. subtsugae coculture vs *B. thailandensis- P. syringae* coculture	0.001	0.001	0.001	0.001
B. thailandensis- P. syringae coculture vs *C. subtsugae-P. syringae* coculture	0.001	0.001	0.001	0.001
3-member community vs *C. subtsugae-P. syringae* coculture	0.001	0.001	0.001	0.001
3-member community vs *B. thailandensis- P. syringae* coculture	0.001	0.001	0.001	0.001
3-member community vs *B. thailandensis-C. subtsugae* coculture	0.002	0.008	0.019	0.025

Supplementary Table S7. Number of predicted biosynthetic gene clusters (BSGCs, first row) followed by the quantity of upregulated BSGCs in cocultures.

	B. thailandensis	*C. subtsugae*	*P. syringae*
Predicted BSGCs	28	14	10
C. subtsugae-P. syringae coculture	-	0	0
B. thailandensis-P. syringae coculture	8	-	0
B. thailandensis-C. subtsugae coculture	10	1	-
3-member community	11	1	0

Supplementary Table S8. One-way ANOVA[a] comparing the quantitation of identified secondary metabolites between community memberships with *B. thailandensis* membership.

	Df (between)	Df (within)	*F* value	*p*
Bactobolin	6	160	392.10	<2e-16
Capistruin	6	160	77.83	<2e-16
Melleilactone	6	121	150.10	<2e-16
Rhamnolipid[b]	6	136	39.34	<2e-16
Thailandamide	6	121	61.02	<2e-16
Pyochelin	6	136	105.20	<2e-16

[a]Formula: aov(formula = log(Value) ~ Membership, data = .)

[b]Rhamnolipid congener Rha-Rha-C14-C14

Supplementary Table S9. TukeyHSD post-hoc results comparing quantitation of identified secondary metabolites between community memberships with *B. thailandensis* membership. Values represent the adjusted P-value.

	Bactobolin	Capistruin	Melleilactone	Rhamnolipid[a]	Thailandamide	Pyochelin
Monoculture vs *P. syringae* coculture	8.41E-01	8.00E-07	4.00E-07	2.26E-01	1.25E-04	4.85E-01
Monoculture vs *C. subtsugae* coculture	3.54E-01	8.45E-02	< 1.00E-07	2.53E-02	< 1.00E-07	8.55E-01
Monoculture vs 3-member	8.27E-01	5.00E-07	< 1.00E-07	1.00E-05	< 1.00E-07	7.13E-04
***C. subtsugae* coculture vs *P. syringae* coculture**	8.38E-01	6.48E-03	5.45E-02	7.68E-01	9.27E-03	9.11E-01
***P. syringae* coculture vs 3-member**	3.28E-01	9.99E-01	1.00E-07	6.50E-03	4.32E-03	4.24E-02
***C. subtsugae* coculture vs 3-member**	6.08E-02	4.20E-03	1.76E-03	7.76E-02	9.97E-1	6.20E-03

[a]Rhamnolipid congener Rha-Rha-C14-C14

Supplementary Table S10. Relative gene expression of genes in the thailandamide operon across different SynCom conditions. *B. thailandensis* (31 wells) in M9-0.067% glucose was the control condition and *rpoD* was the reference gene.

	thaF	*thaK*	*thaQ*
Bt (62 wells)	0.523	0.550	0.650
Bt (93 wells)	0.303	0.138	0.188
Bt-Ps (31 wells/member)	1.311	1.675	2.163
Bt-Cv (31 wells/member)	2.375	2.304	1.05
Bt-Cv-Ps (31 wells/member)	2.048	2.433	1.742

Supplementary Table S11. Network summary results from interspecies coexpression networks.

Network	***B. thailandensis-C. subtsugae***		***B. thailandensis-P. syringae***	
Member	*B. thailandensis*	*C. subtsugae*	*B. thailandensis*	*P. syringae*
Total nodes	2701	2043	3254	3478
Nodes with only intraspecies edges	2418	1814	2749	2996
Nodes with interspecies edges	283	229	505	482
Total edges	9382	7240	15801	23319
Intraspecies edges	9074	6932	15056	22574
Interspecies edges	308		745	

Supplementary Table S12. Primers used for RT-qPCR analysis of genes in the thailandamide operon.

Primer	Sequence (5' > 3')	Product size (bps)	Reference
*rpoD*_F	ACCGTCGTGGCTACAAATTC	117	[3]
*rpoD*_R	TCGTCTCGATCATGTGAACC		
*thaF*_F	CATGCACGCGTTTCTGTTTC	113	This study
*thaF*_F	TCGTAGCCCAAGATCTCGTT		
*thaK*_F	GGTATTGAGGCCATGAACGT	104	This study
*thaK*_F	CATCAGCAGATTCGCGAAAC		
*thaQ*_F	GAACGCGTCGAAGGATTTTC	115	This study
*thaQ*_F	ATTCGTTCGGGTACTTCTGC		

Supplementary Table S13. RT-qPCR efficiencies of reference and target genes for relative expression analysis of genes in the thailandamide operon.

Gene	Slope	R^2	Efficiency (%)
rpoB	-3.424	0.999	102.6
thaF	-3.204	0.996	105.2
thaK	-3.358	0.995	98.5
thaQ	-3.305	0.997	100.7